Synchronization of Coupled Phase Oscillators — Theory and Modelling

---

Chen Gong

Universitäts-Dissertation

zur Erlangung des akademischen Grades
"doctor rerum naturalium"
(Dr. rer. nat.)
in der Wissenschaftsdisziplin Theoretische Physik

eingereicht an der

Mathematisch-Naturwissenschaftlichen Fakultät

in der Arbeitsgruppe

Statistische Physik und Chaostheorie

am

Institut für Physik und Astronomie
Universität Potsdam

Hauptbetreuer und 1. Gutachter:	Professor Dr. Arkady Pikovsky Universität Potsdam
Betreuer:	Dr. Ralf Toenjes Universität Potsdam
2. Gutachter:	Professor Dr. Francisco Rodrigues Universidade de São Paulo
3. Gutachter:	Dr. habil. Michael Zaks Humboldt Universität zu Berlin

Published online on the
Publication Server of the University of Potsdam:
https://doi.org/10.25932/publishup-48752
https://nbn-resolving.org/urn:nbn:de:kobv:517-opus4-487522

UNIVERSITÄT POTSDAM

Abstract

Institut für Physik und Astronomie

Doctor of Philosophy

Synchronization of Coupled Phase Oscillators — Theory and Modelling

by Chen Gong

Oscillatory systems under weak coupling can be described by the Kuramoto model of phase oscillators. Kuramoto phase oscillators have diverse applications ranging from phenomena such as communication between neurons and collective influences of political opinions, to engineered systems such as Josephson Junctions and synchronized electric power grids. This thesis includes the author's contribution to the theoretical framework of coupled Kuramoto oscillators and to the understanding of non-trivial N-body dynamical systems via their reduced mean-field dynamics.

The main content of this thesis is composed of four parts. First, a partially integrable theory of globally coupled identical Kuramoto oscillators is extended to include pure higher-mode coupling. The extended theory is then applied to a non-trivial higher-mode coupled model, which has been found to exhibit asymmetric clustering. Using the developed theory, we could predict a number of features of the asymmetric clustering with only information of the initial state provided.

The second part consists of an iterated discrete-map approach to simulate phase dynamics. The proposed map — a Möbius map — not only provides fast computation of phase synchronization, it also precisely reflects the underlying group structure of the dynamics. We then compare the iterated-map dynamics and various analogous continuous-time dynamics. We are able to replicate known phenomena such as the synchronization transition of the Kuramoto-Sakaguchi model of oscillators with distributed natural frequencies, and chimera states for identical oscillators under nonlocal coupling.

The third part entails a particular model of repulsively coupled identical Kuramoto-Sakaguchi oscillators under common random forcing, which can be shown to be partially integrable. Via both numerical simulations and theoretical analysis, we determine that such a model cannot exhibit stationary multi-cluster states, contrary to the numerical findings in previous literature. Through further investigation, we find that the multi-clustering states reported previously occur due to the accumulation of discretization errors inherent in the integration algorithms, which introduce higher-mode couplings into the model. As a result, the partial integrability condition is violated.

Lastly, we derive the microscopic cross-correlation of globally coupled non-identical Kuramoto oscillators under common fluctuating forcing. The effect of correlation arises naturally in finite populations, due to the non-trivial fluctuations of the mean-field. In an idealized model, we approximate the finite-sized fluctuation by a Gaussian white noise. The analytical approximation qualitatively matches the measurements in numerical experiments, however, due to other periodic components inherent in the fluctuations of the mean-field there still exist significant inconsistencies.

Zusammenfassung

Oszillatorische Systeme unter schwacher Kopplung können durch das Kuramoto-Modell beschrieben werden. Kuramoto-Phasenoszillatoren besitzen eine Vielzahl von Modellanwendungsfällen von der Kommunikation zwischen Nervenzellen bis zu kollektiven Einflüssen auf die politische Meinungsbildung sowie ingenieurwissenschaftlichen Anwendungen wie Josephson-Kontakten und synchronisierten elektrischen Übertragungsnetzen. In dieser Dissertation werden die Beiträge der Autorin zur Theorie der Kuramoto-Oszillatorensysteme und zum Verständnis nichttrivialer dynamischer N-Körpersysteme durch die Analyse ihrer reduzierten Mittelfelddynamik zusammengefasst.

Der Hauptinhalt dieser Dissertation umfasst vier Teile: Zuerst wird eine teilweise integrable Theorie global gekoppelter, identischer Kuramoto-Oszillatoren so erweitert, dass sie auch den Fall reiner Phasenkopplung höherer Ordnung umfasst. Die erweiterte Theorie wird anschließend auf ein nichttriviales Modell mit harmonischer Kopplung höherer Ordnung angewendet, welches asymmetrisches Clustering aufweist. Die Theorie sagt rein auf Basis der Anfangssystembedingungen einige Eigenschaften des asymmetrischen Clustering erfolgreich voraus.

Im zweiten Teil wird die Phasendynamik von Kuramoto-Oszillatoren mithilfe einer iterierten diskreten Abbildung simuliert. Diese Abbildung – eine Möbius-Abbildung – erlaubt nicht nur eine schnelle Berechnung der Phasensynchronisation sondern spiegelt die zugrundeliegende Gruppenstruktur der Phasendynamik auch exakt wieder. Die Dynamik der iterierten Abbildung wird mit verschiedenen analogen Dynamiken mit kontinuierlicher Zeitachse verglichen. Hierbei werden bekannte Phänomene, wie etwa der Phasenübergang im Kuramoto-Sakaguchi-Oszillatormodell mit einer Verteilung der natürlichen Frequenzen und "Chimärenzustände" (*chimera states*) bei identischen Oszillatoren nichtlokalen Kopplungstypen, repliziert.

Im dritten Teil wird ein Modell von repulsiv gekoppelten, identischen, gemeinsam stochastisch getriebenen Kuramoto-Sakaguchi-Oszillatoren beschrieben, dass teilweise integrabel ist. Sowohl durch numerische Simulationen als auch theoretische Analyse wird gezeigt, dass dieses Modell keine stationären Multi-Cluster-Zustände einnehmen kann, was den Ergebnissen anderer numerischer Studien in der Literatur widerspricht. Durch eine weitergehende Analyse wird gezeigt, dass das scheinbare Auftreten von Multi-Cluster-Zuständen der Akkumulation von inhärenten Diskretisierungsfehlern der verwendeten Integrationsalgorithmen zuzuschreiben ist, welche dem Modell Phasenkopplungen höher Ordnung hinzufügen. Als Resultat dieser Effekte wird die Bedingung der teilweisen Integrabilität verletzt.

Zuletzt wird die mikroskopische Kreuzkorrelation zwischen global gekoppelten, nicht identischen gemeinsam fluktuierend getriebenen Kuramoto-Oszillatoren hergeleitet. Der Korrelationseffekt entsteht auf natürliche Art und Weise in endlichen Populationen aufgrund der nichttrivialen Fluktuation des Mittelfelds. Die endliche Fluktuation wird in einem idealisierten Modell mittels gaußschem weißem Rauschen approximiert. Die analytische Annährung stimmt mit den Ergebnissen numerischer Simulationen gut überein, die inhärenten periodischen Komponenten der Fluktuation des Mittelfels verursachen allerdings trotzdem signifikante Inkonsistenzen.

Acknowledgements

Firstly, I would like to express my sincere gratitude to my advisor Professor Dr. Arkady Pikovsky for the continuous support and guidance of my master and Ph.D. study. Moving to Potsdam in order to study in his group has been the best decision I have made academically. His advice and guidance, his quickness and vigor in scientific research motivate me everyday to work diligently, and I could not have imagined having a better mentor for my Ph.D. study. For the last five years, it has been an honor to witness and to be part of his and Professor Dr. Michael Rosenblum's growing international scientific team. By their life-long collaboration, scientific integrity and friendship, they act as professional and moral role models not just for me but for all of their graduate students.

Besides my main advisor, I would like to thank also my second advisor Dr. Ralf Tönjes for his mentorship and friendship. His patience and generosity helped me not only professionally but emotionally through many of the ups and downs of my Ph.D. It was the opportunity to teach programming exercises in his class that gave me the confidence and experience at teaching undergraduate students. I will remember fondly of our amicable discussions over the lunch and coffee breaks.

My sincere thanks also goes to Professor Francisco Rodrigues of University of São Paulo who provided me an opportunity to join his team as an exchange student. His guidance on complex network has helped me look into areas of research beyond my own group, and his friendly and open approach to not just science but to academia in general has encouraged and motivated me immensely in networking with other scientists.

I thank my fellow graduate student colleagues Chunming Zheng, Dr. Franziska Peter, Erik Gengel and Çağdaş Topçu for the stimulating discussions, for the late nights we were working together, and for all the fun we have had in the last four years. Chunming and Franziska are my first scientific collaborators and I learned so much from them through working together. Also I thank my friends and colleagues at the University of Potsdam, Potsdam Institute for Climate Impact Research, Lobachevsky State University of Nizhny Novgorod, University Pompeu Fabra and University of Exeter. I am especially grateful to the scientific exchanges and comradery of Dr. Hadrien Bosetti, Erik Teichmann, Rok Cestnik, Dr. Gloria Cecchini, Janis Goldschmidt, Michael Voigt, Clément de la Salle, Dr. Peng Ji, Yang Liu, Dr. Paul Schultz, Dr. Tatiana Levanova, Alexander Korotkov, Evgeny A. Grines, Dr. Irene Malve, Dr. Giulia Ruzzene, Dr. Petroula Laiou, Dr. Marinho Lopes and Leonardo Rydin Gorjão.

I would like to thank the many professors, PIs, students and postdocs related to the IRTG 1740 and the COSMOS projects for their insight, their guidance and numerous friendly discussions over the years, especially Dr. Michael Zaks, Professor Tiago Pereira, Dr. Rodrigo Pena, Edmilson Roque dos Santos, Robert Ronge, Rico Berner, Dr. Jan Volkholz, Professor Henrique Barbosa and Professor Andreas Daffertshofer. I thank my friend Marie Brunel for her friendship and her energy. Special thanks to IRTG alumni Dr. Vladimir Vlasov and Dr. Niklas Boers for giving me a glipse of what comes after, and Dr. Thomas Peron for his friendly discussion that even lead to our subsequent academic collaboration.

Besides the IRTG and COSMOS groups, I would like to thank Dr. Denis Goldobin for his scientific advices, as well as Professor Dr. Klaus Lehnertz and Professor Plamen Ch. Ivanov for interesting discussions in the direction of physiological applications and for their outstanding teaching in the Como Summer School. I would like to thank also Dr. Frank Hellmann from PIK for interesting discussion on the topic of power grid.

I am grateful to also the following academic staff at the University of Potsdam: Dr. Oleh Omelchenko for his scientific advices; Professor Dr. Achim Feldmeier for giving me a chance to teach the exercise course on Electromagnetism and for fascinating lectures on logic, philosophy and theoretical physics; and Dr. Udo Schwarz for helping me in teaching the said exercise; Professor Dr. Frank Spahn for the class on non-equilibrium kinematics and his climate related activism on campus; and Professor Dr. Martin Wilkens for his enjoyable and interesting lectures.

I would like to extend my special gratitude towards the two advisors of my work student projects, Professor Dr. Stefan Klumpp and Dr. Noam Libeskind. Through their projects I gained valuable experience in software engineering as well as numerical modelling. Intellectually, it was highly stimulating to work on real-world models of scales from the molecules to galaxies.

I am also grateful to the following administrative staff: David Hansmann, Dr. Caroline Reid and Marlies Path for their friendship, unfailing support and assistance. I thank the IRTG 1740 program for funding my Ph.D. research, and especially Professor Dr. Jürgen Kurths and Professor Elbert Macau for making the project possible.

I thank Marta Enesco, Dr. Eslene Bikoumou, Dr. Sofia K. Forslund, Sarah Ring, Dr. Meredith Sylvia, Kristen Lear, Professor Robert Harmon for their friendship and support.

Last but not the least, I would like to thank my family: my husband and parents for their loving and unwavering support of my physical and emotional well-being throughout the writing of this thesis and my life in general.

Contents

Abstract **i**

Acknowledgements **iii**

List of Figures **viii**

List of Tables **x**

I INTRODUCTION **1**

1 Motivation and Background **3**
1.1 Motivation and Literature Review 4
1.1.1 Applications in Engineering, Applied Sciences and as a Computational Tool 4
1.1.2 Review on Theoretical Background 6
1.2 A Small Contribution to a Larger Theoretical Program 10

2 Concepts and Terminology **12**
2.1 Properties of Autonomous Oscillators 12
2.2 The Nature of Coupling 13
2.2.1 Biological Oscillators as Self-Sustained Oscillators with Limit Cycles — the Winfree Model 15
2.2.2 Topology of the Coupling Connection 16
2.2.3 Mean-Field Theory and the Kuramoto Model 17
2.2.4 Attractive vs. Repulsive Coupling 18
2.2.5 Coupling via Higher-Mode of Phase 19
2.3 Coupling with External Stochasticity 20
2.3.1 Common Noise as a Synchronizing Effect 20
2.3.2 Linear Stability 21
2.4 Chimera States of Non-Locally Coupled Identical Oscillators 22

II THEORETICAL FINDINGS AND NUMERICAL EXPERIMENTS **24**

3 Low-Dimensional Dynamics of Globally Coupled Identical Phase Oscillators **26**
3.1 Watanabe-Strogatz Theory of Partial Integrability 26
3.1.1 WS Theory for the Kuramoto-Sakaguchi Model 26
Choice of Initial Conditions for the Reduced System 28
3.1.2 Watanabe-Strogatz Equations for Higher-Mode Phase Coupling 29
Model Formulation 30
Derivation of the Reduced System 31

3.1.3 Numerical Simulation of the Dynamics in the WS Variables . . 32
3.1.4 Basins of Attraction for Clusters 32
3.2 Numerical Example 34
3.2.1 Higher-Mode Coupling Example: Z^2 Mean-Field 34
3.2.2 Integration of the WS Equations for the Z^2-Mean-Field Model 35
3.2.3 Comparison of the Asymmetrical Clustering under the Z^2-Mean-Field Model: Prediction and Numerics 38
3.2.4 Possibility for Decreasing Mean-Field in the Z^2-Mean-Field Model under Positive Coupling 39
3.2.5 Example of WS Integration for Fifth-Order Phase Coupling . . 40
3.3 Conclusion 41

4 Coupled Möbius Maps – a Tool to Model Kuramoto Phase Synchronization 43
4.1 The Möbius Map and Its Properties 44
4.1.1 Basic Properties 44
4.1.2 Dynamics of the Iterated Möbius Map 45
4.1.3 Real Form of the Möbius Map 47
4.1.4 Low-Dimensional Evolution of Oscillator Ensembles Under Möbius Map 48
4.1.5 Relation to Homographic Maps 49
4.2 Relation to Adler Equation and Construction of Globally Coupled Möbius Maps 50
4.2.1 Möbius Maps as a Solution to the Adler Equation 50
4.2.2 Globally Coupled Möbius Maps 51
4.3 Mean-Field Dynamics for Phases Evolved Under Coupled Möbius Maps 52
4.3.1 Globally Coupled Population of Kuramoto-Sakaguchi Type . . 52
4.3.2 Two-Population Chimera 53
4.3.3 Chimera on a Ring 57
4.4 Conclusion 57

5 Repulsively Coupled Oscillators under Multiplicative Common Noise 59
5.1 Main Model 61
5.2 WS Theory Applied to Globally Coupled Identical Oscillators with Common Noise 62
5.3 Linear Stability Analysis of Two-Cluster States 64
5.4 Deterministic Evolution 69
5.5 Numerical Evaluation of Clustering 71
5.6 Stochastic Evolution 72
5.7 Van der Pol Oscillators: Oscillators with Naturally Occurring Clusters Under Repulsive Coupling and Common Noise 74
5.8 Conclusion 77

6 Finite-Size Induced Cross-Correlation in Non-Identical Populations 78
6.1 Analytical Derivation for the Deterministic Case 79
6.2 Analytical Derivation for the Case with External Gaussian Noise . . . 81
6.3 Conclusion 84

III SUMMARY AND DISCUSSION **85**

7 Conclusion and Future Work **87**
7.1 Future Work and Outlook 89

8 Appendix **91**

Bibliography **105**

List of Figures

1.1 Overview of relevant literature as well as the contribution from author. 11

2.1 Graph comparing the limit cycle of a phase oscillator and a phase- and amplitude-coupled Van der Pol oscillator. 13
2.2 Stability condition for Adler equation visualized. 14
2.3 Formation of two anti-phase clusters under Z^2-mean-field model. . . . 19
2.4 An example of non-local coupling on a ring. 23

3.1 The geometric meaning of the original Möbius transformation used by WS, inspired by a coordinate transformation from astrophysics. 28
3.2 Visualizing three different ways of imposing constraints on the over-determined system after Möbius transformation. 29
3.3 The time-dependent Möbius transformation $\mathcal{M}_2(t)$ for the pure second-mode coupled model visualised for two parameter values corresponding to two degrees of (partial) synchrony. 33
3.4 Numerical simulation of synchronization under the Z^2-model using the reduced WS equations. 37
3.5 Comparison between prediction and simulation of the population sizes of the two clusters at steady state. 38
3.6 A unique phenomenon of decreasing mean-field under positive coupling in the Z^2-model, illustrated by a special initial condition. 40
3.7 Numerical integration of the Z^5-model via the WS formulation. 41

4.1 Bifurcation curves for the globally coupled iterated MM model. 54
4.2 Bifurcation curves for the two-population chimera state. 55
4.3 Kuramoto-Battogtokh chimera state computed using coupled MMs. . . 56

5.1 Illustration of the two types of common noise, additive and multiplicative. 60
5.2 Probability density function of the stationary solution of the Fokker-Planck equation for the phase difference between two clusters. 67
5.3 Contour plot showing the Lyapunov exponent of one of the two clusters as a function of noise strength and cluster size, under pure repulsive coupling. 68
5.4 Time evolution of discretization errors as calculated from the drift in the constants of motion, under the RK4 and Euler integration of a deterministic Kuramoto model. 70
5.5 Clustering as indicated by the increasing second Kuramoto-Daido order parameter appears to correlate with growing errors deviating from the partial integrability under the deterministic model. 71
5.6 Additional clustered states found by numerically integrating the model first considered by Gil et al. 72
5.7 Evolution of the second Kuramoto-Daido order parameter R_2 under integration of the repulsively coupled model with strong noise using Euler-Heun scheme for different step sizes. 73

5.8 Three Euler-Heun integrations of identical initial conditions showing the time series for R_2, under the original model with large and small time steps, as well as with a modified dynamics that explicitly models the discretization error to the next order in time step h. 74
5.9 Simulations of the repulsively coupled model with 1 and 2 noise terms showing the second Kuramoto-Daido order parameter and integrability error as functions of time, using Euler-Heun and stochastic Runge-Kutta 4th order schemes. 75
5.10 Contour plot of the Lyapunov exponent for one of the two clusters of repulsively coupled Van der Pol oscillators with additive noise in one direction. 76
5.11 Direct simulation of Van der Pol oscillator ensemble under weak common additive noise and repulsive coupling results in a stationary two-cluster state with relative sizes $p_1 = 53\%$ and $p_2 = 47\%$ after a transient 77

6.1 Synchronization index of two oscillators in the transformed frame as a function of their effective parameter difference. 84

8.1 Significance of parameter λ in terms of the fixed points of a simplified Möbius map. 94

List of Tables

5.1 Table detailing the reason multi-cluster states are precluded for sinusoidally coupled KS models according to WS theory, and the only possible states are full synchrony and full asynchrony. 62

List of Abbreviations

KS	Kuramoto-Sakaguchi
WS	Watanabe-Strogatz
OA	Ott-Antonsen
MMS	Marvel, Mirollo and Strogatz
l.h.s., r.h.s.	left-hand side, right-hand side
ODE	ordinary differential equation
SDE	stochastic differential equation
MM	Möbius map
NEMS	nanoelectromechanical oscillator
RK4	Runge-Kutta 4th-Order integration algorithm
sRK4	stochastic Runge-Kutta 4th-Order integration algorithm

List of Symbols

Chapter 2 [1]

φ	oscillator phase
t	time
ω_0	constant natural frequency of an oscillator
ω	natural (or intrinsic) frequency of an oscillator, usually in an infinite ensemble if not indexed
Ω	frequency of external periodic forcing
ϕ	phase in the rotating reference frame of the periodic forcing, $\phi = \varphi - \Omega t$
$\upsilon := \Omega - \omega$	detuning parameter
N	the number of oscillators in an ensemble / population size
j, j'	index of individual oscillator
k, k'	oscillator index, usually for summing over oscillators
ε	coupling strength
$G(\varphi)$	phase response function / sensitivity function of the Winfree model
$F(\varphi)$	influence function of the Winfree model
$\{\varphi_j\}$	phases of an ensemble of oscillators indexed by j
$\{\omega_j\}$	natural frequencies of oscillators in an ensemble
Im, Re	imaginary, real part of a complex number
Υ	general coupling function between oscillator phases
$Z = R\exp(i\Theta), Z_1$	complex Kuramoto mean-field
$\Theta = \arg(Z)$	phase of the complex Kuramoto mean-field
$R, R_1 = \lvert Z\rvert$	Kuramoto order parameter (first-order Kuramoto-Daido order parameter)
R'	Kuramoto order parameter, used in the self-consistency calculation
$\tilde{\phi}$	phase φ in the frame of the mean-phase Θ, $\tilde{\phi} = \varphi - \Theta$
i	imaginary number
ε_{cr}	critical coupling strength
$g(\omega)$	natural frequency distribution of non-identical oscillators
α	phase shift parameter in the Kuramoto-Sakaguchi model
$H(t)$	time-dependent general forcing term
l	order of harmonic coupling between phase oscillators / mode number
Z_l	l-th-order Kuramoto-Daido mean-field
R_l	l-th order Kuramoto-Daido order parameter, $R_l := \lvert Z_l\rvert$
$\eta(t)$	scalar Gaussian random variable
σ	noise strength
m, m'	general or noise term index

[1] Symbols are introduced in the order of their appearances. Symbols introduced in earlier chapters are not listed repeatedly.

$\mathbf{X}$	general multi-dimensional stochastic processes
$\bar{\boldsymbol{f}}, \bar{\boldsymbol{g}}$	general multi-dimensional functions
W	Wiener process
$\mathbf{x}$	multi-dimensional stochastic variable
$p(\mathbf{x}, t)$	general time-varying probability function of the multi-dimensional state variable $\mathbf{x}$
$P_{st}(\mathbf{x})$	stationary probability distribution function of the multi-dimensional state variable $\mathbf{x}$
M	total number of noise terms
S	Stratonovich shift

Chapter 3

$\omega(t)$	time-dependent natural frequency of an oscillator
*	complex conjugate
$\mathcal{M}_1$	original WS Möbius transformation for first-order harmonic coupling
$\mathcal{M}_l$	extended WS Möbius transformation for l-th harmonic coupling ($l \geq 2$)
$\tilde{z} = \rho \exp(i\Phi)$	complex WS parameter / quasi-mean-field
$\rho = \lvert\tilde{z}\rvert$	amplitude of the complex WS parameter
$\Phi = \arg(\tilde{z})$	phase of the complex WS parameter
$\tilde{\alpha}$	additional rotational variable in the reduced WS system
$\{\psi_j\}$	WS constants of motion
θ	true anomaly
e	eccentricity
E	eccentric anomaly
$H_1(t), H_2(t)$	two general forcing terms
$\bar{m}, \bar{q}, \bar{p}, \bar{n}$	integers
$\zeta = \varrho \exp(i\Psi)$, $\tilde{\beta}$	parameters of $\mathcal{M}_l$
$\{\vartheta_j\}$	transformed angles via Möbius transform $\mathcal{M}_l^{-1}$
$\tilde{n}$	$\tilde{n} = 0, 1, 2, \ldots, l-1$
Δt	small time interval
ψ_S	singular value of the constant of motion in map $\mathcal{M}_l$
φ_S	the oscillator phase in the original space transformed from singular value ψ_S
$\varphi_{S1}, \varphi_{S2}$	two basin boundaries of second-order harmonic coupled model
N_1	number of oscillators in cluster 1
$\bar{\theta}$	tracer phases for visualizing flow
$\bar{\theta}_{S1}, \bar{\theta}_{S2}$	tracers in numerical simulations which mark the basin boundaries
T_{sync}	time till synchronization is reached in numerical simulations
ϵ	general small number/ general perturbation strength
h	time step in numerical integration
p	discrete probability of R value at steady state in Z^2-model simulation

Chapter 4

S^1	unit circle
$\mathbb{D}$	open unit disk
$\bar{z}$	complex number inside closed unit disk
$\mathcal{R}_\chi(\bar{z})$	rotational map, χ the rotation number
$\mathcal{C}_q(\bar{z})$	contractional map in the direction of $\arg(q)$, degree of contraction

	indicated by $\|q\|$, q a complex map parameter
z, z_j	complex exponential of the phase $\exp(i\varphi)$, $\exp(i\varphi_j)$
$\mathcal{M}_{q,\chi}$	Möbius group, $\mathcal{M}_{q,\chi} = \mathcal{C}_q \circ \mathcal{R}_\chi$
$q = \bar{\rho}\exp(i\bar{\vartheta}), \chi$	parameters of Möbius group $\mathcal{M}_{q,\chi}$
$x^{(n)}$	n-th discrete value in a sequence
n	discrete time index, $n = 0, 1, 2, \ldots$
$\bar{z}_1, \bar{z}_2$	two fixed points of the single-sequence iterated Möbius map dynamics
$\kappa, \bar{\phi}, d$	ansatz parameters for the fixed points $\bar{z}_1, \bar{z}_2$
$\bar{\Psi}$	Möbius map rotation number
Q, Ξ	Möbius group parameters
μ	phase probability density
μ_0	uniform phase probability density on a circle
μ_Q	transformed phase probability density by $\mathcal{C}_Q$
$[[\,]]$	functional transformation of the density of phases via Ruelle-Perron-Frobenius operator
$\tilde{k}$	Fourier mode number
λ, A, β	parameters of Adler equation
τ	kick-time interval
$\mathcal{K}_{\lambda,V,\beta}$	kick map for Adler equation with time-varying parameters
σ, Γ	spurious parameters of the kick map, $\sigma = \sqrt{1-\lambda^2}$, $\Gamma = \tanh\left(\frac{A\tau}{2}\sigma\right)$
V	cumulative impulse of time-varying force over kick interval
T	inter-kick interval
$\mu_Q(\omega)$	phase density for a given frequency ω
$\bar{\omega}$	mean natural frequency of an ensemble of non-identical oscillators (oscillators with distributed natural frequencies)
γ	scale parameter of the Lorentzian natural frequency distribution
$\tilde{R}$	Kuramoto mean-field after kick (but before free rotation)
a_0, b_0	general homographic map parameters
$\tilde{G}, \tilde{H}$	short hand notations in the homographic map form of Möbius map
$\varepsilon_0, \varepsilon_1, \varepsilon_2$	several bifurcation points for coupling strengths
$\tilde{p}$	relative strengths of intra- and inter-population couplings of two populations of identical oscillators
Z_1, Z_2	Kuramoto mean-fields of two populations
$\bar{N}_1, \bar{N}_2$	sizes of two populations of identical oscillators
$z_{1,j}, z_{2,j}$	complex exponential of the phases in two populations, $z_{1,j} = \exp(i\varphi_{1,j})$, $z_{2,j} = \exp(i\varphi_{2,j})$
$Y_1 e^{i\tilde{\Psi}_1}, Y_2 e^{i\tilde{\Psi}_2}$	forces acting on all oscillators in population 1 and 2
$\bar{x}$	coordinate on a ring
$\tilde{g}_{jk}$	kernel function for oscillator pair j, k
$\tilde{B}$	cosine kernel function parameter
$U_j = \bar{R}_j e^{i\bar{\Theta}_j}$	the field acting on oscillator j in ring chimera
$\tilde{r}$	parameter for the initialization of phases in the Kuramoto-Battogtokh ring chimera example
L	length of the square distance kernel

Chapter 5

η_1, η_2, η_3	scalar Gaussian random variables
$\sigma_1, \sigma_2, \sigma_3$	noise strengths
δ	Dirac delta function
$\xi(t) = r(t)e^{i\theta(t)}$	isotropic complex Gaussian random variable
$\tilde{M}$	number of clusters
$\tilde{m}$	cluster index
$\tilde{\Phi}_{\tilde{m}}$	the phase of the $\tilde{m}$-th cluster
$\mathcal{U}$	Lyapunov potential
C_j	constant of motion in the form of cross ratio (MMS)
$U_{jj'}$	$U_{jj'} = \sin\frac{\varphi_j - \varphi'_j}{2}$
e_j	numerical error for integrating j-th oscillator dynamics as assessed by the conservation of the cross ratio (MMS)
$\mathrm{Err}_{\mathrm{WS}}(t)$	maximum numerical error made in integrating N oscillators using WS constants
$\mathrm{Err}_{\mathrm{MMS}}(t)$	maximum numerical error made in integrating N oscillators using MMS cross ratios
$\bar{\lambda}$	transversal Lyapunov exponent
p_1, p_2	relative sizes of the two clusters
$\Delta\tilde{\Phi}$	$\Delta\tilde{\Phi} = \tilde{\Phi}_2 - \tilde{\Phi}_1$
$\tilde{\delta}$	small perturbation away from the cluster
$\bar{h}, \bar{g}$	short-hand functions
$W(\tilde{\Phi}_1, \Delta\tilde{\Phi}, t)$	joint probability density of $\tilde{\Phi}_1$ and $\Delta\tilde{\Phi}$
J	probability flux
σ_{cr}	critical noise strength
N_0	normalization constant
$\bar{u}, \bar{v}, \bar{w}$	functions
$\tilde{a}, \tilde{b}$	constants
T_{int}	integration time
h_0, h_1	integration time steps
x, y	Van der Pol oscillator variables
$\bar{a}, \bar{b}$	Van der Pol oscillator parameters
x_j, y_j	coordinates of the j-th Van der Pol oscillators
$\bar{t}_n$	n-th time at which oscillator crosses the positive half-line

Chapter 6

$P(\varphi\|\omega)$	the conditional probability distribution of the oscillator phase φ given intrinsic frequency ω
$\tilde{\varphi}$	transformed phase into co-rotating frame of the mean frequency $\bar{\omega}$
$\bar{Z}$	Kuramoto mean-field of $\tilde{\varphi}$
$\tilde{\psi}$	Möbius transformed phase of $\tilde{\varphi}$ in the deterministic model
ν	observed frequency of the transformed phase angle $\tilde{\psi}$
λ	ratio between mean-adjusted intrinsic frequency $\bar{\omega} - \omega$ and effective common mean-field forcing εR, playing a similar role as λ in Adler equation
γ_{12}	synchronization index / cross-correlation between two oscillators
$\tilde{\theta}$	Möbius transformed phase of $\tilde{\varphi}$ in the noisy model
$\tilde{\nu}$	observed frequency of $\tilde{\theta}$
$\bar{A}, \bar{B}, \bar{C}$	effective noise strengths

a	phase difference variable, $\tilde{\theta}_1 - \tilde{\theta}_2$
b	phase sum variable, $\tilde{\theta}_1 + \tilde{\theta}_2$
$W(a, b)$	joint probability density of a and b
σ_{eff}	effective noise strength
$\tilde{J}$	ratio between probability flux J and σ^2_{eff}
ci, si	cosine and sine integrals
K	ratio between the observed frequency difference of two oscillators and the effective noise strength

Chapter 8

Appendix A

X, Y	stochastic processes under Itô interpretation
X_S, Y_S	stochastic processes under Stratonovich interpretation

Appendix B

$\bar{\varphi}$	raw vector of phases obtained from back transformation before the continuity check is carried out
$\tilde{w}$	$\tilde{w} = 0, 1$ for second-order harmonic coupling model

Appendix C

$\tilde{\vartheta}$	angle related to the fixed point of the Möbius map
U and S	unstable and stable points on the circle under $\mathcal{K}_{\lambda,V,0}$ when $\lvert\lambda < 1\rvert$
M and N	centers under $\mathcal{K}_{\lambda,V,0}$ when $\lvert\lambda\rvert > 1$
$\overline{\mathcal{M}}$	Möbius map which transforms away the bias term in the Adler equation
Δ	transformation parameter of $\overline{\mathcal{M}}$
$\bar{r}$	integration variable / dummy variable
s	transformed variable
$\mathcal{G}$	Möbius map which transforms the WS group parameter $\tilde{z}$ from before to after a delta kick

Appendix D

f	function
t_0	start of time step

Appendix E

$\mathcal{N}(0, 1)$	normal distribution
$\tilde{x}$	half-step value
$\bar{\eta}, \bar{\xi}$	scalar variables in sRK4 scheme
v, u	two random Gaussian numbers

Appendix F

$p_{\tilde{k}}$	Fourier term of probability density
x	transformed variable from a
$P(a)$	original probability density of phase difference a
$Q(x)$	transformed probability density

To my husband Julian

Part I

INTRODUCTION

Chapter 1

Motivation and Background

Phase synchronization is a fascinating topic where mathematical theories meet with important practical problems of our age. How do neurons in the brain communicate with each other? How do coupled generators in a power grid maintain their collective stability? How does political consensus form through collective influences of different opinions? Surprisingly, these are all questions that can be addressed to various degrees of sophistication via simple models of coupled oscillators. These models describe how oscillators influence each other, and sometimes also under external influences. Notably, one of the models — the Kuramoto model, describes oscillators coupled via a special sinusoidal function of their phases, which simplifies their mathematical descriptions in surprising ways.

Sinusoidal coupling of oscillators, as a theoretical framework has existed for more than 40 years at the time of the writing of this thesis, after the first conception of Yushiki Kuramoto in 1975 [Kur75]. Since then, a plethora of literature has been dedicated to the theoretical treatment, extension and numerical modelling of these sinusoidally coupled oscillators. Successful advances in studying the stability of the phase transition of the original Kuramoto model and other extended models have been made, and so have the discovery of new exotic states of synchrony. This thesis concerns itself with some of these existing models, which are mostly centered around the reduced mean-field dynamics of high-dimensional dynamics. Specifically, we study the partial integrability property of sinusoidally coupled globally connected oscillators of identical frequencies and the underlying Möbius group properties.

The structure of the thesis is as follows. In the introductory chapter, first we discuss the motivation of the thesis from an applied as well as a theoretical point of view (Sec. 1.1). We review the empirical motivation for studying synchronization, and specifically the Kuramoto model as a simplified model for synchronization phenomena in the natural world and in experiments. From the point of view of engineering and applied sciences, the Kuramoto model can be used as a computational tool for machine learning (Sec. 1.1.1). To give a historical context, we review existing literature on the development of the field of dynamical systems, as well as on the more specific sub-field of the theory of phase synchronization (Sec. 1.1.2). Lastly, we tie the content of the thesis to an existing larger theoretical framework in Sec. 1.2.

In the following chapters, we first present a more technical introduction, containing the historical development and theoretical background of the research topics presented here (Ch. 2). This detailed introduction serves to make this thesis more or less self-contained with minimal pre-knowledge on the subject, and also to emphasize various otherwise easily-confused concepts for readers not used to the terminologies in the particular discipline of phase synchronization.

Ch. 3 introduces the first main research topic — the partially integrable model of sinusoidally coupled identical phase oscillators on an all-to-all network. We first introduce the first-order sinusoidally coupled model, which has been shown to be partially

integrable by Watanabe and Strogatz, and then extend it to higher-mode coupled models. In Ch. 5 we add common noise to a first-order sinusoidally coupled model, and find that even with common noise, the system remains partially integrable, with conserved quantities forbidding the formations of synchronized clusters. Motivated by the underlying group structure of the Kuramoto-type dynamics, we developed a numerical method of integrating sinusoidally coupled phase dynamics via iterated Möbius maps on a circle (Ch. 4). Last but not the least, in collaboration with Dr. Franziska Peter, we studied an ensemble of oscillators with distributed natural frequencies and the role of the finite-sized fluctuation of the mean-field on the otherwise completely incoherent sub-population (Ch. 6).

Appendices include longer derivations that otherwise would disrupt the flow of the main text. Some passages of this thesis have been quoted verbatim from the following sources published by the author: [Gon+19; GP19; GTP20].

1.1 Motivation and Literature Review

The motivations for this doctoral thesis are twofold, one is from the perspective of applications and the explanation of real-world phenomena, and a second one from the perspective of the extension and addition to an existing pure theoretical framework.

1.1.1 Applications in Engineering, Applied Sciences and as a Computational Tool

The Kuramoto model of globally coupled oscillators has been a standard tool used by diverse scientific communities, particularly within the fields of nonlinear dynamics, computational neuroscience and network science to describe synchronization transition in ensembles of interacting oscillatory sub-systems. It can be directly applied after justifiable *phase reduction* of the original system — reducing the state of every sub-system to a one-dimensional description by an angle. Despite its mathematical simplicity, the Kuramoto model captures the essential characteristics of synchronization phenomena.

The synchronization phenomenon is ubiquitous in nature. Male fireflies synchronize their flashings to attract their mates [Buc88]. Crickets chant in synchrony [Wal69; GR93; Har+05]. Neurons fire in the brains of humans and animals in synchronous pattern as an information processing strategy [Ste+00; Fri15]. The human heart's pacemaker cells synchronize to generate pumping rhythms to circulate the blood throughout the body [Yan+14]. Plant cells in vitro have been observed to synchronize their cell division and differentiation cycles [FK79]. Birds and fish flock in synchronized motion across the sky and the sea [SW13]. Even on a macroscopic human level, we can observe the dramatic effect of self-feedback loop encoded in the positive weak coupling between the motions in a large group of people: human pedestrians fall in synchronized step on the London Millennium Bridge [Str+05]. Synchronization has even been hypothesized as a way that societal and cultural hegemony can be reached via opinion dynamics [PLR05; Lor07].

There are many examples where real-world oscillatory systems can be justifiably reduced to the Kuramoto phase oscillator model, such as Josephson Junctions [WS95], atomic recoil lasers [JPP08], power networks and smart grid [FNP08; DB12; NM15], functional connectivity in the human brain [Cab+11; PPJ18] and in C. elegans [MA19], neuronal oscillations which are created by excitatory and inhibitory mechanisms working together [Sin93; Buz06; TFS08; BHD10; PR15b; MP18], and even hypothesized ways of neural encoding [Doe+09; Mal+15; SMC18]. Besides playing a

role in communication and temporal binding [FA11], synchronization may also protect the communication from noise and therefore raise the precision of the communication channel [TSP10], where thanks to synchronization the coupled systems are almost at their noise-free behaviors.

As a computational tool, phase synchronization has been used in oscillatory neural networks [HI00; Cha+14; Vod+16; Zha+19] — a popular approach for potential hardware implementation of computational neural networks. For instance, the so-called phase-locked loop neural networks allow the phase-locked patterns to become images that can be "memorized" by the algorithms. The neural network can achieve patterns, for example, by converging to limit cycle attractors, which results in some synchronized state of the network with certain sustained relations between the "phases" of neurons.

Recent developments show that in many real-world oscillators, higher modes of coupling play a significant role in the dynamics. For a higher-mode coupled phase dynamics, the connection topology is equivalent to that of hypernetwork models, which may play an important role in neuronal coupling [Pet+14; GGB16; Siz+18]. Often, a pure higher-mode global coupling of this type can be achieved in laboratories through capturing the first-order mean-field value, computing its higher-order function digitally and driving the system with the result as a feedback (e.g. the experimental setup in Ref. [Tot+18]). Moreover, as suggested by Ref. [RP07], and experimentally demonstrated in Ref. [Tem+12] with a population of electronic Wien-bridge oscillators, coupling terms can be nonlinear functions of the global mean-field.

Exotic synchronization states also have captured the imagination of both experimentalists and theorists in recent years. This time the numerical experiments lead the physical experiments in discovery (also see Sec. 2.4). In 2002, Dorjsuren Battogtokh [KB02] first found the exotic state later coined by Steven H. Strogatz as the "chimera" state [AS04], where oscillators with identical intrinsic dynamics and identical coupling behave in drastically different ways in one ensemble — some oscillate coherently in sync, while the others drift incoherently as if they are not coupled to anything. Later such an exotic state has been observed in various settings: in chemical oscillators [TNS12], in two subpopulations of coupled identical metronomes [Mar+13], spontaneously in photoelectrochemical experiments [Sch+14], and more are listed in review articles such as Refs. [PA15; Sch16]. There are still theoretical open questions related to the chimera states [PA15].

Most recently, experiments with a ring of eight nanoelectromechanical oscillators (a.k.a. NEMS) displayed a large array of exotic synchronized states [Mat+19]. The NEMS are coupled to their nearest neighbors, but many states after transient behavior consist of remote synchronization, i.e., a given NEM is decoupled from its nearest connected neighbors and instead is locked to some remote oscillator in the ring. The NEMS are not phase oscillators, and their amplitudes are determined by their frequencies, allowing a variety of ways for the symmetry to be broken in the system, which generates the diversity of states observed. By reducing the dynamics to emergent higher-mode phase coupled dynamics, these phenomena can be explained. A recent popular science article Ref. [Wol19] gave a good overview for the general reader on the discovery of some of these exotic states, along with a historical overview of the field of synchronization.

1.1.2 Review on Theoretical Background

First, there was nonlinear dynamics

The area of phase synchronization falls largely under a sub-area of theoretical physics — the theory of dynamical systems mostly developed in the mid-20th century, although there were certainly even earlier pioneers such as French mathematician Jules Henri Poincaré in the mid- to late-19th century. In relation to the real-world phenomenon, dynamical systems are idealized models of a physical system, where natural fluctuations of the system's parameters and other inevitable sources of noise in the real world are for the most part ignored.[1] Dynamical system theory is frequently concerned with not just the solutions to the system — usually written as differential equations or maps — but the stability properties of these solutions. Steven Strogatz's book on nonlinear dynamics and chaos is a good introductory source on the basic tools and framework of nonlinear dynamics [Str00b]. Important historical discoveries in dynamical system theory include chaotic attractors (e.g. the Lorenz model [Lor63]), period-doubling transition to chaos (e.g. logistic maps), reaction-diffusion systems (e.g. the Kuramoto-Sivashinsky model [Siv77; Kur78; Siv80], the complex Ginzburg-Landau equation [GL50] and activator-inhibitor systems or "excitable systems", such as the FitzHugh-Nagumo model [Fit61]), coupled conservative oscillators (especially the Fermi–Pasta–Ulam–Tsingou problem [FPU55; Dau08] and the soliton solution to the Korteweg–de Vries equation [Miu76]), and coupled dissipative (biological) oscillators with stable limit cycles (see the Winfree model [Win67], also Sec. 2.2.1), among many others. These discoveries mostly date from the period between 1950 and 1990.

The period from 1950 to 1990 in the history of dynamical system saw the amazing development of the theory of "nonlinear dynamics". Nonlinear dynamics was developed comparatively much later than the development of linear dynamics, i.e., those systems that can be written as linear differential equations. In linear equations, only at most the first power of the unknown solution (function) or its derivatives can appear in each term of the equation. Linear equations are simple to solve because they obey the superposition principle. Basically, because differentiation is a linear operator, this means that any linear combination of the solutions of a linear differential equation is also a solution of the equation. Therefore methods such as Fourier transform could be applied to express general solutions as an added series of basic solutions. However, for the nonlinear case where the superposition principle fails, drastically different and new methods are needed, such as inverse scattering theory [Gar+74] (analogous to the Fourier transform in the linear case).

Phase synchronization, especially in the case of the canonical Kuramoto model, can be seen as a theoretically advantageous extension of the Winfree model for coupled nonlinear biological oscillators. The development of the Kuramoto model, according to the inventor himself [Kor], has been inspired by the similarity between the coupling of ferromagnetic spins and the coupling between Winfree model for biological oscillators. The former has a well-known second-order phase transition, which Kuramoto suspected would be also possible for coupled biological oscillators. His main discovery was to realize that the product form of the coupling in Winfree model, though natural and realistic, does not allow for a solvable model. This is the practical motivation for the sinusoidal coupling that forms the basis for the Kuramoto model. Based on the theoretical assumptions that the units are all-to-all coupled and the oscillators have a

[1] In the scope of this thesis, sometimes we deal with noise via established theoretical traditions. In these cases we usually use a type of noise with certain convenient theoretical properties, such as Gaussian white noise, which can be seen as idealized noise.

strongly attractive limit cycle orbit, a sinusoidal form of coupling can be derived from the complex Ginzburg-Landau equation. Later, Kuramoto showed in Ref. [Kur84] how the long-term dynamics of any system of "weakly coupled", nearly identical limit-cycle oscillators can be described by a universal form of phase equations from averaging (see Sec. 5.2 of Ref. [Kur84]). The oscillators are said to be "weakly coupled" if their mutual perturbations via their interactions are small (1) when compared to the characteristic strong stability of the oscillators amplitudes, and (2) when compared to their intrinsic natural frequencies (the changes in period are small compared to the period itself). A comprehensive review on the history and development of the Kuramoto model can be found in Ref. [Str00a] or in Ref. [Ace+05]. Besides the synchronization of regular or deterministic oscillators, chaotic systems have also been shown to be synchronizable [PC90; OPK02]. Under many practical cases where phases can be defined for chaotic oscillators, it is possible to have phase synchronization among the units while their amplitudes remain uncorrelated and chaotic [RPK96].

Phase synchronization — a second boom in the 1990s and 2000s

After a period of relatively slow development, the Kuramoto-model started to gain traction again in the 1990s and early 2000s with the theoretical community. This second phase of development was partially due to the availability of the personal computer and cheap computational power for conducting numerical experiments, and partially due to two important theoretical developments which in one way or another reduce the complex dynamics to lower dimensions. The generalized Kuramoto model — the Kuramoto-Sakaguchi model (Sec. 2.2.4) — contains a low-dimensional description [WS94; OA08; PR15a; CEM17], i.e., a 2- or 3-dimensional dynamics can be shown to be sufficient to describe an N-body interaction. The low-dimensional variables turn out in both cases to be closely connected or identical to the mean-field of the oscillator phases. Therefore we sometimes also call them mean-field or quasi-mean-field theories.

The two "mean-field" theories are the Watanabe-Strogatz (WS) theory and the Ott-Antonsen (OA) theory, named after their authors. The WS theory was developed for oscillators with identical natural frequencies in a system of any size, whereas the OA theory was developed for oscillators with distributed natural frequencies in the infinite-sized system limit. Between the two, the latter has been enjoying more attention from the modelling and complex network community due to its ability to handle heterogeneous populations (coupled sub-units have different natural frequencies). However, OA utilizes an ansatz, which although shown to be attractive [OA09], is technically only valid at the infinite system-size limit (and there has been a report of the OA ansatz as a poor fit of the experimental data for biological oscillators [HFB18]). WS on the other hand reduces the complex dynamics of N bodies to the dynamics of 3 parameters and is not bound by any ansatz or assumptions about system size. The only limitation of the WS theory is that it is solely applicable to identical oscillators. Nevertheless, a perturbation theory exists for frequency distribution deviating weakly from identical common frequencies [VRP16], as does an extension of the WS theory for non-identical oscillators in the thermodynamic limit [PR11]. Regardless of their intrinsic and external limitations, both WS and OA theories afford us powerful tools at analyzing potentially highly complex N-dimensional dynamics by the reduced dynamics of the population's mean-field.

While being extremely powerful theoretical approaches, reductions via the WS or OA theories still suffer from several limitations. First, the WS and OA theories are applicable mostly to ensembles of oscillators where every element is identically connected

(even though certain types of deviations from all-to-all connection are allowed, see below). Second, the WS and OA theories can only be applied to systems with a single harmonic in the coupling function [MMS09]. The second limitation does not necessarily mean that the theories can only be applied to a first-order harmonic coupling (or sinusoidal coupling). In fact, the OA theory has been extended to pure higher-mode coupling in the thermodynamic limit for non-identical oscillators [SOGR11], and for the WS theory, we have extended it in this thesis to pure higher-mode coupling for identical oscillators (see Ch. 3). Thirdly, the WS theory and OA ansatz are not valid for systems whose oscillators evolve with individual noisy components. Each of these three limitations could hinder the applicability of OA or WS theory to biological systems or other real-world systems, even if these systems can be justifiably described by one-dimensional phase oscillator models. For instance, coupling between biological oscillators often features higher-mode components, which might not necessarily be of pure harmonic functions [HMM93; BHD10], and biological oscillators are almost always noisy [BHD10].

In the following paragraphs we list recent advances in overcoming the limitations of these paradigms of mean-field dynamics.

Theoretical extension to complex networks

In the real-world systems of coupled dynamics, often the connection topologies are non-trivial — they are not simple topologies such as lattices or regular graphs. We call such a topology a complex network, and understanding the dynamics of the interacting agents on a complex network has been the main objective of complexity science. Complexity science is still in its infancy, with the networks considered being mostly simple networks, such as regular networks, random scale-free networks, and Erdős–Rényi networks.

Because of the obvious numerical and theoretical advantages of reducing the general complex oscillatory behaviors of agents on a network to simpler descriptions, phase-reduction techniques of complex oscillatory systems can be and have been applied. Many of which have been summarized by Ref. [PD19]. Depending on different phase reduction techniques, different phase dynamics may result from them.

For Kuramoto-type phase oscillators, mean-field theories such as WS and OA have been generalized in some cases by theorists to certain types of complex networks, such as star graphs [VZP14], random scale-free networks or other types of random networks [BAO11; Cou+13; Yoo+15; Lop+16]. Using WS theory, Ref. [PR08] described hierarchical populations of identical oscillators with heterogeneous coupling between populations.

In the context of power-grid networks, a particularly noteworthy paper [Pec+14] discussed cluster formation induced by structural symmetry in a complex network. In terms of pattern formations via chimera states, Omel'chenko et al. [OK19] has applied OA theory to oscillators coupled non-locally on a ring, a torus and a three-dimensional torus.

Theoretical extension to higher-mode coupling in phase

Despite the canonical status of the Kuramoto model, many oscillators interact with each other beyond the simple picture of the first-order harmonic coupling. Higher-order mode coupling usually means that the coupling function $\Upsilon(\varphi_k, \varphi_j)$ between each pair of oscillators is a generic 2π-periodic function of the phase difference $\varphi_k - \varphi_j$, containing a few or many harmonics of the phase difference variable. The phase angles can be coupled to each other and/or to an external mean-field. Phenomenologically,

when higher-order modes are dominant in an interaction, the synchronous state of the system is characterized by the formation of multiple synchronized groups (or "clusters") of oscillators, each with a common phase [HMM93]. This differs from the cases where only the first-order harmonics exist, which can result in at most one cluster.

Recently there has been an increasing interest in second-order harmonic coupling functions and other forms of coupling via higher-order modes. Such models of globally coupled phase oscillators are often called Kuramoto-Daido models [Dai92; SOGR11; KP13; Xu+16; Yua+16; WHY17]. There are indeed many situations where the second-order harmonic coupling is large and even dominates over the first-order harmonics [KZH05; KZH06; Gol+11; Gol+13; Czo+13]. Second-order harmonic coupling can imply non-pairwise connections, which have been shown to exhibit multistability and chaos [TA11; KP15; BAR16; SA19]. Recent theoretical research also points to a more general type of coupling taking place on simplicial topologies, which can be seen as being equivalent to having a mixture of more than one mode of phase coupling, e.g. Refs. [BAR16; SA19].

In terms of mean-field theories for higher-mode coupling models, Skardal et al. [SOGR11] extended the OA theory to pure higher-mode coupling in the thermodynamic limit for non-identical oscillators. The author of this thesis extended the WS theory to pure higher-mode coupling of arbitrary sized ensemble of identical oscillators in Ref. [GP19].

Theoretical extension to nonlinearity in coupling

A series of papers by Pikovsky, Rosenblum and others [RP07; PR09; Bai+09] have highlighted the possibility of having "nonlinearities" in global coupling, where the parameters of the coupling functions, such as frequency and phase shift, depend on the amplitude of the force that acts on the oscillators. This is to be distinguished from the "nonlinear" oscillators which have nonlinear phase response functions such as the Kuramoto oscillators with harmonic phase response functions. A coupling can be nonlinear if a large perturbance does not simply have a "scaled-up" effect from that of a small perturbance. Another scenario is if the oscillators are coupled not directly to each other but through some dynamical medium (e.g. pendulums swinging on a common beam, Josephson junctions or electrochemical oscillators coupled via a common load). The coupling in this case is nonlinear if the equations for the mediator of the interaction are nonlinear. Under such models, the synchronous state becomes unstable and the system settles in a state between synchrony and asynchrony, known as partial synchrony. Remarkably, these phenomena could be fully described by WS theory. In this thesis (Sec. 3.2), we also provide a nonlinear global coupling model and its mean-field reduction treatment.

Theoretical extension to noisy systems

Real-world systems are inevitably subject to noise, both intrinsic due to the variability of the coupled individual elements, and extrinsic due to the fluctuating environment. There have been many theoretical efforts to understand the effect of noise on the synchronization of phase oscillators. Intrinsic noise usually inhibits synchronization [Kur84; Sak88; SM91], while at the same time it is able to drastically change the stability properties of the incoherence solution (by stabilizing it), as shown in Ref. [SM91]. More recently, Ref. [Tyu+18] extended the OA formulation to coupled oscillators with intrinsic noise via perturbation theory through the "circular cumulant" method. Extrinsic noise, on the other hand, usually facilitates synchronization of phase oscillators under conditions which allow for phase reduction. This problem might be particularly

relevant in biological or neurological contexts, since external noise might enhance the synchronization of biological signals. These oscillators can usually be treated by phase reduction. Ref. [NK10] extended the OA theory to include multiplicative "common noise" — an externally imposed noise common to all oscillators in an ensemble. However, only weak noise — like weak coupling, can be theoretically treated via phase reduction as mentioned above. Under strong noise, the noise-induced synchronization will not occur for nonisochronous oscillators (i.e., those whose phase response functions are not perfect sine or cosine functions). Instead, the nonisochronous oscillators will desynchronize under strong noise [GP05; GP06].

1.2 A Small Contribution to a Larger Theoretical Program

In connection to the aforementioned historical development in theory, Fig. 1.1 summarizes the contribution during the past three years by the author and her colleagues in relation to existing literature on the mean-field reduction approach of Kuramoto-type oscillators. Due to limited space, only a few exemplary works from the literature are shown, especially those relevant to the theoretical development (mainly the mean-field dynamical theories) of phase oscillators.

The four studies contained in this thesis are as follows. The model of higher-mode coupled identical phase oscillators on an all-to-all network is treated via WS formulism in Ch. 3 and published in Ref. [GP19]. A discrete-time method for integrating sinusoidally coupled phase dynamics is shown in Ch. 4, published in pre-print [GTP20], and has been accepted by Physical Review E with revision. The globally coupled identical Kuramoto-Sakaguchi oscillator ensemble under common isotropic multiplicative noise is studied via WS formulism and numerical simulations in Ch. 5 and published in Ref. [Gon+19]. The finite-sized-noise induced cross-correlation of coupled non-identical Kuramoto-Sakaguchi oscillators is derived in Ch. 6 and published in Ref. [PGP19], where the author only participated in the analytical treatment of the model.

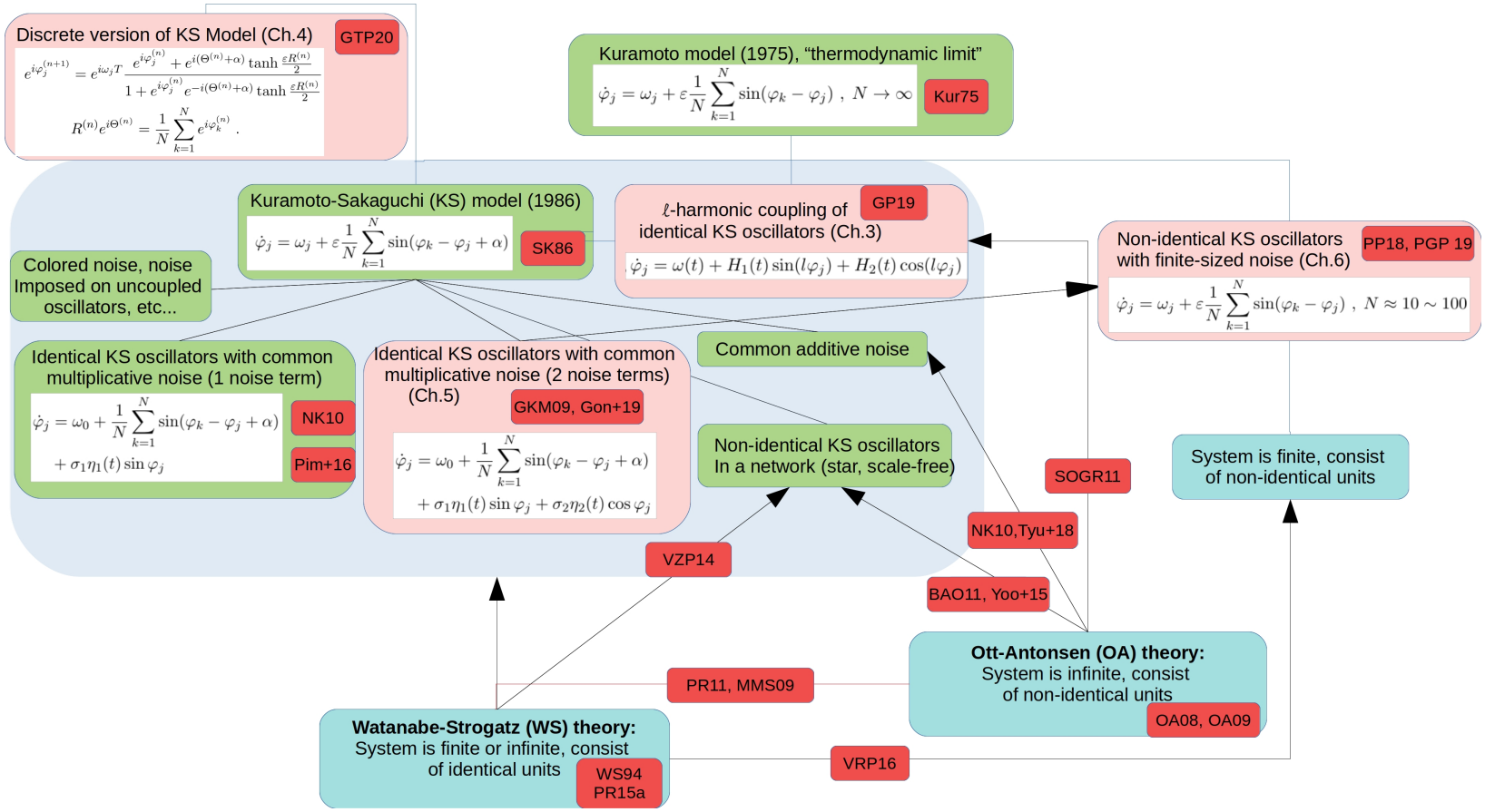

FIGURE 1.1: A summary diagram of the various derivatives of the Kuramoto model that concern this thesis, the relevant literature (citation abbreviation in small red boxes), as well as the contribution from the author and her colleagues (in pink boxes with corresponding chapter numbers). The large grey box contains all models that could be treated using the WS formulism (or using mathematical tools similar to the WS theory). Lines indicate relevance or expansion on existing models (red line between WS and OA theories). Arrows from $A \to B$ indicate that A is applied to B. Unless otherwise noted, coupling connection of the system is via all-to-all topology.

Chapter 2

Concepts and Terminology

In this chapter, we introduce relevant concepts and terminology regarding oscillators and their coupling, such that the thesis can be read and understood self-contained.

2.1 Properties of Autonomous Oscillators

The simplest autonomous oscillator is just an oscillator with a phase rotating on the unit circle at a constant speed

$$\dot{\varphi} := \frac{d\varphi}{dt} = \omega_0 \ , \tag{2.1}$$

where $\varphi(t) \in \mathbb{R}$ denotes the time-varying phase of the oscillator, and $\omega_0 \in \mathbb{R}$ is the so called *natural frequency* (or "intrinsic frequency") of the oscillator. Because such an oscillator only has one scalar variable, its phase, it is called a *phase oscillator*. The phase of an oscillator can be best thought of as a spatial angular coordinate, indicating the state of the oscillator within one recurring oscillatory cycle.

This idealized model of isolated oscillator assumes essentially no net dissipation of energy — it will rotate perpetually on its own. This more general type of oscillator is called a *self-sustained oscillator*. A wound clock is a good real-world example of a self-sustained oscillator. If the state variable(s), e.g. phase angle for one-dimensional oscillator, of such an oscillator repeats itself after a period $\tilde{T}$, and the trajectory corresponds to a closed curve in the phase space[1], then such a curve is called a *limit cycle*.

Phase oscillators are to be distinguished from more complicated oscillators such as Stuart-Landau oscillators, Van der Pol oscillators, and many other "real-world" self-sustained oscillators, where the oscillations can not be described by its phase alone, but also by its amplitude. This type of oscillator cannot be described by one-dimensional phase oscillator models because their state is not constrained on a unit circle. As a simple example, the limit cycle of the Van der Pol oscillator, an electric circuit oscillator, shown in Fig. 2.1, deviates greatly from the unit circle, and the position of the oscillator in the limit cycle cannot be described only by a single variable.

From a theoretical point of view, the major analytical advancements in the theories of synchronization have only been concerned with phase oscillators due to their mathematical simplicity. However, from an application point of view, limiting the description of potentially complex oscillatory dynamics to one scalar phase variable may appear to be highly restrictive at a first glance. Nevertheless, it has been shown that within appropriate parameter ranges, oscillators' dynamics can be approximately described by their phases alone. For example, the Kuramoto model approximates the

[1]Note that here "phase space" is used in the conventional sense, i.e., the space containing all possible states of the dynamical system, and has nothing to do with the oscillator phase, i.e., the angular variable of an oscillation.

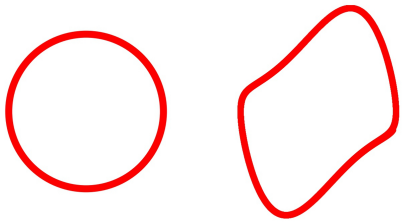

FIGURE 2.1: Graph comparing the limit cycle of a phase oscillator (a unit circle) and a phase- and amplitude-coupled Van der Pol oscillator.

long-term behavior of any ensemble of interacting oscillatory systems, so long as the coupling is weak and the sub-units are nearly identical [Kur84]. The oscillator is said to be *weakly coupled* if the perturbation via the coupling forces is small when compared to its intrinsic natural frequency. If the coupling is strong, and the limit cycle is perturbed away from the unit circle, phase alone might not be sufficient at accurately describing the dynamics, since the coupling now also involves the amplitude of the oscillatory motion.

When studying a complex network of oscillatory sub-units, it is important to differentiate two main types of ensemble: the *non-identical* and the *identical* ensemble of oscillators. Identical oscillators share a common frequency, which is to say when they are observed in isolation ("autonomous" systems), they oscillate at the same frequency. Non-identical oscillators on the other hand have a spread of various natural frequencies. In studying synchronization phenomena, the distribution of their natural frequencies is an important source of heterogeneity, which works against the ordering effect of a collective synchronizing tendency of the oscillators. Depending on the frequency distribution of the oscillators, and in particular on certain symmetry properties of the distributions (see Ref. [PP18]), one might obtain drastically different collective behaviors of the oscillators once they are coupled. However, when the distribution is a delta function, i.e., all oscillators are identical, the situation becomes much simpler, since the synchronization of the oscillators will not include phenomena such as frequency entrainment, but is only concerned with phase synchronization — the effect of the phases coming close to a common value over time.

2.2 The Nature of Coupling

After having established the type of oscillators which we are interested in — self-sustained oscillatory systems with a stable limit cycle on a unit circle, oscillating at a designated natural frequency, now we can drive such an oscillator with an external force and observe its reaction. In the simplest case, this is described by **Adler equation** [Adl46] [2], where a self-sustained oscillator of natural frequency ω_0 ($\omega_0 \in \mathbb{R}$) and described by its phase φ is driven externally by a periodic force with frequency Ω ($\Omega \in \mathbb{R}$)

$$\dot{\varphi} = \omega_0 + \varepsilon \sin(\varphi - \Omega t) \ , \tag{2.2}$$

After defining a new variable $\phi = \varphi - \Omega t$, we obtain the Adler equation

$$\dot{\phi} = -\upsilon + \varepsilon \sin \phi \ , \tag{2.3}$$

[2] In Adler equation, it is assumed that the amplitude perturbation rapidly decays compared to the time scale of the frequency detuning between the drive and the oscillator.

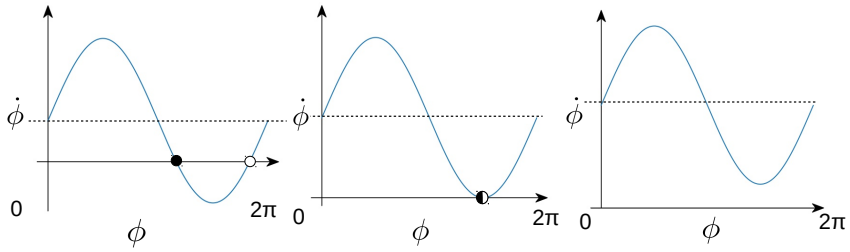

FIGURE 2.2: Stability condition for Adler equation (2.3) visualized for three values of detuning parameters υ (marked by dashed lines), which acts as a bias term to the phase velocity $\dot{\phi}$. For small value of υ (left), it can be seen that there is a stable point (solid circle) that corresponds to phase locking. This changes when the stable and unstable (open circle) merge to become a semi-stable point (half filled circle) as detuning increases (middle). When detuning is large enough (right), no phase locking is possible as phase velocity is never zero.

where ϕ is the phase in the rotating reference frame of Ωt, under a 2π-periodic forcing term, $\varepsilon \sin \phi$, proportional to the sine of the phase. $\varepsilon \in \mathbb{R}$ is a fixed parameter denoting the strength of the sinusoidal forcing. $\upsilon := \Omega - \omega_0$ is the so-called *detuning parameter*. Depending on the size of υ, a phase locking state may or may not exist (see Fig. 2.2).[3]

In the case where the forcing frequency is different from the natural frequency of the oscillator ($\upsilon \neq 0$), the latter will adjust its frequency to that of the forcing. The flashing of a male firefly under an external electric light flash reflects such a detuning phenomenon perfectly. When experimentalists, for example in Ref. [Buc88], exposed the male fireflies of Pteroptyx cribellata of New Britain to rhythmic light flashes, they discovered that the fireflies flashed at the same time as the driving light if the imposed "driving" rhythm was the same as that of their spontaneous flashing; the fireflies appeared to flash later than the driving signal when the driving light flashed faster than their natural rhythms; and they lead the driving signal when the driving period was longer. In other words, the frequencies of the fireflies' flashes were shortened by faster external driving flashes, and lengthened by slower external driving flashes.

In the real world, dynamical systems rarely live in isolation. They are frequently coupled to external fields and to each other. In most applications, a network of sub-systems can be identified and be considered as a closed system subject to an external environment, which imposes forces on this system but is not influenced by the system in return. Hence the dynamics of the external environment will be ignored and only the closed system of interacting sub-units will be considered.[4] One can speak of

[3] If the oscillator is completely in phase as the external driving force, we say it is phase-locked.

[4] This assumption might seem general and implicit in most context, but it might be non-trivial when it comes to real-world systems. For example, when we apply phase reduction technique on coupled oscillatory dynamics which contains amplitude dynamics, in order to reduce it to coupled phase dynamics, we normally require the weak-perturbation limit of the oscillators in question. The existence of the weak-perturbation presumes an "unperturbed" stable limit-cycle of the autonomous dynamics. However, an "unperturbed" limit-cycle simply might not exist. For instance, it is technically not possible to describe an unperturbed limit-cycle of a human heart, because a healthy heart cannot beat in isolation, in the absence of the signals from the central nervous system and many

external forcing in general terms, when such a forcing is not dependent on the states of the closed system of interest. As an example, one can think of the heart as coupled to the brain via the vagus nerve and the sympathetic cardiac nerve, but within the heart, heart cells are coupled to each other in a complex network. The stimuli from the brain to the heart can be seen as external to the heart network, the latter being a closed system of interest. The hidden assumption in this example is that the heart does not influence the brain in the steady state that we are interested in, which would require a justification from experiments.

2.2.1 Biological Oscillators as Self-Sustained Oscillators with Limit Cycles — the Winfree Model

The **Winfree model** [Win67] is one of the first attempts at examining the internal coupling of nonlinear oscillators. Inspired by experimental observations on real biological oscillators, Arthur Winfree intuited that the oscillators can either advance or delay in their cycle, depending on when a kick, or a perturbation, happens in the cycle. As Steven Strogatz pointed out in his book [Str12], the novelty of the Winfree model lies in the fact that the oscillators are not coupled linearly. Before Winfree, physicists were mostly concerned with linear oscillators, e.g. the simple harmonic oscillator, exemplified by a mass on a spring, which obeys Hooke's law. For linear oscillators, the solution is a simple one of normal modes. However, Winfree realized that for biological systems, the coupling must be nonlinear. Capable of consuming energy, a biological oscillator is best described as a self-sustained oscillator with stable limit cycles — which means it can cycle at any amplitude, not just at those described by a fixed harmonic or anharmonic function. Winfree's general framework is adequate in describing many pulse-like interactions, e.g. between fireflies, crickets or neurons, as well as the regulation of the menstrual cycle via a constant adjusting of pheromones.

For simplicity, Winfree made a mean-field approximation, and assumed all oscillators in the population have the same phase response function as well as the same influence on the mean-field. He allowed for heterogeneity in the population by giving the oscillators Gaussian distributed intrinsic frequencies. Winfree was the first to realize that the widths of these Gaussian frequency distributions determine how well the population will synchronize to a large degree. He discovered during this inquiry that the synchronization transition, like phase transitions in thermodynamics, e.g. from liquid to solid, was sudden and not gradual. Therefore he deduced the existence of a critical transition and an accompanying critical parameter, which corresponded to either the degree of heterogeneity, or the strength at which the oscillators were coupled. This was an important step that connected the area of biological coupling to the behavior of molecules in the area of thermal physics.

The Winfree model is

$$\dot{\varphi}_j = \omega_j + G(\varphi_j)\frac{\varepsilon}{N}\sum_{k=1}^{N} F(\varphi_k) \ , \tag{2.4}$$

where φ_j is the j-th oscillator's phase, $j = 1, 2, ..., N$, indicating its position on the limit cycle, and ω_j is its intrinsic frequency. ε is the coupling strength. Winfree found that with different combinations of the *phase response function* (or in his terminology "sensitivity function") $G(\varphi_j)$, and the influence function $F(\varphi_k)$, which describes how the other oscillators k, $k = 1, 2, ..., N$, act to pull or push the observed frequency

other chemical receptors. In order to function, the heart must always be coupled to external signals and is therefore always "perturbed".

of oscillator j, completely different behaviors could arise. In some cases the phases stay completely apart on their limit cycles and the system is dominated by apparent incoherence, while in other cases the phases stuck more or less together, exhibiting some degree of synchronization. As we will see in Sec. 2.2.3, Kuramoto later greatly simplified Winfree's description of the interaction to obtain the same observation for the synchronization transition, and even with an analytical solution of the critical transition at the infinite system size limit.

2.2.2 Topology of the Coupling Connection

The most direct way of conceptualizing coupled oscillator system is by placing them in a network (or a hypernetwork topology where oscillator simplexes are concerned, e.g. see Ref. [SA19] as well as a partially integrable model in Sec. 3.2.1). If two or more oscillators are connected to each other via an edge (or simplex), they are considered coupled to each other. There are mainly two ways the edges in a network (or the connection between nodes) can be established. The connections can be based on the existence of physical connections, such as a nation's electric grid, where electric generators are physically connected to each other and to the users. In cases where the exact physical connections are hard or difficult to ascertain through direct imaging or measurements (such as those between biological cells or neurons), the coupling connections can be established based on mutual information, or cross-correlation between time series [BM+16]. The latter technique is well established in recent years in the area of computational neuroscience in terms of brain functional connectivity [BS09; Lyn+10], as well as in bio-informatics in terms of genetic regulatory networks [SH01; ZSD06; ZSD08]. On a network of oscillators where every sub-unit is connected to and is influenced by every other sub-unit, the network is called an *all-to-all network* or fully connected network, and we call the coupling a *global coupling* of the units.

Theoretical treatment of the complex interaction of oscillatory units on a network — especially in terms of the reduction of many-body dynamics to a mean-field dynamics — is possible under certain limit or assumptions. Fortunately, the assumptions required in many cases are general enough that they allow for a theory to be applied as a first-order approximation to the true dynamics. For example, parts of the brain network are very densely connected, so at least in a small region of the brain, the neuronal connections can be approximated by those on a fully connected network [Cha+17].

Currently, mean-field or quasi-mean-field theories such as OA or WS require certain symmetries in the networks (see Sec. 1.1.2 for references). For this reason, symmetrical topologies will be for the most part assumed in this thesis. The topologies which allow the mean-field dynamics reduction via either WS or OA theory are: fully-connected graphs, scale-free graphs [BAO11; Cou+13; Yoo+15; Lop+16], star graphs [VZP14], and other random networks [Cou+13; Lop+16]. Throughout this thesis, we mostly focus on fully-connected graphs, although the theories used can be easily generalized to scale-free or star graphs within their designated limits of assumptions and regimes.

An extension of the mean-field reductions to more general networks is possible. For example, Ref. [HFB18] discussed how the ansatz used by theoreticians might not always adhere to the data, but modified version(s) of it could (even though one should also take care of the convergence property of the macroscopic variables with an alternative ansatz [GD19]). In cases of heterogeneous networks, one can apply a heterogeneous mean-field such as in Ref. [Ves11], making a mean-field approximation

within each degree class, that is, a class of all the oscillators that are connected to the same number of neighbors on a network.

2.2.3 Mean-Field Theory and the Kuramoto Model

A mean-field formulation is a formulation for an N-body model under which each individual oscillator can be thought of as being coupled to a mean-field, which in turn is a function of the states of all the oscillators. For oscillators, the most famous mean-field model — **the Kuramoto model** [Kur75; SK86] — has a canonical status after its more than 40 years of history. It is a model of an all-to-all coupled ensemble of phase oscillators, with each oscillator represented by a scalar variable — its phase.

Kuramoto's original intention was to devise a model for coupled biological oscillators such as those proposed by Winfree (Sec. 2.2.1), but for which there is an analytically solvable transition to synchronization (unlike the Ising model for ferromagnetism, whose transition is analytically unsolvable). Kuramoto accomplished this, at least in the infinite system size limit, or the *thermodynamic limit*, by choosing an all-to-all coupling topology with a first-order harmonic coupling function. That is, the coupling term between two interacting oscillators is proportional to the sine or cosine function of the difference of two phases. The oscillator coupling is global, i.e., averaged over all pairs of interactions in an ensemble of N oscillators

$$\dot{\varphi}_j = \omega_j + \frac{\varepsilon}{N}\sum_{k=1}^{N}\Upsilon(\varphi_k - \varphi_j) \ , \tag{2.5}$$

where $j = 1, 2, ..., N$, and the coupling function Υ is

$$\Upsilon(\varphi) = \sin(\varphi) \ . \tag{2.6}$$

ω_j is the j-th oscillator's natural frequency as an autonomous oscillator. (For infinite-sized Kuramoto model, see Sec. 6.1.) Equation (2.5) can be written in a mean-field representation

$$\dot{\varphi}_j = \omega_j + \varepsilon \mathrm{Im}\left[Z(t)e^{-i\varphi_j(t)}\right] = \omega_j + \varepsilon R(t)\sin[\Theta(t) - \varphi_j(t)] \ , \tag{2.7}$$

where the complex Kuramoto mean-field Z , $Z \in \mathbb{C}$, is

$$Z(t) = R(t)e^{i\Theta(t)} = \frac{1}{N}\sum_{k=1}^{N} e^{i\varphi_k(t)} \ . \tag{2.8}$$

The mean-field nature of the model is apparent from the form in Eq. (2.7). Each oscillator seems to be "uncoupled" from all the other ones and is only coupled to the mean-field Z, which is an average of the complex exponential of the phases over the entire ensemble. Since the effective strength of the coupling is proportional to the degree of coherence $R(t)$, the model includes a positive feedback loop between coupling and coherence. Namely, when the population becomes more coherent and synchronized, R increases, and so does the effective coupling strength. This leads to the oscillator being coupled more strongly, which in turn leads to more coherence. When $R = 1$, the system is said to be in full synchrony — meaning all oscillators are in phase. When $R = 0$, the system is in complete asynchrony — meaning they are completely out of phase, or decoherent, and their mean-field has zero amplitude, which exerts zero influence on individual oscillators.

The main result of Kuramoto's mean-field analysis is that, for a uni-modal and symmetric natural frequency distribution $g(\omega)$, and assuming the order parameter R and mean-phase Θ are constant (meaning the oscillators are now effectively decoupled, and only coupled to the constant mean-field Z), the model returns essentially a form of Adler equation

$$\dot{\tilde{\phi}}_j = \omega_j - \varepsilon R \sin \tilde{\phi}_j \ ,$$

where $\tilde{\phi}(t) = \varphi(t) - \Theta$. This shows that the population is separated exactly into one locked region and two drifting regions depending on the relation between frequency $|\omega_j|$ and the value of εR (see also Fig. 2.2 and Sec. 2.2). At steady state, one can add together the centroid (the mean of the first harmonics) of the locked oscillators and the centroid of the drifting oscillators, which together contribute to an order parameter value R'. For the model to be self-consistent, R' must by definition be the same as R. Having obtained the self-consistency equation, Kuramoto derived the critical coupling strength ε_{cr} from the bifurcation of the partially synchronized solution.

For identical oscillators, the synchronization picture is much simpler, because the intrinsic frequencies $\omega_j = \omega_0$ is common to all oscillators. The coupling of the identical oscillators is fully described by the WS partial integrable theory [WS94; PR15a; Gon+19], which reduces N-body dynamics to low-dimensional quasi-mean-field dynamics. There are only two possible end states: either under attractive coupling all oscillators are synchronized, or under repulsive coupling (or if they have initially zero mean-field such that they will not evolve at all) all oscillators are completely decoherent. We can set coupling strength $\varepsilon = 1$ without loss of generality, since it is simply equivalent to rescaling time.

A summary of the known result of Kuramoto-type mean-field models is as follows. For non-identical oscillators, R usually takes a value between 0 and 1, because not all the oscillators lie within the synchronizable group. Only those with natural frequencies that lie within a detuning range from the average rotational frequency of the ensemble are entrained by the mean-field, while the other ones outside this range are freely rotating. For identical oscillators, only $R = 0$ or $R = 1$ are possible at steady states according to the WS theory, allowing for one *solitary state* [MPR14], where only one oscillator with a different phase exists apart from the fully synchronous cluster. We show in this thesis that this result can be generalized to higher-mode coupling. Namely, that for pure higher-mode coupling, a possible steady state is either the completely incoherent state, or multi-cluster states where the number of clusters is smaller or equal to the mode number. As in first-order coupling, there still could exist solitary states, but now instead of one oscillator, there can be multiple ones corresponding to the multiple singular points of the dynamics. See also Sec. 3.1.

2.2.4 Attractive vs. Repulsive Coupling

An important constant parameter which was later added to the Kuramoto model, is the *phase shift parameter* (sometimes called "phase lag") [SK86], which we call α, $\alpha \in [0, 2\pi)$. α enters into the model as a constant phase shift to the mean-field phase $\Theta(t) = \arg[Z(t)]$

$$\dot{\varphi}_j = \omega_j + \frac{\varepsilon}{N} \sum_{k=1}^{N} \sin(\varphi_k - \varphi_j + \alpha) = \omega_j + \varepsilon \mathrm{Im}[H(t) e^{-i\varphi_j})] \ , \tag{2.9}$$

where the forcing term

$$H(t) = e^{i\alpha}\frac{1}{N}\sum_{k=1}^{N} e^{i\varphi_k(t)} = Z(t)e^{i\alpha} = R(t)e^{i[\Theta(t)+\alpha]} \tag{2.10}$$

is equal to mean-field $Z(t)$ rotated by a constant phase angle α. The phase shift parameter α parametrizes the degree of repulsion and attraction in the coupling term. In particular, when $\alpha = 0$, the coupling between the oscillators is purely attractive, when $\alpha = \pi$, it is purely repulsive, and when $\alpha = \pi/2$ the coupling is neutral — it is neither attracting, nor repelling.

When the common coupling force is not the Kuramoto mean-field, but is simply a generic global forcing field $H(t)$, it is called the **Kuramoto-Sakaguchi model** [SK86].

2.2.5 Coupling via Higher-Mode of Phase

Daido [Dai92; Dai93; Dai95] introduced the idea that the phase coupling function can be generalized to a Fourier series of phase differences, and with it he introduced the concept of *Kuramoto-Daido mean-fields* (a.k.a. *Kuramoto-Daido order parameters*)

$$Z_l = \frac{1}{N}\sum_{k=1}^{N} e^{il\varphi_k} \ , \tag{2.11}$$

where $l \in \mathbb{Z}$ is the mode number.

Phases coupled via a pure higher-mode with mode number l usually "self-organize" to form l clusters (although cluster numbers smaller than l are also possible depending on initial conditions, see the example in Sec. 3.2.5). If these l clusters have spatial symmetry, e.g. an anti-phase 2-cluster state under second-harmonic coupling (see Fig. 2.3(D)), then a straight-forward calculation shows that $|Z_l|$ is 1. This is true even if the clusters are not equally sized. Therefore $|Z_l|$ is a good measure of the formation of l-cluster states with spatial symmetry of the clusters (but not necessarily distribution symmetry of the phases) under l-th order harmonic coupling.

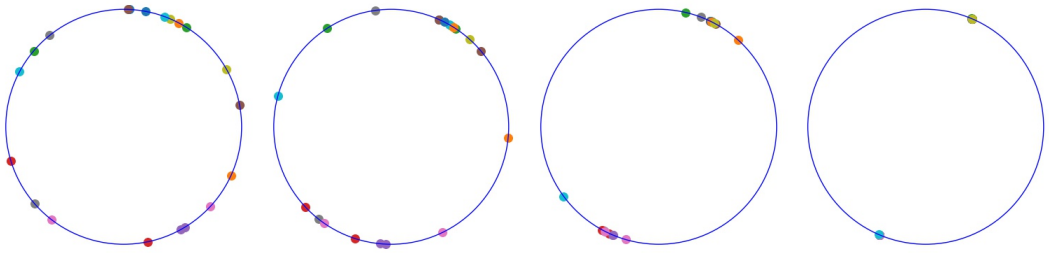

(A) (B) (C) (D)

FIGURE 2.3: From left to right the synchronization of phase oscillators under the Z^2-mean-field model (see Sec. 3.2.1) is depicted. At steady state two clusters are formed at the opposite sides on the unit circle (anti-phase). 20 initial phases are drawn randomly from a uniform distribution from 0 to 2π.

2.3 Coupling with External Stochasticity

2.3.1 Common Noise as a Synchronizing Effect

When an oscillator experiences a force which is randomly fluctuating in time, the dynamics becomes stochastic. Depending on the source of such fluctuations, as well as on the nature of the noise, it often plays a decisive role in determining the system's long term behavior. Units which have inherent noisy dynamics can usually be treated as a coupled ensemble with *individual noise* (or "uncommon noise", "intrinsic noise" in the literature). Under external noisy forces, the coupled units can be treated as an ensemble under the influence from *common noise* — that is, the fluctuating force is common to all of the oscillator phases, so every phase experiences the same random kick at any given time.

Intuitively, noise should destroy order or coherence in a collective dynamics. However, an ensemble of coupled or uncoupled phase oscillators under the influence of weak and common noise will experience only a synchronizing effect. The "weakness" of the noise is relative to the strength of the coupling. The synchronizing effect of common noise on either coupled or uncoupled oscillators is well known since the 80s, usually demonstrated by the calculation of Lyapunov exponents [Pik84; PRK01; GP04; GP05; NK10; Pim+16], also known as *noise-induced synchronization*.

Mathematically, there are several ways of introducing stochasticity into coupled Kuramoto-type or uncoupled limit-cycle phase oscillator models (see Sec. 1.1.2). For uncoupled oscillators, Refs. [GP04] and [GP05] gave a stability analysis of the models with general multiplicative noise (one or more terms). By one-term multiplicative noise we mean a model in which the time derivative of phase linearly depends on one arbitrary 2π-periodic function of the phase $f(\varphi)$ multiplied with a random real Gaussian variable $\eta(t)$ fluctuating in time

$$\dot{\varphi} = 1 + f(\varphi)\eta(t) \ . \tag{2.12}$$

Multiple such terms result in a model

$$\dot{\varphi} = 1 + \sum_{m}^{M} \sigma_m f_m(\varphi)\eta_m(t) \ , \tag{2.13}$$

with a special case with two noise terms where $f_1 \propto \sin(\varphi)$ and $f_2 \propto \cos(\varphi)$ discussed for uncoupled oscillators in Ref. [GP04]. M here is the total number of noise terms, each indexed by m.

In general, weak common noise, either of the additive or multiplicative type, has phase-synchronizing effects on the oscillators, regardless of individual dynamics or initial phase distribution. This has been shown by Ref. [TT04], where together with uncommon additive noise, common multiplicative noise causes intermittent phase slips (phase slips are known to occur for strong unbounded noise such as Gaussian noise)[5]. Individual additive noise alone usually shows desynchronizing tendencies [TT04; NYK12]. In this sense, it is similar to the effect of dissimilarity of the natural frequencies of the oscillators which is a source of heterogeneity that acts against collective synchronizing tendencies.

[5]For the concept of phase slips, see Sec.7.1.7 of [PRK01].

2.3.2 Linear Stability

Given a stochastic dynamics, the microscopic variables, such as individual phases, as well as the macroscopic variables, such as the mean coherence and mean phase of the ensemble, are constantly fluctuating. However, we can still answer the question of stability of the system at certain macroscopic states via the Fokker-Planck equation combined with the standard technique of Lyapunov exponents.

The *Fokker-Planck equation* is a frequently employed technique in calculating the distribution of the fluctuating macroscopic variable in a stochastic system[6]. Similarly it is employed in coupled or uncoupled oscillator models with stochasticity. The Fokker-Planck equation was first used by Fokker and Planck [Fok14; Fok17] to describe the Brownian motion of particles. In general, for an N-dimensional stochastic process $\mathbf{X}$ with multiple noise terms, indexed m for each term

$$d\mathbf{X}(t) = \bar{\boldsymbol{f}}(\mathbf{X}(t), t)\, dt + \sum_m \bar{\boldsymbol{g}}_{\boldsymbol{m}}(\mathbf{X}(t), t)\, dW_m(t) \ , \tag{2.14}$$

where $W_m(t)$ is a Wiener process (i.e. Brownian motion)[Ris96]. To avoid confusion with the frequency distribution function $g(\omega)$ we use $\bar{f}$ and $\bar{g}$ as general functions instead. The stochastic differential equation corresponding to Eq. (2.14) is

$$\dot{\mathbf{x}} = \bar{\boldsymbol{f}}(\mathbf{x}, t) + \sum_m \bar{\boldsymbol{g}}_{\boldsymbol{m}}(\mathbf{x}, t)\eta_m(t) \ , \tag{2.15}$$

where $\{\eta_m\}$ are Gaussian variables with zero mean and correlation functions proportional to the δ function. It is usually normalized such that

$$\langle \eta_m(t) \rangle = 0, \qquad \langle \eta_m(t)\eta_{m'}(t') \rangle = 2\delta_{mm'}\delta(t - t') \ . \tag{2.16}$$

The Fokker-Planck equation [Ris96] which describes the evolution of the probability distribution function $p(\mathbf{x}, t)$ of the state $\mathbf{x}$ is then [7]

$$\begin{aligned} &\frac{\partial p(\mathbf{x}, t)}{\partial t} \\ &= -\sum_{j=1}^{N} \frac{\partial}{\partial x_j} \left[\bar{f}_j(\mathbf{x}, t)\, p(\mathbf{x}, t) \right] + \frac{1}{2} \sum_{m=1}^{M} \sum_{j=1}^{N} \frac{\partial}{\partial x_j} \left\{ \bar{g}_{jm}(\mathbf{x}, t) \sum_{k=1}^{N} \frac{\partial}{\partial x_k} \left[\bar{g}_{km}(\mathbf{x}, t)\, p(\mathbf{x}, t) \right] \right\} \ , \end{aligned} \tag{2.18}$$

where j and k are both dimensional indices of $\mathbf{x}$, and $p(\mathbf{x}, t)$ is the probability distribution of the microscopic variables $\mathbf{x}$ at time t. From the Fokker-Planck equation, we look for its stationary solution which gives us the stationary probability distribution

[6] Besides the Fokker-Planck equation, the Boltzmann equation and the master equation have also been used for describing macroscopic variables in stochastic systems. The Fokker-Planck equation is usually used for smaller systems, as when the system is large enough deterministic treatment is often sufficient [Ris96].

[7] The Fokker-Planck equation can be also written in the form

$$\frac{\partial p(\mathbf{x}, t)}{\partial t} = -\sum_{j=1}^{N} \frac{\partial}{\partial x_j} \left\{ [\bar{f}_j(\mathbf{x}, t) + S_j(\mathbf{x}, t)] p(\mathbf{x}, t) \right\} + \sum_{j=1}^{N} \sum_{k=1}^{N} \frac{\partial^2}{\partial x_j\, \partial x_k} \left[D_{jk}(\mathbf{x}, t) p(\mathbf{x}, t) \right] \tag{2.17}$$

where $D_{jk}(\mathbf{x}, t) = \frac{1}{2} \sum_{m=1}^{M} \bar{g}_{jm}(\mathbf{x}, t)\bar{g}_{km}(\mathbf{x}, t)$ and $S_j(\mathbf{x}, t) = \frac{1}{2} \sum_{k,m} \bar{g}_{km}(\mathbf{x}, t)\partial_{x_k}\bar{g}_{jm}(\mathbf{x}, t)$ is the Stratonovich shift (see Appendix A). Equation (2.17) can be shown straightforwardly to be the same as Eq. (2.18).

function $P_{st}(\mathbf{x})$ of $\mathbf{x}$. The stationary solution is found by letting the probability flux — the time derivative of the phase's probability density — equal to a constant.

The *Lyapunov exponents* are a standard measure of the convergence (stability) and divergence (instability) properties of infinitesimally close dynamical trajectories in the area of nonlinear dynamics. In phase space, if nearby trajectories converge along some directions, the Lyapunov exponent along this direction is negative, whereas divergence corresponds to positive Lyapunov exponent. Furthermore, the absolute value of the Lyapunov exponent characterises the rate of convergence or divergence. Neutral stability (neither converging nor diverging but only shifting along the direction of interest) corresponds to a zero Lyapunov exponent. For example, for a limit cycle the Lyapunov exponent is 0 in the tangential direction to the limit cycle. For an unstable limit cycle, there exists a positive Lyapunov exponent in the transversal direction to it, and for a stable limit cycle, the Lyapunov exponent in the transversal direction is negative.

For simplicity, the Lyapunov exponent of a given state of a one-dimensional random variable x under white noise is equal to the average change of the logarithm of an infinitesimal perturbation δx (see Sec. 9.2.2 of [PRK01] for derivation). The average is usually expressed by an integral of the stationary probability density function $P_{st}(x)$ of variable x — derived from Fokker-Planck equation (2.18) — multiplied with $d\ln(\delta x)/dt$, which is obtained by linearizing the SDE.

In previous literature there have been several examples using Lyapunov exponents to determine the stability of cluster states of Kuramoto oscillators under common Gaussian white noise. For example, to quantify the degree of stability of a fully synchronous cluster, the transversal Lyapunov exponent (a.k.a. "evaporation" or "split Lyapunov exponent" [Pim+16]) is calculated, which describes the evolution of oscillator phases slightly deviated from the cluster. The transversal Lyapunov exponent is these test phases' average exponential rate of approach towards a cluster (or the rate of moving away from the cluster if the exponent is positive).

2.4 Chimera States of Non-Locally Coupled Identical Oscillators

While non-identical oscillators are known to exhibit complex phenomena including frequency locking, phase synchronization, partial synchronization, and complete asynchrony, identical oscillators were thought to only be able to form steady states that are either coherent or completely incoherent — that is, at least before the discovery made by Kuramoto and Battogtokh [KB02] in 2002. They connected identical oscillators placed on a ring with identical non-local (or "non-global") connections and phase lag (see Sec. 2.2.4), and found that for certain initial conditions, oscillators with identical intrinsic frequency which are connected to others identically behave in drastically dissimilar ways. This is the first existence of a special state called *chimera*. According to Abrams and Strogatz [AS04], a chimera state is a spatio-temporal pattern occurring in systems of identical oscillators, where the population splits into coexisting coherent (phase synchronized and frequency locked) and incoherent (drifting, asynchronous) regions. Oscillators are said to be non-locally coupled (see Fig. 2.4), when they are only connected to a number of their spatial or topological neighbors (i.e., not all-to-all connected). Non-local coupling, together with non-zero phase-lag is required to induce chimera states. Chimera is not limited to phase oscillator model like the Kuramoto oscillators. It has also been observed in coupled amplitude oscillators such

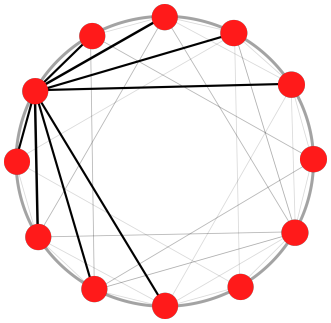

FIGURE 2.4: An example of non-local coupling on a ring. On this ring, each node is connected to its eight neighbors. We call such a connection configuration "non-local", because it is neither a local coupling, where each oscillator on a node is connected only to its two nearest neighbors on the ring, nor is it an all-to-all coupling, where every oscillator is connected to every other oscillator.

as Stuart-Landau oscillators [BPR10], and even real-world mechanical oscillators like coupled metronomes [Mar+13].

In the subsequent years, researchers have found out that chimera states are stable at the thermodynamic limit when the system is infinite. However, in finite systems, a chimera state is not attracting or stable, but is merely a very long-lived transient state. The basins of attraction for chimera states are normally smaller than that of the fully synchronous state, but chimeras are robust against many types of perturbations, as well as able to occur in many types of coupling topologies. Chimeras are robust enough to have been observed in experiments [TNS12; Mar+13; Sch+14].

Even though Ref. [KB02] has shown the chimera state to be self-consistent, the exact mechanism through which the asymmetry of the initial conditions gives rise to the chimera state is not clear. However, as we show in this thesis, the asymmetry in the initial conditions could give rise to asymmetrical clustering for identical oscillators coupled via pure high-order harmonics. It is not known whether these two "symmetry-breaking" phenomena are connected.

Part II

THEORETICAL FINDINGS AND NUMERICAL EXPERIMENTS

Chapter 3

Low-Dimensional Dynamics of Globally Coupled Identical Phase Oscillators

Globally coupled identical oscillators can be seen as a minimal model for coupled nonlinear oscillator models in general. Despite its simple mathematical description, it can demonstrate a host of different spatial configurations from various underlying structural complexity: complete synchrony, where all phases are synchronized, partial synchrony (a nontrivial continuous distribution of phases, where all individual phases can be different, including the evolution towards fully synchronized state) [RP07; PR09], clusters [Dai92; Dai93; Dai95], chimeras [MPMA16], and solitary states [MPR14].

Recent advance in theoretical understanding, namely WS theory, points to a low-dimensional underlying quasi-mean-field dynamics which can explain the various phenomena observed from different parameters and initial conditions. In this chapter, first, in Sec. 3.1, we introduce the WS theory and extend the theory to include pure higher-mode coupled models. Then we give an analytical and numerical example of such higher-order models in Sec. 3.2, and discuss new phenomena not seen in first-order models.

3.1 Watanabe-Strogatz Theory of Partial Integrability

3.1.1 WS Theory for the Kuramoto-Sakaguchi Model

In 1994, in modelling arrays of N identical overdamped Josephson junctions, Watanabe and Strogatz [WS94] showed that such a system has hidden low-dimensional dynamics, for which $N-3$ constants of motion exist. This theory, which we shall call the WS theory, is applicable to N-dimensional dynamics of a system of identically driven identical phase oscillators described by

$$\dot{\varphi}_j = \omega(t) + \mathrm{Im}[H(t)e^{-i\varphi_j}], \quad j = 1, \ldots, N \ , \tag{3.1}$$

where $\omega(t)$ and $H(t)$ are arbitrary real and complex-valued functions of time, respectively. When ω is a constant, it represents the common natural frequency of the oscillators. When $H(t) \sim Z(t)$, $Z(t)$ the Kuramoto mean-field, this system corresponds to the Kuramoto-Sakaguchi model of globally coupled identical oscillators.

A coordinate transformation $\mathcal{M}_1$ is central to the WS theory (see Refs. [WS94; MMS09] for a detailed presentation). $\mathcal{M}_1$ formally belongs to the class of Möbius maps (or Möbius groups). Möbius map is a type of fractional linear transformation mapping the unit circle in the complex plane to itself in a one-to-one way. Explicitly,

the time-dependent Möbius transformation and its inverse[1] can be written as

$$\mathcal{M}_1 : \psi_j \to \varphi_j(t), \quad e^{i\varphi_j(t)} = \frac{\tilde{z}(t) + e^{i(\psi_j + \tilde{\alpha}(t))}}{1 + \tilde{z}^*(t)e^{i(\psi_j + \tilde{\alpha}(t))}} \,, \tag{3.2}$$

$$\mathcal{M}_1^{-1} : \varphi_j(t) \to \psi_j, \quad e^{i\psi_j} = e^{-i\tilde{\alpha}(t)} \frac{\tilde{z}(t) - e^{i\varphi_j(t)}}{\tilde{z}^*(t)e^{i\varphi_j(t)} - 1} \,. \tag{3.3}$$

Here $\{\varphi_j\}$ are the phases of the oscillators, the complex parameter $\tilde{z}(t)$ satisfies $|\tilde{z}(t)| \leq 1$ (in closed unit disk), and the parameter $\tilde{\alpha}(t)$ is a rotation angle, $\tilde{\alpha}(t) \in \mathbb{R}$. To distinguish from later use of z in Ch. 4 and Ch. 6, we use $\tilde{z}(t)$ here. Similarly we use $\tilde{\alpha}$ here to distinguish from the phase shift α. If the phases evolve according to Eq. (3.1) and the WS parameters $\tilde{z}$ and $\tilde{\alpha}$ evolve according to

$$\begin{cases} \dot{\tilde{z}} &= i\omega(t)\tilde{z} + \frac{1}{2}H(t) - \frac{1}{2}H^*(t)\tilde{z}^2, \\ \dot{\tilde{\alpha}} &= \omega(t) + \mathrm{Im}[\tilde{z}^* H(t)] \,, \end{cases} \tag{3.4}$$

then the transformed phases $\psi_j = \mathcal{M}_1^{-1}(\varphi_j(t))$ are conserved quantities ("constants of motion"). Thus, WS theory implies partial integrability of the system of identical oscillators. Equation (3.4) can be shown to be a Riccati equation, and its integrability follows from the transformation of the Riccati equation to a linear form [Goe95; Che17].

Under the Möbius transform Eq. (3.2), constants ψ_j are rotated by the time-varying angle $\tilde{\alpha}(t)$ and then contracted along the circle into the direction of $\arg[\tilde{z}(t)]$, the degree of contraction controlled by $|\tilde{z}(t)|$ (see also a visualization of second harmonic example in Fig. 3.3). In fact, akin to the Kuramoto order parameter $|Z|$, $|\tilde{z}|$ can typically be used as a measure of synchronization, since both parameters become equal to unity at full synchrony.

The Möbius transformation (3.2) is inspired from a transformation between two representations of orbital angular position in celestial mechanics, namely the true anomaly and the eccentric anomaly, for a given eccentricity (see Fig. 3.1 left). From this geometric point of view, it transforms between a unimodal distribution and a uniform one (see Fig. 3.1 right). The unimodal distribution corresponds to the distribution of phases being synchronized, and the uniform one, which stays uniform, corresponds to the constants of motion.

The astrophysical transformation (as shown at the top of left figure of Fig. 3.1) differs from the form we use throughout the thesis Eq. (3.2) [2], but qualitatively they are the same. To illustrate how WS theory essentially reduces an N-body dynamics to a low-dimensional one using a geometric "trick", we look at how the Möbius transform turns an equidistant set of phases into a discrete unimodal distribution in Fig. 3.1 right panel, under an idealised situation where $\tilde{\alpha} = 0$ and $\arg(\tilde{z})$ is constant. As the

[1] Distinguishing forward and inverse transformations is rather arbitrary; here we just use one possible formulation.

[2] The original Möbius transformation as used by Ref. [WS94], is the same one as used in celestial mechanics

$$\tan(\frac{\psi_j + \tilde{\alpha}(t)}{2}) = \sqrt{\frac{1 + |\tilde{z}(t)|}{1 - |\tilde{z}(t)|}} \tan(\frac{\varphi_j(t) - \arg[\tilde{z}(t)]}{2}) \,, \tag{3.5}$$

whereas the transform Eq. (3.2) used in the rest of the thesis is equivalent to

$$\tan(\frac{\psi_j + \tilde{\alpha}(t)}{2}) = \frac{1 + |\tilde{z}(t)|}{1 - |\tilde{z}(t)|} \tan(\frac{\varphi_j(t) - \arg[\tilde{z}(t)]}{2}) \,. \tag{3.6}$$

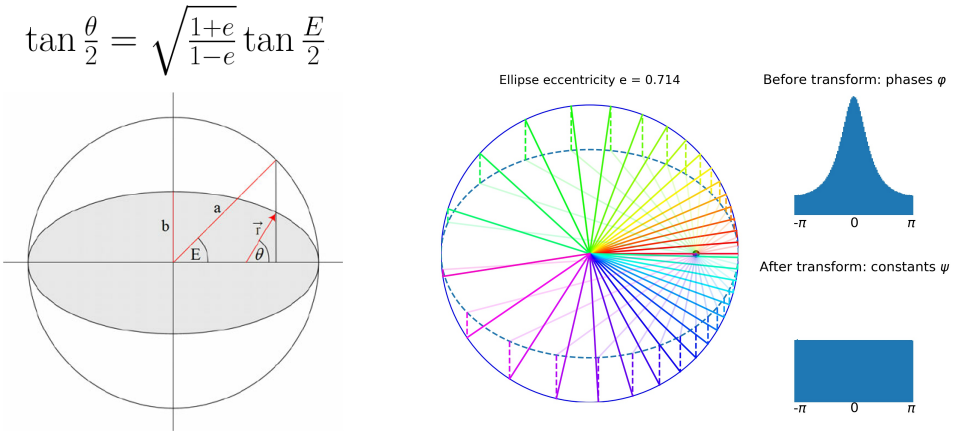

FIGURE 3.1: The equation on the top left shows the original transformation between the true anomaly θ and the eccentric anomaly E (also used by Ref. [WS94]). The eccentricity e, of which the WS parameter $|\tilde{z}|$ plays the role, is the only parameter in the transformation. Right: the transformation between an equidistant set of phases and a unimodal one on the ellipse, under an idealized condition where $\tilde{\alpha}(t) = 0$ and $\arg(\tilde{z})$ is constant. The true anomaly θ corresponds to the constant of motion ψ, whereas the eccentric anomaly E corresponds to the phase φ.

WS parameter $|\tilde{z}(t)|$, which plays the role of eccentricity, increases, the unimodal distribution gets narrower, in alignment with the observation of phases becoming closer together during synchronization. Effectively, the N-dimensional phase dynamics is reduced to only the one-dimensional dynamics of $|\tilde{z}(t)|$. As coherence measured by $|\tilde{z}(t)|$ increases, the eccentricity of the ellipse increases. While the distribution of the true anomaly stays uniform, the distribution of the eccentric anomaly becomes narrower, the values of these angles get closer to their mean value.

Choice of Initial Conditions for the Reduced System

Because we have introduced three extra parameters via the Möbius transform, to make the Möbius transform unique, we must impose the same number of conditions on the new system Eq. (3.4). We have the choice of either imposing three conditions on the constants of motion, or, we can impose conditions on the initial values of the parameters themselves. The conditions themselves are rather arbitrary. In practice however, there are a number of ways of choosing conditions such that the system evolves more "naturally". For the WS reformulation of higher-mode coupled systems (see Sections 3.1.2 and 3.2.2), we focus on the latter option, namely, imposing conditions on the parameters' initial values.

As argued by Watanabe et al. [WS94], the three required constraints are best to be imposed on the initial values of the constants $\{\psi_j(0)\}$ instead of on the initial values of the three reduced variables ρ_0, Φ_0 and $\tilde{\alpha}_0$ (e.g. by letting each of them equal 0), where $\rho = |\tilde{z}|$ and $\Phi = \arg(\tilde{z})$, even though imposing constraints on the latter is also valid. Imposing fixed initial conditions on the reduced variables (Fig. 3.2 (b)) was deemed "unnatural" by Watanabe et al. [WS94]. They argued that under this initial condition, regardless of different initial phases, the starting coordinate of the new system is always the same, while the flow is different. This makes the evolution of the reduced system unnatural.

Among the three constraints proposed by Watanabe et al. [WS94], two of them are significant. The two significant constraints imposed on the Watanabe-Strogatz

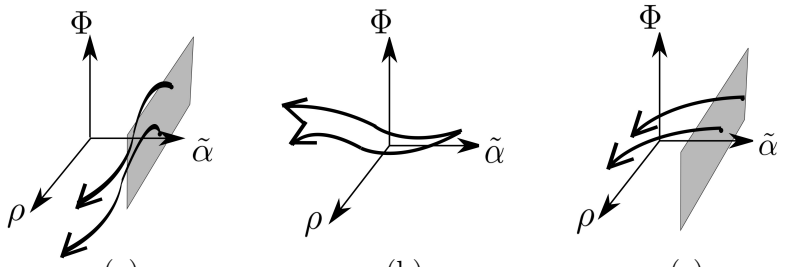

(a) (b) (c)

FIGURE 3.2: Visualizing different ways of imposing constraints on the over-determined system Eq. (3.4) after Möbius transformation. (a) The "incoherent" initial condition Eq. 3.7, suggested by Watanabe et al. [WS94]. (b) The "unnatural" condition suggested by Watanabe et al. [WS94], where the initial values of the three newly-introduced parameters are set to an independent value, serves as a contrast to condition (a). (c) A new set of constraints proposed, where we set the initial condition of the WS order parameter $\tilde{z}(0)$ (or $\zeta(0)$ for the higher harmonic coupling case in Sec. 3.1.2) to be the same as the general forcing term $H(0)$.

constants of motion are described in Ref. [WS94] as:

$$\langle \cos\psi_j \rangle = \frac{1}{N}\sum_{j=1}^{N} \cos\psi_j = 0 \ , \langle \sin\psi_j \rangle = \frac{1}{N}\sum_{j=1}^{N} \sin\psi_j = 0 \ , \tag{3.7}$$

or simply, $\langle e^{i\psi_j} \rangle = 0$, i.e., the centroid of the N constants $\{\psi_j\}$ vanishes. This is defined as the "incoherent" condition (Fig. 3.2 (a)). Under this constraint, the flow is preserved for all dynamical systems, and the starting coordinates in the phase space of the new dynamics are different depending on different initial phases.

However, for the WS reformulation of higher-mode coupled system, we focus on the latter option, namely, imposing constraints on the parameters' initial values. We argue later in the simulation Sec. 3.2.1 this can also be made "natural", which is to say, they can be made dependent on the initial conditions of the phases (see Fig. 3.2 (c)). One crucial difference between Fig. 3.2 (a) and (c), at least as observed in the simulations, is that in (a) for certain initial conditions of phases under attractive coupling, the amplitude ρ will first decrease to 0 then grow to 1, while the angle Φ abruptly changes by π as ρ hits 0. In the complex plane this corresponds to the WS parameter $\tilde{z} = \rho\exp(i\Phi)$ crosses the origin. In (c) such an effect will not happen. In (a) (b) and (c) the starting coordinate lies on a plane with the rotation angle $\tilde{\alpha}(0) = 0$ ($\tilde{\beta}$ for higher-mode cases). The initial value of $\tilde{\alpha}$ has so far been found to have no significant meaning in terms of the behavior of the transformed dynamics, in contrast to the WS order parameter. Setting its initial value therefore becomes truly arbitrary.

3.1.2 Watanabe-Strogatz Equations for Higher-Mode Phase Coupling

As we have seen in Sec. 3.1.1, sine or cosine coupled identical oscillators which are globally connected can be reduced to low-dimension and the system is partially integrable. Perhaps surprisingly, a similar model coupled via pure but arbitrarily higher-order harmonic functions is also partially integrable. Building on the first-order models, we reformulated the higher-order problems using a similar method as employed by Watanabe and Strogatz for first-order coupling in phase.

Model Formulation

First we introduce the higher-mode phase coupled model. We consider a population of N identical phase oscillators with phases $\{\varphi_j\}$, $j = 1, 2, \ldots, N$, subject to a global coupling. Here, unlike in the standard Kuramoto-Sakaguchi model [SK86], the coupling term is purely of an arbitrary higher order l ($l \geq 2, l \in \mathbb{Z}$),

$$\dot{\varphi}_j = \omega(t) + \mathrm{Im}[H(t)e^{-il\varphi_j}] \ , \tag{3.8}$$

where $\omega(t)$ and $H(t)$ are arbitrary scalar and complex functions, respectively. Equivalently we can write Eq. (3.8) as

$$\dot{\varphi}_j = \omega(t) + H_1(t)\sin(l\varphi_j) + H_2(t)\cos(l\varphi_j) \ . \tag{3.9}$$

When ω is constant, it represents the identical natural frequency of the oscillators. While in the problem formulation and theory derivation we write generically $\omega(t)$, in the numerical part we use a constant ω, to be comparable to previous numerical studies in the literature. $H(t)$ represents an arbitrary complex forcing term, which can be dependent or independent of the phases $\{\varphi_j\}$, deterministic or stochastic, and also can be external time-dependent forces. The latter case is not considered in this chapter; see Ch. 5 or Ref. [Gon+19] for exploration of external driving within the scope of the reduced WS theory for the first-order coupling.

Global coupling (a.k.a. "all-to-all" coupling) of the oscillators corresponds to the case where $H(t)$ depends on the Kuramoto-Daido order parameters (mean-fields of the higher modes of phases)

$$Z_l = \frac{1}{N}\sum_{k=1}^{N} e^{il\varphi_k} \ .$$

For simplicity, in the rest of the chapter we use Z_1 and Z interchangeably to denote the Kuramoto order parameter, which is also the first Kuramoto-Daido order parameter.

The simplest example of higher-mode coupling of type Eq. (3.8) is a model of identical phase oscillators globally coupled via the second-order harmonic coupling function of their phase differences:

$$\dot{\varphi}_j = \omega_0 + \frac{1}{N}\sum_{k=1}^{N}\sin(2\varphi_k - 2\varphi_j + \alpha) \ = \omega_0 + \mathrm{Im}(Z_2 e^{i\alpha}e^{-2i\varphi_j}) \ , \tag{3.10}$$

where α is the phase shift parameter, tuning the nature of the coupling between various degrees of attractiveness or repulsiveness (see also Sec. 2.2.4). Here the global forcing term $H(t)$ is just the second Kuramoto-Daido mean-field Z_2 rotated by the phase shift α.

This system is trivial to solve due to its similarity with the Kuramoto model, with phases φ now replaced by 2φ and everything else remaining the same (Ref. [Del19] has shown that they are fully equivalent). Below we focus on more complex models, where $H(t)$ is a generic function of order parameters, which satisfies the phase shift invariance property (i.e., under $\varphi \to \varphi + \text{const.}$ the dynamics are the same). In particular, the complex forcing can take any form such as $(Z_{\bar{q}})^{\bar{m}}(Z^*_{\bar{p}})^{\bar{n}}$, with $\bar{m}\bar{q} - \bar{p}\bar{n} = l$, or a combination of these terms, where $\bar{m}, \bar{q}, \bar{p}, \bar{n}$ are integers. So for example, for $l = 2$ one can have $H(t) \sim Z_2$ like in Eq. (3.10), but also $H(t) \sim Z^2$ like in Ref. [KP15], or, e.g., $H(t) \sim Z_4 Z_2^*$.

Derivation of the Reduced System

We now demonstrate that the WS theory can be generalized easily to higher-mode coupling of the general form of Eq. (3.8), using derivation extremely similar to those outlined in Ref. [PR15a]. Due to the algebraic similarity, we only sketch out a general idea, and leave the details to be inferred from Ref. [PR15a].

N phase oscillators coupled via higher-modes obey the general equations of motion Eq. (3.8). It can be rewritten as

$$\frac{d}{dt}(e^{il\varphi_j}) = ile^{il\varphi_j}\omega(t) + \frac{l}{2}\left[H(t) - H^*(t)e^{2il\varphi_j}\right] \ . \tag{3.11}$$

We transform the phases φ_j into phases ϑ_j via Möbius transform

$$e^{il\varphi_j} = \frac{\zeta + e^{i\vartheta_j}}{1 + \zeta^* e^{i\vartheta_j}} \ , \tag{3.12}$$

with an additional complex parameter ζ, $\zeta \in \{\mathbb{D} \cup \mathrm{S}^1\}$ is in the closed unit disk. Equations (3.11) can be transformed in terms of $\{\vartheta_j\}$, ζ and their time derivatives $\{\dot{\vartheta}_j\}$ and $\dot{\zeta}$. Going through a similar procedure of picking out terms in the orders of $e^{i\vartheta_j}$ as done in Ref. [PR15a], we obtain

$$\begin{cases} \dot{\zeta} = l\left[i\omega(t)\zeta + \frac{1}{2}H(t) - \frac{1}{2}H^*(t)\zeta^2\right] \ , \\ \dot{\vartheta}_j = l\left\{\omega(t) + \mathrm{Im}[H(t)\zeta^*]\right\} \ , \end{cases} \tag{3.13}$$

which satisfy all N transformed equations, and hence also the N original equations (3.8). We notice that the right-hand side of the second equation of Eqs. (3.13) is independent of oscillator index j, indicating that all the angles $\{\vartheta_j\}$ rotate at the same speed. Therefore, we can create a new time-dependent parameter $\tilde{\beta}$, $\tilde{\beta} \in \mathbb{R}$, which has the same rotational speed as $\{\vartheta_j\}$, $\dot{\tilde{\beta}} = \dot{\vartheta}_j$, and define

$$\tilde{\beta}(t) := \vartheta_j(t) - \psi_j \ , \tag{3.14}$$

where $\{\psi_j\}$ are the constants of motion.

We thus come to the Möbius transformation from constants ψ_j to phases φ_j

$$\mathcal{M}_l : \psi_j \to \varphi_j(t), \quad e^{il\varphi_j(t)} = \frac{\zeta(t) + e^{i\vartheta_j(t)}}{1 + \zeta^*(t)e^{i\vartheta_j(t)}} = \frac{\zeta(t) + e^{i[\psi_j + \tilde{\beta}(t)]}}{1 + \zeta^*(t)e^{i[\psi_j + \tilde{\beta}(t)]}} \ , \tag{3.15}$$

depending on the time-dependent WS variables $\zeta(t), \tilde{\beta}(t)$. The inverse Möbius transformation for higher-mode coupling is

$$\mathcal{M}_l^{-1} : \varphi_j(t) \to \psi_j, \quad e^{i\psi_j} = e^{-i\tilde{\beta}(t)}\frac{\zeta(t) - e^{il\varphi_j(t)}}{\zeta^*(t)e^{il\varphi_j(t)} - 1} \ . \tag{3.16}$$

Compare Eqs. (3.15) and (3.16) to the transform for a first-order coupling Eqs.(3.2) and (3.3), only the original phases are multiplied with the order of coupling l, otherwise the form of the transform stays the same. Comparing the WS equations for the first-order coupling Eq. (3.4) with Eq. (3.13), we find that the equations for pure higher-order harmonic (or "l-harmonic") coupling are merely multiplied by the factor l on the right-hand side.

We can write the equations for the three WS parameters Eq.(3.13) in terms of dot and cross products of $H(t)$ and ζ in the complex plane ($\zeta = \varrho \exp(i\Psi)$, $\varrho \neq 0$):

$$\begin{cases} \dot{\varrho} &= l\frac{1-\varrho^2}{2\varrho} H(t) \cdot \zeta, \\ \dot{\Psi} &= l[\omega(t) + \frac{1+\varrho^2}{2\varrho^2} H(t) \times \zeta], \\ \dot{\bar{\beta}} &= l[\omega(t) + H(t) \times \zeta], \end{cases} \tag{3.17}$$

where parameter Ψ evolves according to $H(t) \times \zeta$, similar to a torque experienced by an object with a magnetic moment under a magnetic field. For the same initial condition, but for a different common forcing $H(t)$, the higher-order quasi-mean-field ζ behaves like a magnet with the same magnetic moment, but now its moves under a different magnetic field $H(t)$.

For a transform of the second-mode coupled model [3]where $l = 2$, we demonstrate in Fig. 3.3 how the WS parameters shape the transform as the parameters are evolved.

3.1.3 Numerical Simulation of the Dynamics in the WS Variables

At first glance, Eqs. (3.17) present an enormous simplification compared to the original model (3.8), as the number of independent variables is reduced from N to 3. However, the difficulty in numerical simulation of the WS equations is that the coupling term $H(t)$ is typically expressed in terms of the original phases via the Kuramoto-Daido order parameters, and not in terms of the WS variables and the constants of motion. Therefore, for each calculation of the right-hand side in Eq. (3.17) one has to perform transformation Eq. (3.15). If the coupling contains only order parameters $Z_{\bar{m}*l}$ with integer $\bar{m}$, then only quantities $\exp(il\varphi_j)$ are needed to compute the coupling term and no transformation step is needed. However, if other order parameters have to be calculated, then one needs to know phases φ_j, which are not uniquely defined through quantities $\exp(il\varphi_j)$. Indeed, one value of a constant ψ maps to l values of the phase variable: $\varphi/l + 2\tilde{n}\pi/l$, where $\tilde{n} = 0, 1, \ldots, l-1$. To choose a proper value, one can use continuity of the dynamics of the phases φ in time. This means, the proper value of the phase at time instant $t + \Delta t$ is the value closest to that at the previous step $\varphi(t)$, for small Δt. In numerical implementations without intermediate steps, like Euler or Adams-Bashforth [BF04] schemes for solving ordinary differential equations, this check is simple. In Runge-Kutta-type schemes, one should also take care that at intermediate calculations of the right-hand side of equations inside a Runge-Kutta step, the proper phase is extracted from the transformation Eq. (3.15).

3.1.4 Basins of Attraction for Clusters

The WS theory implies that a system of globally coupled identical oscillators with an l-harmonic coupling can evolve to at most l clusters at any point in time. Indeed, if the initial phase distribution has no clusters, then all the constants of motion ψ are different. Then, for any $|\zeta| < 1$, all the phases are different as well. The only way for clusters to form is $|\zeta| \to 1$ under attractive coupling.

[3]By the convention in existing literature, Kuramoto-Sakaguchi oscillators refer to those phase oscillators that are coupled via their first-order harmonics, i.e., when $l = 1$. Hence to be consistent, phase oscillators coupled via higher-modes should not be referred to as Kuramoto-Sakaguchi oscillators. Additionally, second-order-harmonic (or more compactly, "higher-mode") coupled models should also be distinguished from "second-order Kuramoto models". The latter type of models involve inertia term, i.e. the second-order time derivatives of phases, and is frequently used in simulations of power grid.

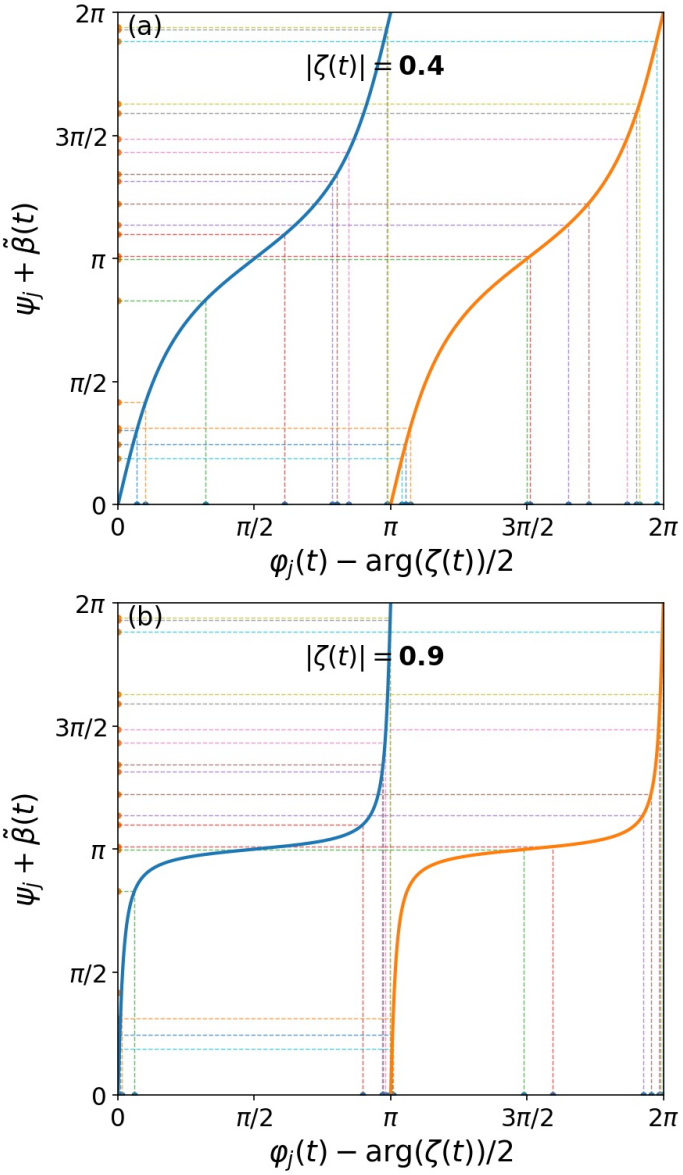

FIGURE 3.3: The Möbius transformation $\varphi_j(t) \leftrightarrow \psi_j$ for the second-mode coupling is visualised for two parameter values of $|\zeta(t)|$. Horizontal axis: phases φ_j are shifted by the parameter $\arg[\zeta(t)]/2$; Vertical axis: constants ψ_j are shifted by the parameter $\tilde{\beta}(t)$. Transforming the same set of constants to the phases results in a more spread out set of phases (panel (a)) for small values of $|\zeta|$, and in a more clustered state of phases for $|\zeta|$ close to one (panel (b)). The two branches of the mapping illustrate the non-uniqueness of $\mathcal{M}_2(t)$. Figure reprinted with permission from Ref. [GP19].

For attractive l-harmonic coupling, in general it is expected that eventually the phases form l clusters, i.e., l distinct attractive subgroups of oscillators (there are special initial states for which this is not true, see discussion in Sec. 3.2.4 below about the solutions in which $|\zeta|$ does not grow). Thus, the circle is divided in l basins of attraction of these clusters. The boundaries of these basins of attraction are hence special points of the collective motion, since they will not be synchronized to any final cluster, and can be described as "unsychronizable" ("solitary states" in the terminology of Ref. [MPR14]). Because basins evolve in time, the boundaries are unstable trajectories of the dynamics on the unit circle. Below we relate these boundaries to the mathematical singularity occurring in the WS formulation of the

system, specifically, to the pole in the Möbius transformation Eq. (3.15).

Because basin boundaries are not trajectories of real oscillator phases, we have to consider the transformation Eq. (3.15) for all possible values of ψ. One can see that this transformation becomes singular at the limit $|\zeta| \to 1$. For $|\zeta| = 1$, all values of ψ are mapped to the cluster states $\varphi = \Psi/l + 2\tilde{n}\pi/l$, where $\tilde{n} = 0, \ldots, l-1$, except for the singular value $\psi_S = \Psi + \pi - \tilde{\beta}$, where $\Psi = \arg(\zeta)$ as defined in Section 3.1.2 . This singular constant is mapped via Eq. (3.15) (at $|\zeta| \to 1^-$ when the map is not singular) to the basin boundaries at the end of the evolution $t \to \infty$: $\varphi_S = \Psi/l + (2\tilde{n}+1)\pi/l$.

In a particular case under $l = 2$ to be explored numerically below, we have two such basin boundary trajectories. At the end of the evolution, at $t \to \infty$, where clusters are formed and $|\zeta(\infty)| = 1$, the boundary points are $\varphi_{S1}(\infty) = \Psi(\infty)/2 + \pi/2$ and $\varphi_{S2}(\infty) = \Psi(\infty)/2 + 3\pi/2$. To find these boundaries at all times, and in particular at the initial moment in time, one can trace these states back in time according to the oscillator dynamical equation, but even that is not necessary. In fact, to find $\varphi_{S1,S2}(t)$, it is sufficient to know the singular value of the constant ψ_S at the final stage of the evolution: $\psi_S = \Psi(\infty) - \tilde{\beta}(\infty) + \pi$. Then, for each $0 \leq t < \infty$, the basins can be calculated according to the transformation Eq. (3.15):

$$e^{2i\varphi_S(t)} = \frac{\zeta(t) + e^{i(\psi_S + \tilde{\beta}(t))}}{1 + \zeta^*(t) e^{i(\psi_S + \tilde{\beta}(t))}} \,. \tag{3.18}$$

At each moment in time the basin boundaries φ_S can be obtained via the above expression using a combination of the corresponding constant of motion ψ_S, as well as the instantaneous transform parameters $\zeta(t)$ and $\tilde{\beta}(t)$. Expression (3.18) also tells us that the sizes of the basins are equal (in the case of $l = 2$, the sizes are π). However, the positions of the basins depend on the final point of integration of both WS variables $\zeta(t = \infty)$ and $\tilde{\beta}(t = \infty)$: thus to find them one first has to perform integration up to large enough time, and only after that formula Eq. (3.18) is applicable. Below we will also discuss an approximate way to define these boundaries solely from the initial state, and will see that even though it does not provide an exact prediction of the clustering, it could predict certain features of the final state of clustering.

3.2 Numerical Example

In this section we numerically simulate a particular model of second-mode coupling which has been studied in previous literature. The approach can be generalized to arbitrary higher-mode phase coupling, and we offer one example with the fifth-order coupling for completeness.

3.2.1 Higher-Mode Coupling Example: Z^2 Mean-Field

As discussed above, for $l = 2$, a coupling scheme via the second Kuramoto-Daido order parameter Z_2 is trivial, because it can be reduced to the standard Kuramoto model. Instead, we can choose a simple nontrivial example, such as a coupling via the square of the first-order mean-field, i.e., $H(t) = Z^2$. This model has appeared in previous literature [KP15], where an ensemble of identical phases at steady state is always found to exhibit a curious strictly non-symmetric two-cluster distribution (or "asymmetrical clustering" in literature), starting from phases drawn randomly from a uniform distribution on the circle. It is "strictly" asymmetric because one cluster always contains more phases than the other in the final state.

The asymmetrical steady state might look a little puzzling at first because the underlying dynamics are completely symmetrical — the ensemble contains only identical oscillators which are identically driven in the absence of noise or other potential symmetry-breaking dynamical mechanisms. The only source of asymmetry must therefore come from the initial states of the oscillators. The initial phases are drawn randomly from a uniform distribution on a circle, thus they are unlikely to be symmetrically distributed for each given draw.

To further study the asymmetrical two-cluster formation under the $H(t) = Z^2$ model, we use the extended WS formulation above and its prediction of the boundaries of the two basins of attraction to partially explain the source of this apparent symmetry breaking.

The equations for the Z^2-mean-field model of identical oscillators can be written as the following

$$\dot{\varphi}_j = |Z|^2 \sin\left[2\arg(Z) - 2\varphi_j\right], \quad Z = \frac{1}{N}\sum_{k=1}^{N} e^{i\varphi_k}, \tag{3.19}$$

or in non-mean-field coupled form

$$\dot{\varphi}_j = \frac{1}{N^2}\sum_{k=1}^{N}\sum_{k'=1}^{N} \sin(\varphi_k + \varphi_{k'} - 2\varphi_j). \tag{3.20}$$

Eq. (3.19) (or Eq. (3.20)) corresponds to the general higher-mode coupled system Eq. (3.8) with mode number $l = 2$ and general forcing $H(t) = Z^2$. Moreover, we assume the natural frequency ω_0 to be a constant and fix its value to zero (one can accomplish this by choosing a rotating reference frame).

Since we can rescale time, we have set the coupling strength to 1 without loss of generality. The coupling term in Eq. (3.20), instead of being between pairs of phases, as in the Z_2-mean-field model (Eq. 3.10), now involves a triplet of phases indexed by k, k', and j. This coupling form corresponds to a hypernetwork topological connection between the oscillators. In this hypernetwork, three nodes jointly form a coupling connection, as opposed to those in a conventional network where two nodes form a coupling connection. Dynamics on a hypernetwork could play an important role in neuronal coupling [Pet+14; GGB16; Siz+18].

As discussed above, for $t \to \infty$, two clusters will form with some constant final value of Z, one with the phase of the mean-field $\arg(Z)$ and the other one shifted by π: $\arg(Z) + \pi$, as can be easily found from Eq. (3.19) by equating the right-hand side to zero. A simple metric for describing the distribution of the phases among the clusters is $R := |Z|$, the Kuramoto order parameter amplitude. It relates to the population of one of the clusters by $R = |2N_1/N - 1|$, where N_1 is the number of oscillators in one of the two clusters. When $R = 0$, the two clusters have equal size. When $R = 1$, all the oscillators are in one cluster.

3.2.2 Integration of the WS Equations for the Z^2-Mean-Field Model

Before we carry out numerical integration of WS equations, we introduce a method of visualizing the basins. As discussed above, one needs to follow the evolution not only of the set of coupled oscillators, but of all possible values of phases that can be mapped to the space of the constants ψ. Equivalently, we can use Eq. (3.19), and unidirectionally couple an arbitrary number of oscillators to the field. These oscillators, which we denote $\bar{\theta}$ as passive tracers, are influenced by but do not contribute to the global field

which depends on the "active" phases φ_j only,

$$\dot{\bar{\theta}} = \mathrm{Im}[Z^2 e^{-2i\bar{\theta}}] \ , \tag{3.21}$$

where the mean-field is defined in Eq. (3.19). The variable of a tracer $\bar{\theta}$ is not indexed since we can use any number of them and they take on any value between 0 and 2π.

Introducing passive oscillators gives us the advantage of visualizing the field on the entire circle, because we can place them anywhere on the circle to "test" the strength of the field, and not just at those places where the active oscillators happen to be. In this sense they are analogous to fluid tracers in hydrodynamical simulations or experiments. These tracers make the motion of the points on the circle under the field obvious to the eye, especially those near the unstable points.

For the Z^2-mean-field model Eq. (3.19), the WS parameters obey

$$\begin{cases} \dot{\zeta} = Z^2(t) - [Z^*(t)]^2 \zeta^2 \\ \dot{\tilde{\beta}} = 2\,\mathrm{Im}[Z^2(t)\zeta^*] \ . \end{cases} \tag{3.22}$$

Initial values of the WS parameters in our numerical simulation are chosen as $\zeta(0) = Z^2(0)$ and $\tilde{\beta}(0) = 0$. Under such an initial condition, the second WS equation is $\dot{\tilde{\beta}} = 0$ at $t = 0$, therefore, it can be considered as a natural initial condition, although it is not the only reasonable one. For instance, previous literature Ref. [WS94] has given two initial conditions as options. One is the "identity conversion", with the introduced WS parameters all set to 0: $|\zeta(0)| = 0$, $\arg[\zeta(0)] = 0$ and $\tilde{\beta}(0) = 0$, which corresponds to the case when $\mathcal{M}_1$ is just the identity operator at $t = 0$. The other is the "incoherent state", which corresponds to the case when the constants of motion are maximally incoherently distributed, i.e., choose $\zeta(0)$ and $\tilde{\beta}(0)$ such that $\langle \exp(i\psi_j) \rangle = 0$ (if no majority cluster exists). "Identity conversion" was deemed unsuitable because even with different initial sets of phases, the WS parameters start at the same point in the three-dimensional phase space. However, our chosen initial condition for the parameter, $\zeta(0) = H(0)$, does depend on the initial phases. This initial condition is also more suited to the complex representation of the WS system, as opposed to the three real equations in Ref. [WS94] or like Eq. (3.17), since $\varrho(0) := |\zeta(0)| = 0$ is a singularity there, and $\arg[\zeta(0)]$ would be undefined. For clarity, we define explicitly the argument of ζ: $\Psi = \arg(\zeta)$ as before. Also see the discussion in Sec. 3.1.1.

As outlined above, numerical integration can be performed either directly in variables $\varphi, \bar{\theta}$ or in WS variables $\zeta, \tilde{\beta}$ with additional transformation at each integration step from the constants ψ_j to the phases φ_j, to calculate the mean-field Z. Both methods match to a very good accuracy. The numerical procedure for integrating via the WS variables can be found in Appendix B. Two examples of the time evolution shown in Fig. 3.4 for two random initial conditions ($N = 20$) illustrate this.

In Fig. 3.4, we highlight the trajectories of the two tracers that end up exactly at asymptotic basin boundaries $\varphi_{S1} = \Psi(t = T_{\mathrm{sync}})/2 + \pi/2$ and $\varphi_{S2} = \Psi(t = T_{\mathrm{sync}})/2 - \pi/2$ in φ-space (corresponding to the pole of $\mathcal{M}_2$ in ϑ-space at the final synchronous state), where T_{sync} is the time at which some synchronization threshold is reached during the integration process. These trajectories are time-varying basin boundaries. This variation in time of basin boundaries is typically the case not just for higher-mode coupling like $\sim Z^2$, but also for the standard Kuramoto model. These variations make it impossible to predict the initial locations of the basins without integration, and therefore also unable to predict the numbers of oscillators in the final two clusters explicitly from the initial condition alone. Because the basin boundaries being unstable trajectories in reverse time become attractive, their positions at $t =$

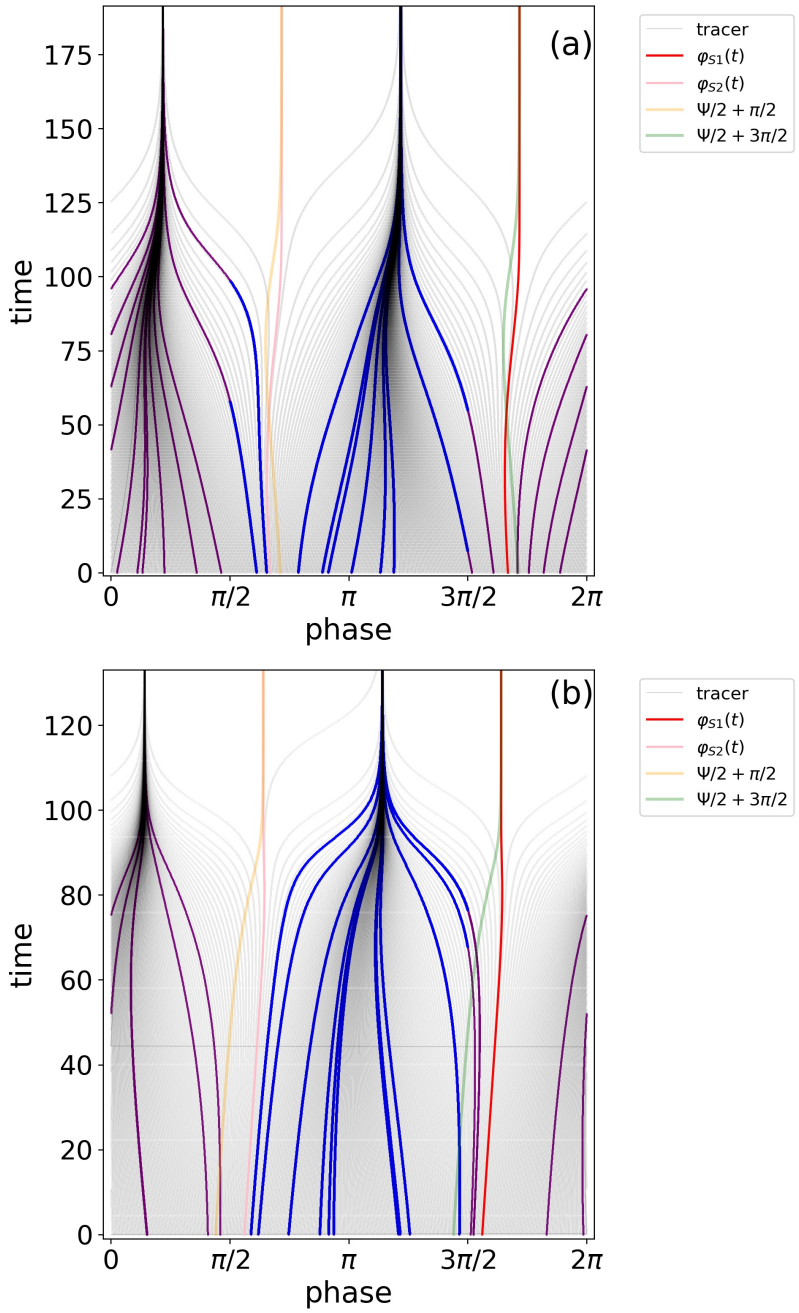

FIGURE 3.4: Euler integration with $h = 0.01$ of the WS equations (3.22) for the Z^2-mean-field model. The model is simulated for two sets of random initial conditions (phases are randomly drawn from uniform distribution from 0 to 2π). Integration is carried out until two synchronized clusters are formed. Gray lines are the tracers $\bar{\theta}$ (Eq. 3.21), which are uniformly spaced initially on a circle, and passively coupled to the global field of the active phases. The flow of 20 active phases φ_j are marked by purple or blue. Purple indicates if at time t, the phase φ_j transformed back from the constant ψ_j does not need to be added π, and blue indicates if it does, to ensure the continuity of the flow of the phases. Trajectories of WS parameter $\Psi(t)/2 + \pi/2$ and $\Psi(t)/2 - \pi/2$ are in orange and green. Pink and red lines are the trajectories of two tracers which end up at singular points $\varphi_{S1}(\infty)$ and $\varphi_{S2}(\infty)$ (as discussed in Sec. 3.1.4). These unstable trajectories are computed via Eq. (3.18) from the singular constant ψ_S and the saved values of $\zeta(t)$ and $\tilde{\beta}(t)$. The intercepts of the red and pink trajectories with horizontal axis match well with the initial position of the basin boundaries, where the tracers split. Figure reprinted with permission from Ref. [GP19].

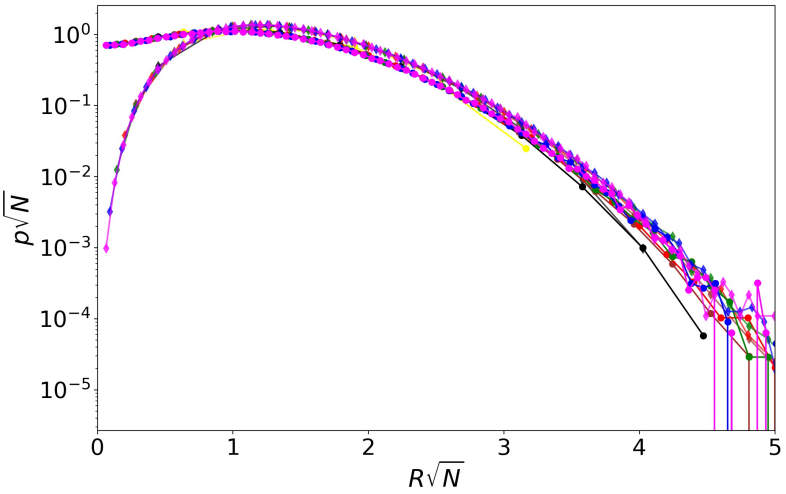

FIGURE 3.5: Comparison between prediction and simulation of the population sizes of the two clusters, plotted as a histogram of R values, based on random initial conditions (uniform distribution on a circle) for ensemble sizes $N = 10, 20, 50, 100, 200, 500, 1000$ (color-coded for N). Round markers: predictions of the cluster size based on the basins estimated from initial states. p is the discrete probability of R value at steady state. Diamond markers: simulated results at steady state (data obtained from Ref. [KP15] with permission of the author). The distributions nearly coincide for $R\sqrt{N} \gtrsim 1$, but for small R the estimated distribution does not reproduce the drop in the density near the totally absent symmetrical clustering state at $R = 0$. Figure reprinted with permission from Ref. [GP19].

0 can be obtained by integrating back in time (under the correct mean-field time evolution calculated forward in time), starting from any point on the circle outside a small neighborhood around the two poles of $\mathcal{M}_2^{-1}$. The size of the neighborhood $\epsilon \to 0$ under infinite forward integration time. Alternatively, we can simply map the singular constant ψ_S via Eq. (3.18) with $\zeta(0)$ and $\tilde{\beta}(0)$ as transformation parameters to obtain basin boundaries φ_S at $t = 0$. However, ψ_S can only be known after integrating to full synchrony: $\psi_S = \Psi(\infty) - \tilde{\beta}(\infty) + \pi$. Therefore, both methods of determining basin boundaries at $t = 0$ require integration.

3.2.3 Comparison of the Asymmetrical Clustering under the Z^2-Mean-Field Model: Prediction and Numerics

Here we discuss a way of approximating cluster distribution just from initial data. As discussed above, the basin boundaries rotate in the course of evolution. However, this rotation is usually small, which means we could estimate roughly the boundaries using the initial value of ζ (according to our choice of initial condition). This method will therefore naturally involve an error corresponding to the degree of rotations. Using the same expression as the final singular points $\varphi_S : \Psi(\infty)/2 + \pi/2$ and $\Psi(\infty)/2 + 3\pi/2$, we approximate basin boundaries at initial time as $\Psi(0)/2 + \pi/2$ and $\Psi(0)/2 + 3\pi/2$. Since the initial condition is $\zeta(0) = H(0) = Z^2(0)$, this implies $\arg[\zeta(0)] = \Psi(0) = 2\arg[Z(0)]$. The number of oscillators falling into each basin (marked by $\arg(Z) + \pi/2$ and $\arg(Z) + 3\pi/2$ at $t = 0$) therefore yields an estimate for the populations of the final clusters. In Fig. 3.5, this estimation in the form of a probability distribution is compared with the correct final asymmetrical clustering distribution, as a function of the metric $R = |Z|$, both axes scaled by $\sqrt{N}$.

This estimate is naturally not accurate because of the rotation of the basin boundaries, however, it is able to explain several features of the distribution. First, for both

the prediction and the simulation, the distribution is asymmetrical, i.e., the maximum of the distribution is not at $R = 0$ (the symmetric clustering state). However, the location of the maximum is underpredicted by theory. Second, the $\sqrt{N}$ scaling law with respect to the ensemble size applies to both. In fact, the successful scaling of the prediction based only on initial conditions implies that the source of the steady state scaling law lies in the initial conditions and their finite sampling, not in the dynamics.

According to the first observation, the source of this "symmetry breaking" in terms of particle distribution should in part be related to the geometrical fact that the angle of the particle mean-field $\arg[Z(0)]$ is not isotropic relative to the particle positions on the circle, even if the underlying particle distribution is isotropic on average. Because if $\arg[Z(0)]$ has no preferred direction relative to the particles, we should see a final cluster-size distribution more akin to the binomial distribution. This is intuitive when one reflects on the meaning of $\arg[Z(0)]$ as the direction of the average over-density of the initial phase distribution. There will, by definition, be more phases on the side where $\arg[Z(0)]$ is pointing towards, and fewer on the side opposite to it. Naturally, the half circles spanning these two sides marked by $\arg[Z(0)] + \pi/2$ and $\arg[Z(0)] + 3\pi/2$ will have unequal numbers of phases in these "approximate basins". This confirms our initial intuition that the source of asymmetry must come from the non-symmetrically distributed phase particles, since the underlying dynamics is entirely symmetric and isotropic.

We must note that our estimate of the basin position is completely reliant on our particular choice of initial conditions for the WS variable $\Psi(0)$. The choice is arbitrary due to over-determinedness of the transformed equations. Therefore, another choice of initial conditions will give another completely different estimate. The fact that our estimate seems to explain some features of the final distribution speaks only for the "naturalness" of our choice of initial conditions, justified by the WS equation (3.22), namely that the second WS equation has zero r.h.s. for the choice $\Psi(0) = 2\arg[Z(0)]$. Conversely, another better choice might be able to exactly predict the final distribution, if such a choice exists generally for all initial conditions.

Despite the partial explanation for the final asymmetrical clustering, the estimate fails to predict the lack of states near $R = 0$, as well as the complete absence of the symmetrical state (two clusters being equally sized). This failure can only be due to the dynamics of the system, which is not inferrable directly from the initial conditions, even though the system is fully deterministic. Specifically, in simulations, the $R = 0$ final state is completely absent, which is in fact due to the weak instability at the symmetry state. An elementary linear stability analysis of the symmetry states with $N = 2$ or $N = 4$ shows that the states (two clusters with sizes 1-1 or 2-2) are weakly unstable, thus giving evidence of the weak instability at the symmetrical state and justifying their absence from the distribution.

3.2.4 Possibility for Decreasing Mean-Field in the Z^2-Mean-Field Model under Positive Coupling

The Kuramoto model with first-order mean-field coupling is known to possess a Lyapunov function [WS94]. This means that generic initial conditions (i.e., with an initially non-zero order parameter) monotonously evolve towards a synchronous clustered state under attractive coupling (only initial states with a zero mean-field do not evolve). This property is not shared by the Z^2-coupling model we consider here. It is possible, using symmetry, to construct special initial conditions which lead to a monotonic decrease of the order parameter. For example, we consider a special symmetric set of initial phase values as shown in Fig. 3.6(b) inset. The initial value

of the Kuramoto order parameter is nonzero, $R > 0$, i.e., the system will evolve under Z^2. However, the evolution preserves the symmetry, so a formation of asymmetric clusters is not possible. Numerical integration shown in Figure 3.6(a) demonstrates convergence towards an unstable configuration with $R = 0$. One should note, that numerical errors could eventually destabilize this symmetric state due to symmetry breaking, with a formation of two clusters of unequal sizes, which should eventually be observed on a long timescale.

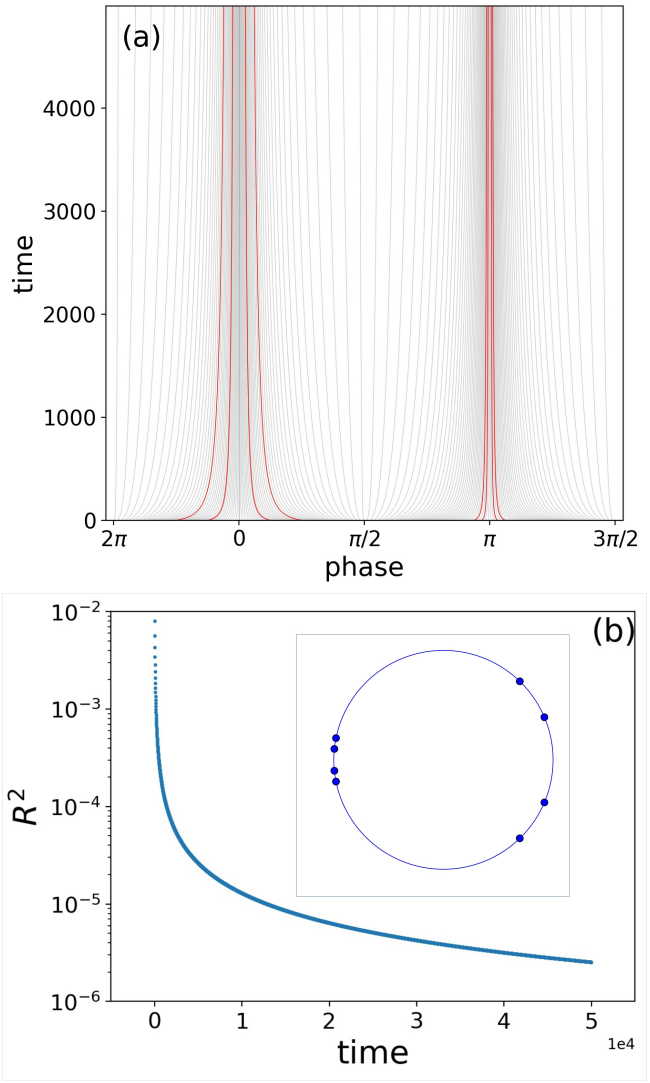

FIGURE 3.6: A unique phenomenon of decreasing mean-field under positive coupling in the second-mode coupled model, illustrated by a special initial condition. A decreasing mean-field under positive coupling can never occur in first-order-harmonic coupled models. (a): Flow of passive (gray) and active oscillator phases (red). (b): Evolution of the mean-field amplitude R^2. Inset in panel (b): Special symmetric initial conditions. Figure reprinted with permission from Ref. [GP19].

3.2.5 Example of WS Integration for Fifth-Order Phase Coupling

Since the theory proposed in this chapter — that phase variables with identical frequency globally coupled via pure higher-mode coupling is partially integrable — is in fact valid at any order l, we provide in Fig. 3.7 an example where $l = 5$ for 20 oscillators with random uniform initial conditions.

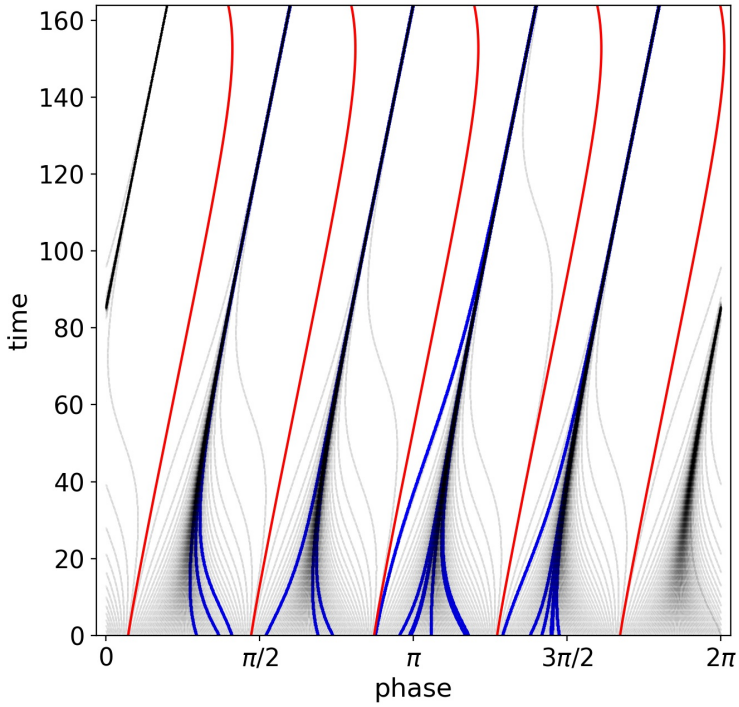

FIGURE 3.7: Analogous to the Z^2 case in Fig. 3.4, here a flow plot for model $\dot{\varphi}_j = \mathrm{Im}[Z^5 e^{-i5\varphi_j}]$, for $N = 20$. Red curves are the basin boundaries $\varphi_S(t)$. Figure reprinted with permission from Ref. [GP19].

Analogous to Fig. 3.4, where a second-mode coupled example is provided, for $l = 5$ and a forcing term $H = Z^5$ where Z is the Kuramoto mean-field, Fig. 3.7 shows the phase flow plot (along with passive tracers). As with the $H = Z^2$ model, we can find the basin boundaries of the cluster formation numerically. Also note that it is generally possible to arrive at a number of clusters smaller than l which gives the maximal number of clusters; in this case four clusters under fifth-order coupling.

3.3 Conclusion

This chapter provides an analytical extension of the dimension-reducing formulation of globally coupled identical phase oscillators under pure higher-mode coupling, and carries the analytical tradition of Watanabe-Strogatz theory further, the same way Ref. [SOGR11] did in terms of the OA theory for the Kuramoto model. Similar to the WS formulation for a first-order harmonic coupling, we apply an analogous type of Möbius transformation from the space of the original phases into the space of the transformed phases (constants of motion) to obtain the three-dimensional WS equations. We invoke the continuity condition to solve the apparent non-unique transformation from the constants back to the original phases. Numerical integration shows that the simulation based on reduced WS equations matches the simulation based on the phase equations.

As an example, the WS formulation of the Z^2-mean-field model, which exhibits asymmetrical clustering, is tested with good numerical agreement to the phase model. The boundaries of the basins of attraction under such a model match the pole in the Möbius map at the final steady state. The asymmetric clustering can be explained, albeit partially via the theory, explicitly from the initial distribution of phases. The main obstacle is the fact that the pole only appears in the Möbius map at the final synchronous steady state, and neither at intermediate nor initial states. This makes

it impossible to find the initial basin boundaries without following the dynamics to the end state.

We also report on a possibility for (unstable) desynchronization to happen in the attractively coupled Z^2-mean-field model, a situation not observed in the classic Kuramoto setup. This is an indication for complex non-monotonous transient behaviours in identical ensembles with higher-mode coupling.

Chapter 4

Coupled Möbius Maps – a Tool to Model Kuramoto Phase Synchronization

In this chapter, we propose a discrete-time analogue of the Kuramoto-Sakaguchi model, a system of globally coupled maps that has similar dynamical properties, and which also provides fast and exact computation of the dynamics in discrete-time steps.

Globally coupled maps [Kan90; Kan91; Noz92; PK94; Jus95; TKP01] have been extensively studied in the literature, often with emphasis on the collective dynamics of intrinsically chaotic units. Among the existing coupled maps, globally coupled circle maps are ideal for studying synchronization phenomena due to their periodic domains. The simplest and most widely used circle map is the sine circle map $\varphi \to \varphi+\Omega+\varepsilon \sin \varphi$, which has been explored in the context of global coupling [Kan91; CG96; OK02] as well as in non-trivial coupling networks such as computational neural networks [BM09]. However, the coupled sine circle maps have several properties different from that of the Kuramoto-Sakaguchi model. For example, a known property of the continuous-time Kuramoto-Sakaguchi model is that clustering, i.e., the formation of several distinct synchronized groups, cannot occur [Gon+19]. However, for the sine circle maps, when the map parameters are tuned to regions which do not produce chaos in a single map (i.e., the mapping remains one-to-one), the iterated map dynamics for identical units governed by the same mean-field nevertheless produces various complex cluster states.

As shown in previous literature, the propagator of continuous-time sinusoidally forced phase oscillators has the form of a Möbius Map (MM) [MMS09]. The Möbius transform lies at the heart of the low-dimensional dynamical theory for globally forced populations of continuous-time phase oscillators formulated by Watanabe and Strogatz (WS) [WS94; PR08; MMS09; PR15a; CEM17]. There, the Möbius transform is used to convert the original phase variables to new conserved quantities, such that the time-varying transformation parameters obey a simple low-dimensional system of ordinary differential equations.

In this chapter, we implement an MM, inspired by the aforementioned Möbius transform, as the basic circle map. The main arguments for studying synchronization using an MM are threefold. First, one distinct feature of MMs over other circle maps is that a single map does not possess higher-order phase-locked states (higher-order Arnold tongues), and instead exhibits only the simplest first-order Arnold tongue (see Ref. [PRK01] for the concept of Arnold tongue). Therefore, by using an MM, complex clustering can be avoided by default. Second, coupled MMs under positive coupling reach qualitative agreement with the dynamics of Kuramoto-type coupled oscillators in continuous time, and can be used for fast computation of desired Kuramoto dynamics

by making larger computational steps. Third, MMs under negative coupling produce new and interesting dynamics, different from the continuous-time counterparts.

By using an MM model, the fundamental properties of the continuous-time models are preserved and many synchronization phenomena can be reproduced. One such property is the WS integrability mentioned above. Another property is the applicability of the Ott-Antonsen (OA) ansatz [OA08], under which the existence of a low-dimensional manifold can be established for an infinite population of globally coupled continuous-time phase oscillators. Similarly, for maps, we can establish a low-dimensional dynamics in an ensemble of phase oscillators evolved under identical Möbius mapping.

The plan of the chapter is as follows. In Sec. 4.1, we first review the general form of the complex MM and discuss its group properties. We discuss its single-map dynamics under function iteration and fixed parameters. Then we present a real form of the MM to be used in numerical calculations. Next, by allowing the parameters of the map to vary in time and applying the group properties, we study the low-dimensional dynamics in globally coupled identical maps, and make a connection to the WS and OA theories. We also briefly discuss the connection of MMs to homographic maps. In Sec. 4.2, we find the MM which solves the Adler equation (Eq. 2.3) with piecewise constant parameters, and suggest a model of globally coupled, non-identical Möbius maps analogous to the Kuramoto-Sakaguchi model. Lastly, in Sec. 4.3, we compute synchronizing dynamics using the map analogues of several systems which have been studied extensively before in the context of Kuramoto-Sakaguchi dynamics. We discuss globally coupled MMs with frequency heterogeneity, chimera states in two populations of identical phase oscillators with different intra- and inter-population coupling [Abr+08], and chimeras on a periodic lattice of identical oscillators with nonlocal coupling [AS04; KB02; Kal+17]. In all examples, known dynamical behaviour of the smooth dynamics can be qualitatively reproduced under positive coupling, and an interesting new dynamical behaviour can be found for negative couplings, under which the familiar continuous-time dynamics would simply be incoherent or asynchronous.

4.1 The Möbius Map and Its Properties

4.1.1 Basic Properties

In order to model the coupled phase oscillator dynamics in discrete-time steps we are looking for a map from the unit circle S^1 to itself. Examples of global coupling of such one dimensional maps on a periodic domain include the sine circle map [Arn65; Kan91; CG96; OK02; BM09], more general circle maps [Noz92], as well as chaotic maps such as the Bernoulli map [TKP01]. The MM we propose is a one-to-one mapping on the open unit disc $\mathbb{D}$ in the complex plane and its boundary S^1. The set of these maps is a Lie group, the Möbius group, with parameters $(q, \chi) \in \mathbb{D}\times\mathrm{S}^1$, i.e., $|q| < 1$ and $\exp(i\chi) \in \mathrm{S}^1$. The map for any complex number $\bar{z}$ in the closed unit disk, $\bar{z} \in \{\mathbb{D}\cup\mathrm{S}^1\}$, can be written as a composition of a rotation by an angle χ,

$$\mathcal{R}_\chi : \bar{z} \to e^{i\chi}\bar{z} \ , \tag{4.1}$$

and a directional contraction

$$\mathcal{C}_q : \bar{z} \to \frac{q + \bar{z}}{1 + q^*\bar{z}} \tag{4.2}$$

in the direction of complex parameter q, and with the degree of contraction controlled by $|q|$. To distinguish from later use of z in this chapter and Ch. 6, as well as WS parameter $\tilde{z}$ from previous chapter, we use $\bar{z}(t)$ here. We adopt the standard form of the MM [MMS09] as

$$\mathcal{M}_{q,\chi}(\bar{z}) = \mathcal{C}_q \circ \mathcal{R}_\chi(\bar{z}) = \frac{q + e^{i\chi}\bar{z}}{1 + q^* e^{i\chi}\bar{z}} , \tag{4.3}$$

with q^* denoting the complex conjugate of q. We distinguish the MM here with the MM from Ch. 3 by its subscript: The MM used in this chapter has two subscripts, corresponding to the two map parameters, whereas the MM used in Ch. 3 has one positive integer subscript, which corresponds to the order of harmonic coupling. The phase φ on the unit circle, $\exp(i\varphi) = z$, $z \in \mathrm{S}^1$, is therefore transformed by

$$\mathcal{M}_{q,\chi}\left(e^{i\varphi}\right) = \frac{q + e^{i(\varphi+\chi)}}{1 + q^* e^{i(\varphi+\chi)}} . \tag{4.4}$$

The rotational actions commute: $\mathcal{R}_{\chi_1} \circ \mathcal{R}_{\chi_2} = \mathcal{R}_{\chi_2} \circ \mathcal{R}_{\chi_1} = \mathcal{R}_{\chi_1+\chi_2}$, with the inverse of the rotation $\mathcal{R}_\chi^{-1} = \mathcal{R}_{-\chi}$. The inverse of the contraction is $\mathcal{C}_q^{-1} = \mathcal{C}_{-q}$ such that

$$\mathcal{M}_{q,\chi}^{-1} = \mathcal{R}_{-\chi} \circ \mathcal{C}_{-q}. \tag{4.5}$$

Rotational symmetry is expressed as

$$\mathcal{C}_q = \mathcal{R}_{-\chi} \circ \mathcal{C}_{qe^{i\chi}} \circ \mathcal{R}_\chi . \tag{4.6}$$

The identity map is $\mathcal{M}_{0,0}$.

Under a functional composition of two MMs, a very useful property is that the new map parameter of the composite map is itself expressed by a MM using the parameters of the component maps:

$$\begin{aligned} \mathcal{M}_{q_2,\chi_2}(\bar{z}) &= \mathcal{M}_{q_1,\chi_1} \circ \mathcal{M}_{q_0,\chi_0}(\bar{z}) \\ &= \frac{\mathcal{M}_{q_1,\chi_1}(q_0) + \mathcal{C}_{q_1 q_0^*}(e^{i\chi_1}) e^{i\chi_0}\bar{z}}{1 + \mathcal{M}^*_{q_1,\chi_1}(q_0)\, \mathcal{C}_{q_1 q_0^*}(e^{i\chi_1})\, e^{i\chi_0}\bar{z}} , \end{aligned} \tag{4.7}$$

or equivalently,

$$q_2 = \mathcal{M}_{q_1,\chi_1}(q_0) , \quad e^{i\chi_2} = \mathcal{C}_{q_1 q_0^*}\left(e^{i\chi_1}\right) \cdot e^{i\chi_0} . \tag{4.8}$$

Hence MMs form a group under functional composition.

4.1.2 Dynamics of the Iterated Möbius Map

Here we shortly discuss the iterated map dynamics of a single MM with constant parameters q and χ:

$$\bar{z}^{(n+1)} = \mathcal{M}_{q,\chi}\left(\bar{z}^{(n)}\right) , \tag{4.9}$$

where $n = 0, 1, \ldots$ is a discrete time index.

To find the fixed points of the discrete dynamics under Eq. (4.9), we solve the quadratic equation

$$\bar{z}^2 - \frac{e^{i\chi} - 1}{q^* e^{i\chi}}\bar{z} - \frac{q}{q^* e^{i\chi}} = 0 . \tag{4.10}$$

Equation (4.10) has two solutions $\bar{z}_1$ and $\bar{z}_2$ with the properties

$$\bar{z}_1\bar{z}_2 = -\frac{q}{q^*}e^{-i\chi} \ , \quad \bar{z}_1 + \bar{z}_2 = \frac{e^{i\chi}-1}{q^*e^{i\chi}} \ . \tag{4.11}$$

From the first property it follows that $|\bar{z}_1||\bar{z}_2| = 1$, which means that either the two fixed points are on the unit circle, or one fixed point is inside and the other outside the unit circle. We make the general ansatz

$$\bar{z}_1 = \kappa e^{i(\bar{\phi}+d)} \ , \qquad \bar{z}_2 = \frac{1}{\kappa}e^{i(\bar{\phi}-d)} \ . \tag{4.12}$$

Denoting $q = \bar{\rho}\cdot\exp(i\bar{\vartheta})$ with $0 \le \bar{\rho} < 1$ (using an overbar to distinguish from the variables ϕ, ρ and ϑ used in previous chapters), we obtain from (4.11) the following two relations:

$$\bar{\phi} = \bar{\vartheta} - \frac{\chi-\pi}{2} \ , \tag{4.13}$$

$$\sin\frac{\chi}{2} = \frac{\bar{\rho}}{2}\left[\left(\kappa+\frac{1}{\kappa}\right)\cos d + i\left(\kappa-\frac{1}{\kappa}\right)\sin d\right] . \tag{4.14}$$

The two fixed points do not uniquely determine the Möbius group parameters q and χ. In the first regime, the two fixed points are on the unit circle, which means $\kappa = 1$. As a result, the second relation (4.14) is simplified to

$$\bar{\rho}\cos d = \sin\frac{\chi}{2} \ . \tag{4.15}$$

The condition for fixed points on the unit circle is therefore

$$\bar{\rho} > \left|\sin\frac{\chi}{2}\right| \ . \tag{4.16}$$

One of the fixed points is stable and the other unstable, so the dynamics of the single MM are trivial, and the rotation number is 0. When equality holds in Eq. (4.16), it corresponds to the tangent bifurcation point, where the two fixed points merge into one.

In the second regime, $\kappa < 1$, i.e., $\bar{z}_1$ is inside the unit circle, then Eq. (4.14) yields two results

$$d = 0 \tag{4.17}$$

$$\kappa = \bar{\rho}^{-1}\left(\sin\frac{\chi}{2} \pm \sqrt{\sin^2\frac{\chi}{2} - \bar{\rho}^2}\right) \ . \tag{4.18}$$

For κ to be a real number, $\bar{\rho} \le |\sin(\chi/2)|$ must be satisfied, which is the exact opposite condition from Eq. (4.16). Under this set of map parameters, i.e., $\bar{\rho} \le |\sin(\chi/2)|$, map (4.9) shows rotational dynamics, which can be reduced to a pure rotation by virtue of a transformation which is also an MM

$$\bar{y}^{(n)} = \mathcal{C}_{-\bar{z}_1}\left(\bar{z}^{(n)}\right) \tag{4.19}$$

The resulting pure rotational dynamics are

$$\bar{y}^{(n+1)} = \mathcal{C}_{-\bar{z}_1}\circ\mathcal{M}_{q,\chi}\circ\mathcal{C}_{\bar{z}_1}\left(\bar{y}^{(n)}\right) = \mathcal{R}_{\bar{\Psi}}\left(\bar{y}^{(n)}\right) , \tag{4.20}$$

with the fixed point $\bar{z}_1 = \kappa \cdot \exp(i\bar{\phi})$ as the group parameter, and the rotation number is

$$\bar{\Psi} = 2 \arctan \left(\tan \frac{\chi}{2} \sqrt{1 - \frac{\bar{\rho}^2}{\sin^2 \frac{\chi}{2}}} \right) . \tag{4.21}$$

Note that to distinguish from Ψ in the previous chapter and $\tilde{\Psi}$ later in this chapter, we have used $\bar{\Psi}$ here. Also to distinguish from coordinate y, we have used $\bar{y}$.

Equation (4.21) shows that in this second regime, the rotation number $\bar{\Psi}$ is a smooth function of the map parameters χ and $\bar{\rho}$. Altogether, the above analysis shows that the iterated single (uncoupled) MM dynamics with fixed parameters have only one Arnold tongue given by Eq. (4.16), a region of synchronous phase locking, with rotation number zero (and when rotational map parameter $\bar{\Psi}$ takes its values on a real line, it has an Arnold tongue with an integer rotation number). For all other non-zero rational values of $\bar{\Psi}$ there are no extended regions of phase locking as found typically in other types of circle maps. Explicitly, this implies that clustering dynamics cannot occur under an iterated MM-dynamics with constant parameters.

Incidentally, like all invertible circle maps (those mapping the unit circle to itself in a one-to-one way), chaotic phase dynamics cannot occur under the iterated map dynamics of MM, regardless of whether the map parameters are constant or time-varying, even including chaotic sequences of map parameters.

4.1.3 Real Form of the Möbius Map

Compared to the complex form of the MM (4.3), the following real form of the MM is more suitable for numerical implementation in programming languages that do not natively support a data type for complex numbers. Denoting $z^{(n)} = \exp(i\varphi^{(n)})$, $q = \bar{\rho} \cdot \exp(i\bar{\vartheta})$, and using the identity $\exp(i\phi) = (1 + i \tan \frac{\phi}{2})(1 - i \tan \frac{\phi}{2})^{-1}$, we obtain from (4.3)

$$\tan \frac{\varphi^{(n+1)} - \bar{\vartheta}}{2} = \frac{1 - \bar{\rho}}{1 + \bar{\rho}} \tan \frac{\varphi^{(n)} + \chi - \bar{\vartheta}}{2} . \tag{4.22}$$

A further transformation yields still another form of the MM

$$\begin{aligned} \sin(\varphi^{(n+1)} - \bar{\vartheta}) &= \frac{(1 - \bar{\rho}^2) \sin(\varphi^{(n)} + \chi - \bar{\vartheta})}{1 + \bar{\rho}^2 + 2\bar{\rho} \cos(\varphi^{(n)} + \chi - \bar{\vartheta})} , \\ \cos(\varphi^{(n+1)} - \bar{\vartheta}) &= \frac{(1 + \bar{\rho}^2) \cos(\varphi^{(n)} + \chi - \bar{\vartheta}) + 2\bar{\rho}}{1 + \bar{\rho}^2 + 2\bar{\rho} \cos(\varphi^{(n)} + \chi - \bar{\vartheta})} . \end{aligned} \tag{4.23}$$

This allows for a straightforward numerical implementation of the MM via the ATAN2 function[1]

$$\varphi^{(n+1)} = \bar{\vartheta} + \mathrm{ATAN2} \left[(1 - \bar{\rho}^2) \sin(\varphi^{(n)} + \chi - \bar{\vartheta}), (1 + \bar{\rho}^2) \cos(\varphi^{(n)} + \chi - \bar{\vartheta}) + 2\bar{\rho} \right] . \tag{4.24}$$

[1] Function ATAN2(y, x) is defined as the angle (given in radians) in the Euclidean plane, between the positive x-axis and the line crossing the origin and the point (x, y), where $(x, y) \neq (0, 0)$.

4.1.4 Low-Dimensional Evolution of Oscillator Ensembles Under Möbius Map

The group property of the MM, as shown by Eqs. (4.7) and (4.8), means that the evolution under MM dynamics from any set of initial states is reducible to a three-dimensional evolution of the parameters of the map q and χ. In particular, consider single-map dynamics (4.9) with discrete sequence of parameters $q^{(n)}, \chi^{(n)}$ that vary in time

$$e^{i\varphi^{(n)}} = \mathcal{M}_{q^{(n)},\chi^{(n)}}\left(e^{i\varphi^{(n-1)}}\right) . \tag{4.25}$$

The evolution over any time interval from the initial state $\exp(i\varphi^{(0)})$ to the final state $\exp(i\varphi^{(n)})$ can be expressed as an MM

$$e^{i\varphi^{(n)}} = \mathcal{M}_{Q^{(n)},\Xi^{(n)}}\left(e^{i\varphi^{(0)}}\right), \tag{4.26}$$

with the composite group parameters governed by the following MM

$$\begin{aligned} Q^{(n)} &= \mathcal{M}_{q^{(n)},\chi^{(n)}}\left(Q^{(n-1)}\right) , \\ e^{i\Xi^{(n)}} &= \mathcal{C}_{q^{(n)}Q^{*(n-1)}}\left(e^{i\chi^{(n)}}\right) e^{i\Xi^{(n-1)}} , \end{aligned} \tag{4.27}$$

due to the group property (4.7). We note that the MM governing Q is the same as the original MM (4.25) that governs the phase. The evolution of any ensemble of oscillators governed by an identical sequence of MMs is always restricted to a three-dimensional manifold described by (4.27) and parametrized by $(Q^{(n)}, \Xi^{(n)})$. Hence the discrete-time dynamics (4.27) for an ensemble of oscillators identically forced (i.e., under common forcing) are fully analogous to the Watanabe-Strogatz quasi-mean-field equations in the continuous-time case (also see Sec. 4.2.1 below).

In fact, the transformation of any measure on the unit circle via the Ruelle-Frobenius-Perron operator corresponding to the mapping of the phases is restricted to such a three-dimensional manifold. In the special case of a continuous, uniform phase density $\mu_0(\varphi) = 1/(2\pi)$, its invariant manifold (MM transformed density) is the family of wrapped Cauchy distributions, a.k.a. a univariate Poisson kernel, as shown by Ref. [MMS09]. The invariant manifold exactly corresponds to the Ott-Antonsen invariant manifold in the continuous-time case, so we shall call this family the OA manifold. Consider $\mu_Q = \mathcal{M}_{Q,\Xi}[[\mu_0]] = \mathcal{C}_Q[[\mu_0]]$, where the double brackets denotes the functional transformation of the density of phases, via Ruelle-Perron-Frobenius operator of the maps $\mathcal{M}_{Q,\Xi}$ and $\mathcal{C}_Q$, both transforming the phases on the unit circle. Because μ_0 is uniform, and is invariant under rotation, i.e., $\mathcal{R}_\Xi[[\mu_0]] = \mu_0$, the density μ_Q is independent of Ξ. Then the following holds for the characteristic function or Fourier transform of the phase density

$$\begin{aligned} \left\langle e^{i\tilde{k}\varphi}\right\rangle_{\mu_Q} &= \int_0^{2\pi} e^{i\tilde{k}\varphi}\mu_Q(\varphi)d\varphi \\ &= \frac{1}{2\pi}\int_0^{2\pi}\left(\mathcal{M}_{Q,\Xi}\left(e^{i\varphi}\right)\right)^{\tilde{k}} d\varphi \\ &= \frac{1}{2\pi}\int_0^{2\pi}\left(\frac{Q+e^{i(\Xi+\varphi)}}{1+Q^*e^{i(\Xi+\varphi)}}\right)^{\tilde{k}} d\varphi \\ &= \frac{1}{2\pi i}\oint_{|z|=1}\frac{1}{z}\left(\frac{Q+z}{1-Q^*z}\right)^{\tilde{k}} dz = Q^{\tilde{k}} , \end{aligned} \tag{4.28}$$

where $\tilde{k}$ is the Fourier mode of the phases, which is to be distinguished from the oscillator index k. The last integral is a complex contour integral with a simple pole $z = 0$ inside and a $\tilde{k}$th-order pole $z = (Q^*)^{-1}$ outside the unit circle. In the derivation above we have also used the fact that the integral over the unit circle with respect to the transformed density μ_Q is equal to the integral of the transformed circle $\mathcal{M}_{Q,\Xi}(\mathrm{S}^1)$ with respect to the uniform density μ_0.

Equation (4.28) shows that the first circular moment of the phase distribution is $\left\langle e^{i\varphi}\right\rangle_{\mu_Q} = Q$, and all higher moments are integer powers of Q. Therefore, on the OA manifold, the MM parameter Q that transforms a uniform density to the wrapped Cauchy density is the first circular moment of the phase distribution, i.e., the usual Kuramoto order parameter

$$Q = Z = \langle e^{i\varphi}\rangle_{\mu_Q} \ . \tag{4.29}$$

Incidentally, the explicit form of the wrapped Cauchy probability density, corresponding to the set of the moments (4.28), reads

$$\mu_Q(\varphi) = \frac{1}{2\pi}\frac{1-|Q|^2}{|e^{i\varphi}-Q|^2} \ . \tag{4.30}$$

From result (4.29) and the group property (4.27), the evolution of the mean-field Z on the unit disc $\mathbb{D}\cup\mathrm{S}^1$ can then be expressed by the same MM that transforms the phases on the unit circle S^1

$$Z^{(n)} = \frac{q^{(n)} + e^{i\chi^{(n)}} Z^{(n-1)}}{1 + q^{*(n)} e^{i\chi^{(n)}} Z^{(n-1)}} \ . \tag{4.31}$$

Equation (4.31) is in fact a discrete analogue of the Ott-Antonsen equation in continuous-time dynamics. It is interesting to note that, map (4.31) has the exact same form as the the map describing the dynamics of one MM (4.25). This is similar to the fact that for the continuous-time dynamics, the OA equation for the mean-field has the same form as the equation for the individual oscillator, written in terms of $z = e^{i\varphi}$.

As a side note, both time-varying parameters q and χ in Eq. (4.25) can contain noisy components. In this way, more complicated noisy dynamics can also be studied with the discrete map model proposed here for which all the results above still hold.

4.1.5 Relation to Homographic Maps

Griniasty and Hakim [GH94] studied a family of homographic maps, defined for real x

$$x^{(n+1)} = a_0 - \frac{b_0}{x^{(n)}} \ . \tag{4.32}$$

This map leaves a Cauchy distribution density invariant, in the same sense as an MM leaves a wrapped Cauchy distribution invariant. A homographic map (4.32) can be shown to be equivalent to an MM, as the latter (Eq. 4.22) can be rewritten as a fractional linear transformation of the variable $x^{(n)} = \tan(\varphi^{(n)}/2)$ as follows

$$\begin{gathered} x^{(n+1)} = \frac{(1+\bar{\rho})\tilde{G} + (1-\bar{\rho})\tilde{H} + x^{(n)}[(1-\bar{\rho}) - (1+\bar{\rho})\tilde{G}\tilde{H}]}{1+\bar{\rho} - (1-\bar{\rho})\tilde{G}\tilde{H} - x^{(n)}[(1+\bar{\rho})\tilde{H} + (1-\bar{\rho})\tilde{G}]}, \\ \tilde{G} = \tan\frac{\bar{\vartheta}}{2},\ \tilde{H} = \tan\frac{\chi-\bar{\vartheta}}{2} \ . \end{gathered} \tag{4.33}$$

The MM (4.33) can be considered as a shifted homographic map (4.32).

4.2 Relation to Adler Equation and Construction of Globally Coupled Möbius Maps

4.2.1 Möbius Maps as a Solution to the Adler Equation

The Adler equation [Adl46] with constant parameters has the form

$$\dot{\varphi} = A\left[\lambda - \sin(\varphi - \beta)\right] \ , \tag{4.34}$$

where the real-valued parameters consist of the amplitude A, the ratio λ between the constant bias term and the amplitude of the sinusoidal forcing and the phase shift β. It is known (Sec. 2.2) for $|\lambda| \leq 1$ that the Adler equation has a steady state solution, and for $|\lambda| > 1$, it yields phase rotations.

The solution of the Adler equation over a time interval τ can be shown to be an MM, where the fixed parameters consist of A, λ, β and τ, but in the end only the product $A \cdot \tau$ enters the solution. Denoting

$$\sigma = \sqrt{1-\lambda^2}, \quad \Gamma = \tanh\left(\frac{A\tau}{2}\sigma\right) \ , \tag{4.35}$$

and using the conventions $\sqrt{-1} = i$ and $\tanh(ix) = \tan(x)$, we can show the solution of Eq. (4.34) over τ is an MM

$$e^{i\varphi(\tau)} = \frac{(\sigma + i\lambda\Gamma)e^{i\varphi(0)} + e^{i\beta}\Gamma}{(\sigma - i\lambda\Gamma) + e^{i\varphi(0)}e^{-i\beta}\Gamma} = \mathcal{M}_{q,\chi}\left(e^{i\varphi(0)}\right) \tag{4.36}$$

with the group parameters

$$q = e^{i\beta}\frac{\Gamma}{\sigma - i\lambda\Gamma}, \qquad e^{i\chi} = \frac{\sigma + i\lambda\Gamma}{\sigma - i\lambda\Gamma} \ . \tag{4.37}$$

Equation (4.36) has been derived in detail in Appendix C.

If the solution to the Adler equation after τ is an MM, then the evolution under iterated MMs is an MM again, as shown by the group property in Sec. 4.1.1. Therefore the solution to the problem (4.34) is an MM after any time interval for fixed parameters A, λ and β. Additionally, for time-dependent parameters $A(t)$, $\lambda(t)$ and $\beta(t)$, which are arbitrary functions of time, the solution to the problem (4.34) is still an MM.

Consequently, all basic properties of the Adler equation are inherited by the MM. In particular, it is known that for a periodic solution of the Adler equation there is only one Arnold tongue, corresponding to an integer rotation number [BKT10; IRF11]. This matches exactly the property of MMs as discussed in Section 4.1.2, i.e., the MM has at most one stable fixed point in the synchronized state.

Here it is important to note, that Eq. (4.36) can be viewed as an ideal numerical scheme to simulate the continuous-time Adler equation with a small time step τ. In linear order the standard Euler scheme coincides with the MM. However, while a standard Euler scheme breaks the Watanabe-Strogatz partial integrability of the coupled Adler equation [Gon+19], the MM (4.36) preserves this partial integrability. The later is hence similar to the symplectic schemes for Hamiltonian equations.

In the special case where the amplitude $A = A(t)$ has explicit time dependence, the solution is still an MM. Under this condition, the Adler equation (4.34) has the form of a linear phase response to a time-dependent forcing, $\dot{\varphi} = H(\varphi)A(t)$. Separation of variables shows that in this case the product $A\tau$ from Eq. (4.35) is to be replaced by

V, which is the integral of $A(t)$ over the time interval τ

$$V = \int_0^\tau A(t)dt. \tag{4.38}$$

The solution to the Adler equation with time varying parameter $A(t)$ is hence the "kick map"

$$\mathcal{K}_{\lambda,V,\beta}(z) = \frac{(\sigma + i\lambda\Gamma)z + e^{i\beta}\Gamma}{(\sigma - i\lambda\Gamma) + ze^{-i\beta}\Gamma} \tag{4.39}$$

with $\Gamma = \tanh(\sigma V/2)$, mapping a phase under a "kick" V. This way, $A(t)$ can be any generic function, regardless of whether it is a delta pulse or a constant force.

4.2.2 Globally Coupled Möbius Maps

To formulate a model of globally coupled MMs, we can use the result from Sec. 4.2.1, where we show an MM as the solution to an Adler equation. We start with the Kuramoto-Sakaguchi model in continuous time

$$\dot{\varphi}_j = \omega_j + \varepsilon R \sin(\Theta - \varphi_j - \alpha),\ j = 1, \ldots, N\ . \tag{4.40}$$

Here $\{\varphi_j\}$ is the set of phases of oscillators in a population of size N, indexed by oscillator index j. Their natural frequencies ω_j are generally different. The Kuramoto mean-field of the population is defined according to

$$Z = Re^{i\Theta} = \frac{1}{N}\sum_{k=1}^{N} e^{i\varphi_k}\ . \tag{4.41}$$

One can see that for a constant mean-field parameter R and Θ, the dynamics of each oscillator is governed by the Adler equation (4.34), where they are effectively decoupled from each other and are only coupled to the constant mean-field. However, because we do not assume a constant mean-field, we must look for ways to implement the changing mean-field via time-dependent parameters of the map. We notice that the parameters λ and A enter the resulting MM (4.36) in a rather complex manner. Therefore, to get a simple discrete-time model that nevertheless carries essential properties of the Kuramoto-Sakaguchi model, we split the evolution in two stages. In stage one, the phases are transformed according to the kick map $\mathcal{K}_{0,\varepsilon R^{(n)},\Theta^{(n)}-\alpha}$, i.e., with a constant kick $V^{(n)} = \varepsilon R^{(n)}$, setting the kick duration $\tau = 1$ without loss of generality. In the second stage phases undergo free rotation over a time interval T according to their natural frequencies ω_j. Combining stage one and two, the resulting model of globally coupled MMs reads

$$\begin{aligned} e^{i\varphi_j^{(n+1)}} &= \mathcal{R}_{\omega_j T} \circ \mathcal{K}_{0,\varepsilon R^{(n)},\Theta^{(n)}-\alpha}\left(e^{i\varphi_j^{(n)}}\right) \\ &= e^{i\omega_j T}\frac{e^{i\varphi_j^{(n)}} + e^{i(\Theta^{(n)}-\alpha)}\tanh\frac{\varepsilon R^{(n)}}{2}}{1 + e^{i\varphi_j^{(n)}}e^{-i(\Theta^{(n)}-\alpha)}\tanh\frac{\varepsilon R^{(n)}}{2}}\ , \\ R^{(n)}e^{i\Theta^{(n)}} &= \frac{1}{N}\sum_{k=1}^{N} e^{i\varphi_k^{(n)}}\ . \end{aligned} \tag{4.42}$$

This discrete-time system has, similar to the Kuramoto-Sakaguchi model (4.40), the natural frequencies ω_j, the coupling strength ε and the coupling phase shift α as

parameters, with an additional parameter time interval T.

4.3 Mean-Field Dynamics for Phases Evolved Under Coupled Möbius Maps

4.3.1 Globally Coupled Population of Kuramoto-Sakaguchi Type

Here we consider the simplest case of one population of globally coupled MMs (4.42) in the thermodynamic limit. On the Ott-Antonsen manifold, the phase density $\mu_Q(\omega)$ for each value of ω is a wrapped Cauchy distribution with mean-field $Q(\omega) = \left\langle e^{i\varphi} \right\rangle_{\mu_Q(\omega)}$, as derived before from Eq. (4.29). Q then evolves according to the same map for the individual phase with frequency ω (4.42), i.e.,

$$Q^{(n+1)}(\omega) = e^{i\omega T} \frac{Q^{(n)}(\omega) + e^{i(\Theta^{(n)}-\alpha)} \tanh \frac{\varepsilon R^{(n)}}{2}}{1 + Q^{(n)}(\omega) e^{-i(\Theta^{(n)}-\alpha)} \tanh \frac{\varepsilon R^{(n)}}{2}} \tag{4.43}$$

as derived in Sec. 4.1.4. The intrinsic frequency ω is responsible merely for a free rotation of Q by the angle ωT during the interval T between the kick. Therefore we merely need to multiply the right hand side with $e^{i\omega T}$.

Integrating over the frequency distribution, we obtain the global mean-field

$$Z^{(n)} = R^{(n)} e^{i\Theta^{(n)}} = \int_{-\infty}^{\infty} Q^{(n)}(\omega) g(\omega) d\omega \ . \tag{4.44}$$

Similar to the approach of Ott and Antonsen [OA08], we can assume that $Q(\omega)$ is analytic in the upper half-plane, which allows us to calculate the integral via the residue theorem. For a Lorentzian frequency distribution $g(\omega)$ of mean $\bar{\omega}$ (to be distinguished from intrinsic frequency ω) and scale parameter γ (to be distinguished from synchronization index γ_{12} in Ch. 6)

$$g(\omega) = \frac{1}{\pi\gamma} \frac{\gamma^2}{(\omega - \bar{\omega})^2 + \gamma^2} \tag{4.45}$$

we have $Z = Q(\bar{\omega} + i\gamma)$. Accordingly, the global mean-field evolves as

$$Z^{(n+1)} = e^{(i\bar{\omega}-\gamma)T} \frac{Z^{(n)} + e^{i(\Theta^{(n)}-\alpha)} \tanh\left(\frac{\varepsilon R^{(n)}}{2}\right)}{1 + Z^{(n)} e^{-i(\Theta^{(n)}-\alpha)} \tanh\left(\frac{\varepsilon R^{(n)}}{2}\right)}. \tag{4.46}$$

The free rotation $\mathcal{R}_{\omega T}(z) = \exp(i\omega T) z$ for identical oscillators is replaced by a rotation with the mean frequency $\bar{\omega}$ of the ensemble and a decay of the mean-field due to population heterogeneity γ, which denotes the width of the natural frequency distribution.

For this model we can calculate the steady state order parameter $\tilde{R} = R \exp(\gamma T)$ after each kick implicitly. Because we can always go into the co-rotating frame with the mean frequency $\bar{\omega}$, we can set it to 0 without loss of generality. Setting the order parameter $\tilde{R}$ equal on both sides of (4.46)

$$\tilde{R}^2 = \left| \frac{\Gamma e^{-i\alpha} + \tilde{R} e^{-\gamma T}}{1 + \Gamma e^{i\alpha} \tilde{R} e^{-\gamma T}} \right|^2 = \frac{\Gamma^2 + \tilde{R}^2 e^{-2\gamma T} + 2\Gamma \tilde{R} e^{-\gamma T} \cos\alpha}{1 + \Gamma^2 \tilde{R}^2 e^{-2\gamma T} + 2\Gamma \tilde{R} e^{-\gamma T} \cos\alpha} \tag{4.47}$$

where $\Gamma = \tanh\left(\varepsilon e^{-\gamma T}\tilde{R}/2\right)$, we solve a quadratic equation for Γ, and obtain

$$\begin{aligned}\Gamma =& \frac{\tilde{R}}{1-\tilde{R}^4 e^{-2\gamma T}}\Big[-(1-\tilde{R}^2)e^{-\gamma T}\cos\alpha \\ &\pm\sqrt{(1-\tilde{R}^2)^2 e^{-2\gamma T}\cos^2\alpha + (1-e^{-2\gamma T})\left(1-\tilde{R}^4 e^{-2\gamma T}\right)}\Big].\end{aligned} \tag{4.48}$$

Inverting the expression for ε we obtain

$$\varepsilon = \frac{2}{\tilde{R}e^{-\gamma T}}\operatorname{arctanh}(\Gamma). \tag{4.49}$$

Equations (4.48) and (4.49) together allow us to express coupling strength ε explicitly as a function of the steady state synchronization order parameter $\tilde{R}$ and to plot them in a bifurcation diagram, as shown in Fig. 4.1..

The first notable limit of the expression of the bifurcation curve is the existence of two critical coupling strengths for $\tilde{R} \to 0$

$$\varepsilon_{cr} = 2\left(-\cos\alpha \pm \sqrt{\cos^2\alpha + e^{2\gamma T} - 1}\right). \tag{4.50}$$

This implies that there is always a positive and a negative critical coupling strength for the incoherent state in globally coupled MMs. The second limit is the limit of identical oscillators $\gamma \to 0$. Then $\tilde{R} = R$ and

$$\Gamma = \tanh\left(\frac{\varepsilon R}{2}\right) = R\frac{-\cos\alpha \pm |\cos\alpha|}{1+R^2}. \tag{4.51}$$

This indicates two lines of fixed points connecting incoherence at $R = 0$ and complete synchronization $R = 1$.

Under negative coupling and identical frequency, there are several regimes for a transition to synchrony. At $\varepsilon_0 = 0$, the stability of complete synchronization and incoherence is exchanged instantly. At $\varepsilon_1 = -4\cos\alpha$, incoherence $R = 0$ becomes unstable, and at $\varepsilon_2 = \ln[(1-\cos\alpha)/(1+\cos\alpha)]$, complete synchronization $R = 1$ becomes unstable.

The existence of a synchronization transition for strongly repulsively coupled oscillators under discrete time stands in stark contrast to the continuous-time Kuramoto-Sakaguchi model (4.40). In the continuous case, the order parameter R decreases to zero continuously under negative coupling, whereas in the coupled-maps system a negative forcing strong enough can invert the orientation of the mean-field during one step, and even increases its amplitude.

4.3.2 Two-Population Chimera

Here we consider a setup similar to the one studied in Ref. [MPMA16], where two populations of identical continuous-time oscillators interact, with each population more strongly coupled to itself than to the other population. To formulate the corresponding MM model, we denote coupled phases in the two populations by their complex exponentials as before, $z_{1,j} = \exp(i\varphi_{1,j})$ and $z_{2,j} = \exp(i\varphi_{2,j})$, and the corresponding mean-field of each population as

$$Z_1 = \frac{1}{\overline{N}_1}\sum_{k=1}^{\overline{N}_1} z_{1,k}, \quad Z_2 = \frac{1}{\overline{N}_2}\sum_{k=1}^{\overline{N}_2} z_{2,k}\ ,$$

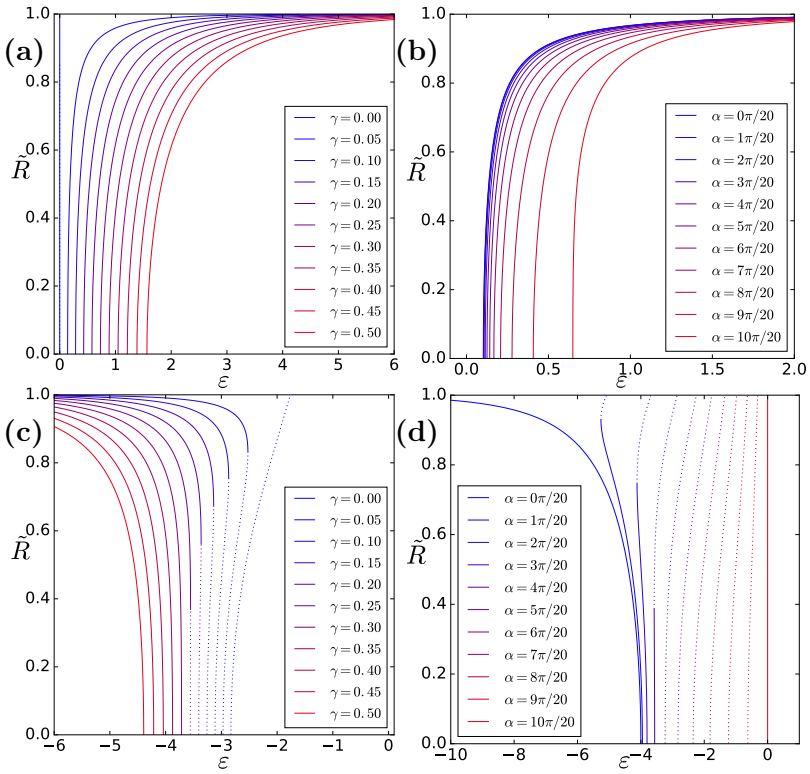

FIGURE 4.1: Steady state order parameter $\tilde{R}$ as a function of coupling strength ε (i.e., the bifurcation curve) in the attractively (a)-(b) ($\varepsilon > 0$) or repulsively coupled (c)-(d) ($\varepsilon < 0$) MM model. Without loss of generality we assume the time interval between discrete kicks to be $T = 1.0$. Linearly unstable and stable partially synchronized states are marked by dotted and solid lines, respectively. In (a) and (c), we keep $\alpha = \pi/4$ constant and vary the natural frequency heterogeneity parameter γ from 0 to 0.5 (from top to bottom). In (b) and (d) we set γ to a constant value, $\gamma = 0.05$ in (b) and $\gamma = 0$ in (d), and vary the parameter α. In (a)-(b) we see the typical second-order synchronization transition as in the classical Kuramoto-Sakaguchi model with frequency heterogeneity. For negative coupling strengths as in (c)-(d) there can be several transitions, both continuous and discontinuous, even for identical oscillators in (d) with $\gamma = 0$. Figure reprinted with permission from Ref. [GTP20].

where $\overline{N}_1, \overline{N}_2$ are the sizes of two populations of identical oscillators. The forces acting on the populations are linear combinations of these mean-fields

$$\begin{aligned} Y_1 e^{i\tilde{\Psi}_1} &= \tilde{p} Z_1 + (1-\tilde{p}) Z_2 \ , \\ Y_2 e^{i\tilde{\Psi}_2} &= \tilde{p} Z_2 + (1-\tilde{p}) Z_1 \ , \end{aligned} \tag{4.52}$$

where parameter $\tilde{p}$ defines relative strengths of intra- and inter-population couplings, to be distinguished from probability density p in Ch. 3. We use $\tilde{\Psi}$ here to differentiate from the WS parameter Ψ in Ch. 3. Substituting these forces into Eq. (4.42), the resulting MMs for the phase variables are

$$\begin{aligned} z_{1,j}^{(n+1)} &= \frac{z_{1,j}^{(n)} + e^{i(\tilde{\Psi}_1^{(n)} - \alpha)} \tanh(\frac{\varepsilon Y_1}{2})}{1 + z_{1,j}^{(n)} e^{-i(\tilde{\Psi}_1^{(n)} - \alpha)} \tanh(\frac{\varepsilon Y_1}{2})} \ , \\ z_{2,j}^{(n+1)} &= \frac{z_{2,j}^{(n)} + e^{i(\tilde{\Psi}_2^{(n)} - \alpha)} \tanh(\frac{\varepsilon Y_2}{2})}{1 + z_{2,j}^{(n)} e^{-i(\tilde{\Psi}_2^{(n)} - \alpha)} \tanh(\frac{\varepsilon Y_2}{2})} \ , \end{aligned} \tag{4.53}$$

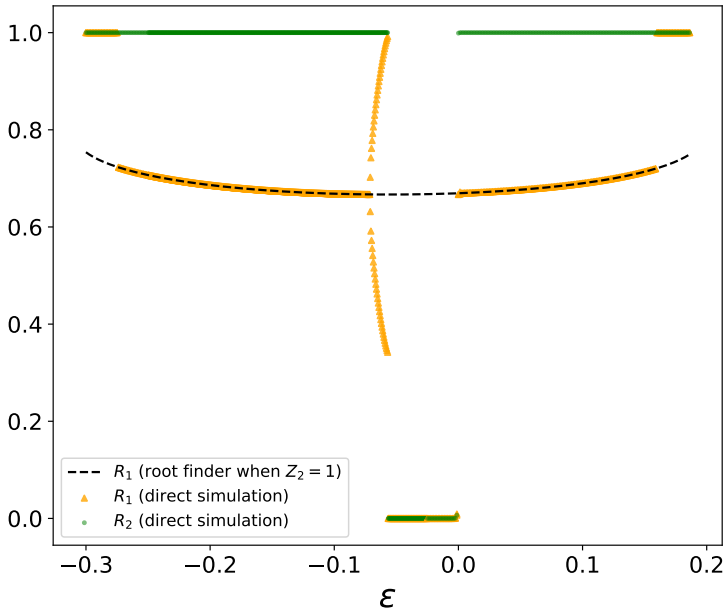

FIGURE 4.2: Bifurcation diagram (order parameter R vs. coupling strength ε) illustrating the stability of the chimera states of the two coupled maps of the mean-fields (4.54) . Scatter plots depict the stable solutions (after transient) obtained from the direct simulation of the coupled maps (4.54), showing $|Z_1|$ (orange) and $|Z_2|$ (green). The dashed line is the fixed point of the coupled map dynamics found via a numerical solver (the `findroot` function of the mpmath package [Joh+13]) while assuming one of the mean-fields is 1 (at full synchrony). Figure reprinted with permission from Ref. [GTP20].

where α is the common phase shift and ε is the common coupling strength. Here we set the identical frequency to zero by transforming into a co-rotating frame with the common natural frequency.

In the thermodynamical limit, i.e., $\overline{N}_1, \overline{N}_2 \to \infty$, assuming that both systems are on the OA manifold, we can write the dynamics of the coupled system as two coupled maps of the order parameters $Z_{1,2}$

$$\begin{aligned} Z_1^{(n+1)} &= \frac{Z_1^{(n)} + e^{i(\tilde{\Psi}_1 - \alpha)}\Gamma_1}{1 + Z_1^{(n)} e^{-i(\tilde{\Psi}_1 - \alpha)}\Gamma_1} \,, \\ Z_2^{(n+1)} &= \frac{Z_2^{(n)} + e^{i(\tilde{\Psi}_2 - \alpha)}\Gamma_2}{1 + Z_2^{(n)} e^{-i(\tilde{\Psi}_2 - \alpha)}\Gamma_2} \,, \end{aligned} \tag{4.54}$$

using Eq. (4.46), $\bar{\omega} = \gamma = 0$ for identical populations. $\Gamma_1 = \tanh(\varepsilon Y_1/2)$, $\Gamma_2 = \tanh(\varepsilon Y_2/2)$. $Y_{1,2}$ and $\tilde{\Psi}_{1,2}$ are expressed by Eq. (4.52).

As in Ref. [MPMA16], we choose $\alpha = 0.5\pi - 0.025$, in-group coupling ratio $\tilde{p} = 0.6$, and start iterations at initial order parameters $Z_{1,2}^{(0)}$ with small amplitudes, either close to in-phase or to anti-phase. We first evolve the coupled maps (4.54) according to various positive coupling strengths ε. We found the results to be qualitatively similar to the continuous limit solutions. Namely, at low coupling strengths, chimera states, where one of the population is in full synchrony and the other in partial synchrony are obtained. At intermediate coupling strengths, depending on the initial conditions $Z_{1,2}(0)$, either chimera or full synchrony of the two populations are possible steady state solutions, where it is appropriate to speak of a basin of attraction, similar to the continuous case [MPMA16]. At high coupling strength, both populations are in full

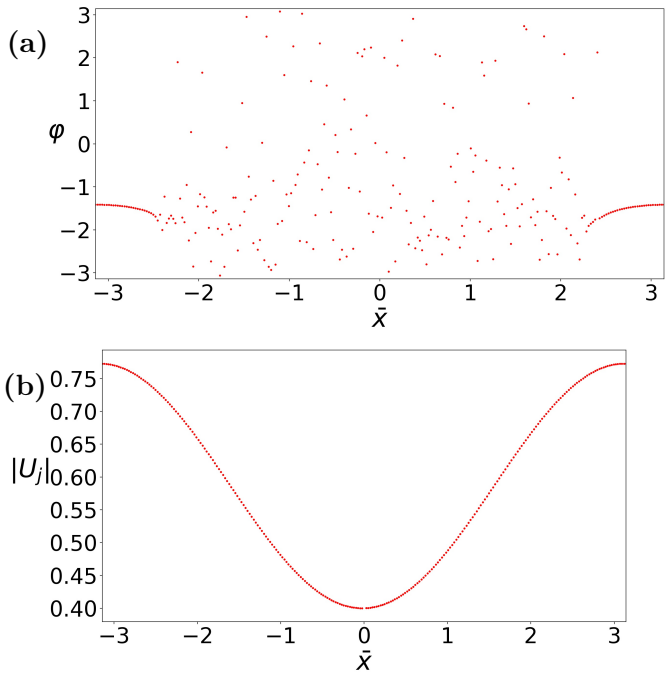

FIGURE 4.3: Chimera states on a ring in model (4.55) and (4.56). Panel (a): configuration of the phases; panel (b): the local field amplitude. This chimera pattern appears stable after 18000 steps. The network size is $N = 256$, coupling strength $\varepsilon = -0.8$, kernel function parameter $\tilde{B} = 0.995$ and phase lag $\alpha = \pi/2 - 0.18$. Same as the initial condition in Ref. [AS04] for the continuous dynamics, we use $\varphi(t = 0) = 6\tilde{r}\exp(-0.76\bar{x}^2)$, where $\tilde{r} \in [-1/2, 1/2]$ is randomly sampled. Figure reprinted with permission from Ref. [GTP20].

synchrony at the steady state.

For negative ε, we see four regimes. At $\varepsilon > \varepsilon_{cr}^{-}$, corresponding to the negative critical coupling strength (derived in Sec. 4.3.1), we observe only the complete asynchronous case with vanishing order parameter. As we decrease ε, we see first a regime where only chimeras are obtained, then a regime where either chimera or full synchrony are possible depending on the initial conditions, and finally the regime where only full synchrony of both populations is obtained.

Therefore it is possible for negative coupling strength under discrete dynamics to create steady states that are either partially (chimera state) or completely synchronized. This is in contrast with continuous-time dynamics, where under negative coupling both order parameters can only decrease to zero at steady state.

To probe the stability of the chimera states of the coupled maps (4.54), we conduct a bifurcation analysis across both positive and negative ε regime (Fig. 4.2). The stable chimera state, as found via integrating the coupled maps, numerically agrees with the fixed points found by a numerical solver (the `findroot` function of the mpmath package [Joh+13]) for stable chimera states. At $\varepsilon \approx -0.07$ a period-doubling bifurcation of the chimera amplitude occurs corresponding to a periodic or quasi-periodic mean-field. As ε continues to increase to about -0.06 the quasi-periodic orbit collides with the full synchrony and both disappear. The asynchronous state becomes stable. In the limit $\varepsilon \to 0^+$ the map dynamics corresponds to the continuous-time dynamics discussed in Ref. [MPMA16]. The loss of stability of the chimera for a larger positive coupling strength at $\varepsilon \approx 0.16$ is again an effect of the discrete map dynamics.

4.3.3 Chimera on a Ring

The first example of a chimera state for continuous-time oscillators was on a one-dimensional ring with non-local coupling [KB02; AS04], first explored by Kuramoto and Battogtokh. The oscillators are coupled via a kernel function, which determines the spatial extend of the interactions with their neighbors. We can find similar chimeras with the coupled map model.

The oscillators on the ring have positions $\bar{x}_j = 2\pi j/N$, where N is the total number of oscillators. Following Ref. [AS04], we have chosen the kernel as $\tilde{g}_{jk} = 1 + \tilde{B}\cos(\bar{x}_j - \bar{x}_k)$, so that the field acting on oscillator j is calculated as

$$U_j = \bar{R}_j e^{i\bar{\Theta}_j} = \sum_{k=1}^{N} \tilde{g}_{jk} \sin(\varphi_j - \varphi_k - \alpha) \ . \tag{4.55}$$

We denote the kernel function $\tilde{g}$ to be distinguished from generic function $\bar{g}$ and the frequency distribution $g(\omega)$. The local mean-field parameters $\bar{R}_j$ and $\bar{\Theta}_j$ are to be distinguished from the Kuramoto mean-field amplitude R and phase Θ. The phases are driven by these local fields according to the MM

$$z_j^{(n+1)} = \frac{z_j^{(n)} + e^{i(\bar{\Theta}_j^{(n)} - \alpha)} \tanh(\frac{\varepsilon \bar{R}_j^{(n)}}{2})}{1 + z_j^{(n)} e^{-i(\bar{\Theta}_j^{(n)} - \alpha)} \tanh(\frac{\varepsilon \bar{R}_j^{(n)}}{2})} \ , \tag{4.56}$$

where, as before, $z_j = \exp(i\varphi_j)$.

Similar to the continuous dynamics, we can obtain a stable chimera pattern for a range of positive values of ε (e.g., $\varepsilon = 0.025$) (not shown). Same as in the two-population case before, under discrete map dynamics, there exists a regime under large negative coupling strength which can give rise to a stable chimera pattern, see for example Fig. 4.3.

Besides the cosine kernel function, we have also simulated the case with a square kernel, i.e., with the local field

$$U_j = \frac{1}{2L+1} \sum_{k=-L}^{k=L} \sin(\varphi_{k+j} - \varphi_j - \alpha) \ . \tag{4.57}$$

Iterating the same map (4.56) using this new local field with $N = 1000$, $L = 130$, $\varepsilon = 0.025$ and $\alpha = 2.71$, we obtained a many-headed chimera state as in the continuous case in Ref. [Mai+14].

4.4 Conclusion

In this chapter we propose a method of modelling synchronizing phase dynamics using an MM. This map precisely reproduces the dynamics of phase oscillators in discrete time. It can be an ideal choice for fast simulation of phase synchronization, since it inherits all the properties of continuous-time phase dynamics. In particular, neither clustering nor chaos under the iteration of a sequence of MMs can occur. All continuous-time models based on the Adler phase equation (i.e., with a pure sinusoidal coupling) can be equivalently studied via MMs. Additionally, phase coupling models with pure higher-harmonics couplings [GP19] can be modelled with correspondingly modified MMs.

With the proposed MM, we have studied map analogues of known continuous-time models for oscillator ensembles with various connection topologies: the globally coupled Kuramoto-Sakaguchi model, two coupled populations of identical oscillators, and identical oscillators on a ring with non-local coupling via cosine or square distance kernel. For small coupling strengths and small free rotation time steps, the coupled maps reproduce the dynamics of their continuous-time dynamical counterparts. In particular, we have reproduced known chimera states with coupled maps under non-local couplings. For large coupling strengths, and in particular for large repulsive coupling, the discrete time dynamics can lead to new synchronization phenomena with continuous and discontinuous bifurcations to synchrony. This phenomenon is not observed in the analogous continuous-time models.

Chapter 5

Repulsively Coupled Oscillators under Multiplicative Common Noise

In this section, we extend the application of WS theory to noisy models, and discuss the restriction on possible attracting states. We discover that the standard numerical integration schemes violate the partial integrability due to discretization that introduces higher-mode coupling into the model.

As we have shown in Ch. 3, the WS approach turns out to be a fruitful one at converting the original complex dynamics into a precise low-dimensional one. One of the important consequences of the WS approach, which we explore below, is that it leads to a restriction on possible states that are not fully synchronous — namely, it excludes the formation of several clusters. This restriction holds not only for noise-free models already discussed, but also certain types of noisy models. As we will see, the violation of the partial integrability in this case might lead to drastically different results in numerical experiments from the correct, theoretically predicted ones. The model we studied originated from Gil et al. [GKM09] and belongs to a type of Kuramoto model with common noise.

There are mainly two ways common noise can be added to a coupled mean-field model as shown in Eq. (5.1), via two directions of multiplicative noise or an additive noise term (also see Fig. 1.1 for a summary of the existing literature)

$$\dot{\varphi}_j = \underbrace{\omega_j}_{\text{intr. freq.}} + \underbrace{\frac{\varepsilon}{N}\sum_{k=1}^{N}\sin(\varphi_k - \varphi_j + \alpha)}_{\text{coupling term}} + \underbrace{\sigma_1\eta_1(t)\sin\varphi_j + \sigma_2\eta_2(t)\cos\varphi_j}_{\text{multiplicative noise}} + \underbrace{\sigma_3\eta_3(t)}_{\text{add. noise}} , \tag{5.1}$$

where $\eta_1(t), \eta_2(t), \eta_3(t)$ are random scalar Gaussian(0,1) variables and $\sigma_1, \sigma_2, \sigma_3$ are the corresponding scalar noise strengths. In the complex plane of the phase space, common additive noise corresponds to a random scalar Gaussian field applied uniformly along the unit circle, whereas the common multiplicative noise corresponds to a vector field on the circle, with the term proportional to the sine of phases pointing along the imaginary axis, and the term proportional to the cosine of phases pointing along the real axis (see Fig. 5.1). The multiplicative common noise is analogous to a flashlight which is randomly shone on a group of synchronizing fireflies. The fluctuating light from the flashlight is added to the common light field of the fireflies — their mean-field. Depending on the position of each firefly, it experiences more or less of the fluctuating light. For additive noise, a similar picture holds, except that now each firefly receives the same fluctuating light from a flashlight regardless of its position.

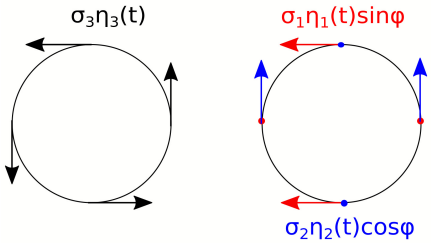

FIGURE 5.1: Illustration of the two types of common noise. Formula see Eq. (5.1). Left: additive common noise, and right: multiplicative common noise. Red and blue code for the sine and cosine multiplicative terms. On the right it is clear that depending on the location on the circle, various degrees of noisy force are exerted.

The model previously studied numerically by Gil et al. had only multiplicative noise with sine and cosine terms, and the two terms have equal coupling strength, such that their sum corresponds to an isotropic random vector field on the circle, i.e., $\sigma_1 = \sigma_2$, and $\sigma_3 = 0$. In Gil et al., stationary states of 2 or 3 clusters were observed in a set of identical oscillators under common multiplicative noise and repulsive coupling. Under strong repulsive coupling a fully synchronized cluster becomes unstable, but it is not evident a priori what will be observed instead. Therefore, Gil et al. conducted numerical simulations and reported that common noise generally causes clustering in globally repulsively coupled Kuramoto interactions.

However, this claim is called into question based on the following reasons. First, clustering is indeed observed in some models of globally coupled identical phase oscillators [HMM93; Gol+92; PRK01], but always in situations where the interaction functions include higher modes of the coupled phases. In the interaction term in the model proposed by Gil et al., no such higher modes are present. Secondly, recent studies of the competition between common noise and repulsive coupling revealed non-trivial distributions for identical and non-identical oscillators [Pim+16; LAP13], but no clustering has been observed. Gil et al., on the other hand, reported that for identical oscillators, clusters formed without a threshold, at any noise intensity. Finally and perhaps most decisively, because the model used by Gil et al. can be fully described by WS theory, there are restrictions due to the general properties of the Möbius transform governing the dynamics [MMS09], i.e., clusters are not allowed to appear (see Sec. 5.2 below). Therefore, a thorough numerical and analytical study is needed to resolve the conflict between the numerical findings of Ref. [GKM09] and known theories.

The observation of clustering in simulations by Gil et al. [GKM09] may be attributed to numerical artefacts, as one cannot expect WS integrability to be preserved by standard numerical methods. In this chapter we explore how different numerical integration methods for integrating deterministic and stochastic equations affect WS integrability and clustering.

The main goal of this chapter is twofold: (i) to demonstrate that the occurrence of clusters in the system studied by Gil et al. is impossible, contrary to their numerical report, and (ii) to identify numerical artefacts that may nevertheless lead to cluster formation in simulations. In the following sections, we first present the WS approach and show that clustering is impossible. Then we study the formation and stability of clusters under the model in Gil et al. both analytically and numerically. We have found that the exact integrability is not preserved by the standard numerical schemes, both for deterministic and stochastic equations. The WS constants of motion have not been preserved during simulation. This is in contrast with similarly repulsively

coupled Van der Pol oscillators under common additive noise, for which higher-order Fourier terms and multiplicative noise are naturally present in the phase reduced dynamics, and form clusters as predicted.

5.1 Main Model

Per Gil et al., we study a population of identical phase oscillators with phases $\{\varphi_j\}$ subject to a global coupling of Kuramoto-Sakaguchi type (Sec. 2.2.4) and two common [1]phase-dependent nonlinear noise terms

$$\dot{\varphi}_j = \omega_0 + \frac{1}{N}\sum_{k=1}^{N}\sin(\varphi_k - \varphi_j + \alpha) + \sigma_1\eta_1(t)\sin\varphi_j + \sigma_2\eta_2(t)\cos\varphi_j \ . \tag{5.2}$$

Here $\eta_{1,2}(t)$ are Gaussian random variables, with $\langle\eta_1(t)\rangle = 0$, $\langle\eta_2(t)\rangle = 0$, $\langle\eta_m(t)\eta_{m'}(t')\rangle = \delta_{mm'}\delta(t-t')$. The parameters σ_1 and σ_2 parametrize the noise strengths for the two noise terms. The Langevin Eq.(5.2) is to be interpreted in the Stratonovich sense so that WS theory is applicable. Indeed, when interpreted in the sense of Itô calculus, for $\sigma_1 \neq \sigma_2$ a noise-induced drift, i.e., Stratonovich shift, exists, and is proportional to the second harmonics in φ_j. The occurrence of higher-order harmonics mixed with first-order harmonic coupling violate the conditions under which WS theory can be applied, since WS theory can only be applied to models with a single order of harmonic coupling (Ch. 3).

Because it is always possible to rescale time, we can, without loss of generality, set the coupling strength between the mean-field and the phases to 1 ($\varepsilon = 1$ in Eq. (5.1)).

Models of Kuramoto-Sakaguchi oscillators under multiplicative common noise have been analysed in Refs. [NK10] and [Pim+16], and in Gil et al. [GKM09] for two noise terms. Gil et al. [GKM09] argued that when the two noise strengths are equal, model Eq. (5.2) is equivalent to the phase-reduced model of a population of weakly coupled identical Stuart-Landau oscillators with a common additive noise isotropic in the complex plane. In this case, the model under the isotropic noise is invariant under rotation. We let $\sigma_1 = \sigma_2 = \sigma$, and rewrite Eq. (5.2) as

$$\dot{\varphi}_j = \omega_0 + \mathrm{Im}\{[Ze^{i\alpha} + \sigma\xi(t)]e^{-i\varphi_j}\} \ , \tag{5.3}$$

where Z is the Kuramoto mean-field and $\xi = -\eta_1 + i\eta_2$ is a complex Gaussian white noise. The identical intrinsic frequency ω_0 can be set to zero by going into a co-rotating frame due to the rotational symmetry. After change of variable $\varphi_j \to \varphi_j - \omega_0 t$, with $\xi(t) = r(t)e^{i\theta(t)}$, Eq. (5.3) becomes

$$\begin{aligned}\dot{\varphi}_j =& \mathrm{Im}\left[\frac{1}{N}\sum_{k=1}^{N} e^{i\varphi_k}e^{-i(\varphi_j-\alpha)}\right] \\ &+ \sigma r(t)\sin[\theta(t)-\omega_0 t]\cos\varphi_j - \sigma r(t)\cos[\theta(t)-\omega_0 t]\sin\varphi_j\end{aligned} \tag{5.4}$$

which is the same as the original model Eq. (5.3). However, one should note here that eliminating identical intrinsic frequency ω_0 by going into co-rotating frame is only valid if the noise is isotropic in the complex plane, i.e., the two multiplicative noise

[1]The noise is common because the vector field itself is common to all oscillators. But depending on the oscillator's position in the field, it experiences different degrees of noise. If the parameter σ is also different for different individual oscillators, then it is individual noise. Also see introduction in Sec. 2.3.1.

terms must have equal noise strength. Because the multiplicative noise term depends on the absolute value of the phase, which in turn depends on the frequency, so if there is a preferred direction in the system, for example, caused by the anisotropic noise in the complex plane, the system loses its rotational invariance and it will no longer be possible to go into a co-rotating frame. Specifically, for a one-noise-term model, it is no longer valid to set $\omega_0 = 0$.

5.2 WS Theory Applied to Globally Coupled Identical Oscillators with Common Noise

As already introduced in Sec. 3.1, expression Eq. (3.2) alone rules out the formation of clustered states from non-clustered initial conditions. Two oscillators with initially different phases are mapped to a single point only at full synchrony for first-order harmonic coupling. Therefore, only a single cluster attracting different phases can exist at a time. Nevertheless, this only prohibits the formation of multiple clusters but not their existence under this model. There is no restrictions on the oscillators to start out in one or several distinct clusters and stay in that configuration.

Table 5.1 shows in detail, that for multiple clusters the Möbius structure of the dynamics cannot hold, and the violation of the Möbius structure in turn is forbidden by WS theory. The Möbius transformation dictates that no more than 1 cluster can be found at the steady state. Even if the model is stochastic with noise terms, as long as it is still within the regime of WS theory, clusters are forbidden to form. Therefore, even though noise is known to result in clustering, as an exception, cluster states cannot form in the first-order harmonic coupled Kuramoto-Sakaguchi models even if they contain noise.

State	WS mean-field	State under Möbius transform
no cluster	$\tilde{z} = 0$	$\varphi_j = \psi_j + \tilde{\alpha}$
1 cluster	$\tilde{z} = e^{i\Phi}$	$\varphi_j = \Phi$, Φ the synchronized phase
$\tilde{M}$ clusters ($2 \leq \tilde{M} < N$)	$\tilde{z} = \rho e^{i\Phi}$	$\mathcal{M}_1$: $e^{i\varphi_{j,\tilde{m}}} = e^{i\tilde{\Phi}_{\tilde{m}}} \neq \frac{\rho e^{i\Phi} + e^{i(\psi_j+\tilde{\alpha})}}{1+\rho e^{-i\Phi} e^{i(\psi_j+\tilde{\alpha})}}$ $\tilde{\Phi}_{\tilde{m}}$ the phase of the $\tilde{m}$-th cluster

TABLE 5.1: Table detailing the reason why multi-cluster states are precluded by WS theory for the KS type models, and the only possible states are full synchrony and full asynchrony. Multiple clusters cannot occur under such a model because on the l.h.s. of the Möbius transform $\mathcal{M}_1$, there are $\tilde{M}$ values, corresponding to $\tilde{M}$ clusters, whereas the r.h.s. has N values, corresponding to the N constants of motion. The equality on the third row therefore cannot hold. Number of clusters $\tilde{M}$ and cluster index $\tilde{m}$ are to be distinguished from the number of noise terms M and noise term index m. $\tilde{\Phi}$ is to be distinguished from the WS parameter Φ (Ch. 3).

When the multiplicative noise is only dependent on one variable, as in our case, the j-th component of the Stratonovich shift $\vec{S}(\varphi)$ is

$$\begin{aligned} S_j(\varphi) &= \frac{\sigma^2}{2} \sum_{j'=1}^{N} \left[\sin\varphi_{j'} \partial_{\varphi_{j'}} (\sin\varphi_j) + \cos\varphi_{j'} \partial_{\varphi_{j'}} (\cos\varphi_j) \right] \\ &= \frac{\sigma^2}{2} \left[\sin\varphi_j \cos\varphi_j - \cos\varphi_j \sin\varphi_j \right] = 0 \ . \end{aligned} \tag{5.5}$$

Therefore for Eq. (5.3) with two equal-strength noise terms, the Stratonovich shift is 0.

Since we expect the partial integrability, guaranteed by the maintaining of Möbius group structure, to be likely not conserved by the numerical integration scheme, we set out to measure the degree that the partial integrability might be violated during numerical integration. The easiest way to measure the potential violation of partial integrability is by the values of the constants of motion. A drift of the constants of motion will directly imply that the partial integrability is violated. As has been outlined in Sec. 3.1.1, the constants of motion of the system can be determined via the Möbius transformation Eq. (3.2) of the N phases $\{\varphi_j\}$. In practice, one must first determine the complex variable $\tilde{z} = \rho e^{i\Phi}$ which characterizes the transformation. Watanabe and Strogatz (see Sec. 4.2 in Ref. [WS94]) have shown that this can be accomplished with the help of a potential function

$$\mathcal{U}(\rho, \Phi) = \frac{1}{N} \sum_{k=1}^{N} \log \frac{1 - 2\rho \cos(\varphi_k - \Phi) + \rho^2}{1 - \rho^2} \ . \tag{5.6}$$

The proper value of $\tilde{z}$ corresponds to the minimum of this function with respect to its modulus ρ and to its argument Φ. The easiest way to determine the minimum is by integrating

$$\dot{\rho} = -\mathcal{U}_\rho \ , \qquad \dot{\Phi} = -\mathcal{U}_\Phi \ ,$$

where subscripts indicate partial derivatives, until the steady state is established. The angles $\psi_j + \tilde{\alpha}$ can then be obtained with the Möbius transformation Eq. (3.2), where ψ_j are the WS constants of motion. It is possible to avoid integrating $\tilde{\alpha}$ by considering only the differences $\psi_j - \psi_1$, $j = 2, \ldots, N$ as constants of motion. The disadvantage of this method lies in the necessity of solving the minimization problem for the potential Eq. (5.6), which can be performed with finite accuracy only. There exists, however, another possibility to determine the constants of motion.

Marvel, Mirollo and Strogatz (MMS) (see Sec. V in Ref. [MMS09]) have demonstrated that the cross ratio of four complex numbers on the unit circle is a preserved quantity under the Möbius transformation. For any four phases $\varphi_j, \varphi_{j+1}, \varphi_{j+2}, \varphi_{j+3}$ (not necessarily ordered on the circle), the constant of motion C_j is defined as

$$C_j = \frac{U_{j,j+2}}{U_{j,j+3}} \cdot \frac{U_{j+1,j+3}}{U_{j+1,j+2}} \ , \text{ where } U_{jj'} = \sin \frac{\varphi_j - \varphi_{j'}}{2} \ . \tag{5.7}$$

Our method of checking the conservation of these quantities is based on Eq. (5.7), but we find it appropriate to avoid calculating fractions, because as the phases synchronize, the denominators can be very small or vanish. Instead, we calculate the numerical errors in the following form

$$\begin{aligned} e_j = & U_{j,j+2}(t) U_{j+1,j+3}(t) U_{j,j+3}(0) U_{j+1,j+2}(0) \\ & - U_{j,j+3}(t) U_{j+1,j+2}(t) U_{j,j+2}(0) U_{j+1,j+3}(0) \ . \end{aligned}$$

In summary, we test for integrability in numerical schemes by calculating the following errors containing changes in the conserved quantities under Möbius action

$$\mathrm{Err}_{\mathrm{WS}}(t) = \max_j \{\sin |[\psi_j(t) - \psi_1(t)] - [\psi_j(0) - \psi_1(0)]|\}, \text{ where } j = 2, \ldots, N \ , \tag{5.8}$$

$$\mathrm{Err}_{\mathrm{MMS}}(t) = \max_j (|e_j|), \text{ where } j = 1, 2, \ldots, N-3 \ . \tag{5.9}$$

In this section we have shown that clusters cannot appear from non-clustered initial conditions. The same arguments can be applied when the dynamics evolve from an initial multicluster state. Here, either the multicluster remains with the same partition, or the fully synchronized state with maximally one additional cluster or oscillator in a solitary state appears. Imperfect clusters, i.e., configurations with phases very close to one another, can also dissolve or contract depending on their dynamical stability.

The conclusion drawn here from WS theory of partial integrability will be further supported below by an analytic and numerical investigation of the Lyapunov exponents of oscillators evolving in the field of two fully synchronized clusters in Sec. 5.3 .

5.3 Linear Stability Analysis of Two-Cluster States

According to WS theory, one expects that not more than one of the clusters can be asymptotically attracting. Otherwise multiclusters would also form from non-clustered initial conditions, a phenomenon which is forbidden by the argument in Sec. 5.2. Additionally, there exist previous results on the stability of the completely synchronous cluster for the model with one noise term, which can be expressed in terms of the transversal Lyapunov exponent [Pim+16]

$$\bar{\lambda} = -\cos\alpha - \frac{\sigma^2}{2} \ . \tag{5.10}$$

where α is the usual phase shift (Ch. 2 and Ch. 4), and σ the noise strength. $\bar{\lambda}$ is to be distinguished from the Adler equation parameter λ (Ch. 2 and Ch. 4). When $\bar{\lambda}$ is negative, complete synchronization is stable, i.e., it attracts nearby phases that are perturbed from it. According to Eq. (5.10), for sufficiently strong noise, the cluster of complete synchrony is stable. For repulsive coupling, with $\cos\alpha < 0$ and sufficiently weak noise, the cluster is unstable. However, contrary to this result, Gil et al.'s result indicated that for two noise terms, clusters formed at any noise intensity. Therefore, in this section we provide a linear stability analysis of a two-cluster state under the stochastic evolution given by model Eq. (5.3) which confirms our expectation that the two-cluster state cannot be attracting.

We write system (5.3) for a two-cluster state as

$$\begin{aligned}
\dot{\tilde{\Phi}}_1 =& \omega_0 + p_1 \sin\alpha + p_2 \sin(\Delta\tilde{\Phi} + \alpha) + \sigma \sin\tilde{\Phi}_1\eta_1(t) + \sigma\cos\tilde{\Phi}_1\eta_2(t) \\
\dot{\tilde{\Phi}}_2 =& \omega_0 + p_2 \sin\alpha - p_1 \sin(\Delta\tilde{\Phi} - \alpha) + \sigma \sin\tilde{\Phi}_2\eta_1(t) + \sigma\cos\tilde{\Phi}_2\eta_2(t) \ .
\end{aligned} \tag{5.11}$$

Here $\tilde{\Phi}_1$ and $\tilde{\Phi}_2$ are the phases of the two clusters. $\Delta\tilde{\Phi} = \tilde{\Phi}_2 - \tilde{\Phi}_1$ is their phase difference. Parameters p_1 and $p_2 = 1 - p_1$ are their relative population sizes.

To evaluate the stability of the two-cluster state in terms of a small perturbation from one of the clusters, say, cluster 1, we perturb two oscillators belonging to cluster 1 by pulling them in opposite directions by a small amount away from the cluster, i.e., $\varphi_{1,2} = \tilde{\Phi}_1 \pm \tilde{\delta}$. For small $\tilde{\delta}$, linearization yields

$$\dot{\tilde{\delta}} = \tilde{\delta}\big[-p_1\cos\alpha - p_2\cos(\Delta\tilde{\Phi} + \alpha) + \sigma\cos\tilde{\Phi}_1\eta_1(t) - \sigma\sin\tilde{\Phi}_1\eta_2(t)\big] \ . \tag{5.12}$$

$\tilde{\delta}$ is to be distinguished from the Dirac delta function δ. This allows us to express stability of cluster 1 via the split/evaporation Lyapunov exponent [Kan89; PPM01;

PP16] as

$$\bar{\lambda}_1 = < \frac{d \ln \tilde{\delta}}{dt} >= -p_1 \cos\alpha - p_2 \langle \cos(\Delta\tilde{\Phi} + \alpha) \rangle + \sigma \langle \cos\tilde{\Phi}_1 \eta_1(t) \rangle - \sigma \langle \sin\tilde{\Phi}_1 \eta_2(t) \rangle \ , \tag{5.13}$$

where $\langle \cdot \rangle$ indicates time average, which in this case also equals to the ensemble average, because as we will see in (5.21), the probability distribution of the phase $\Delta\tilde{\Phi}$ is stationary. Also see Sec. 2.3.2 in the introduction.

While the Stratonovich shift for the Langevin Eqs.(5.11) happens to be zero, that is not the case anymore when Eq.(5.12) is considered as well. It is important to keep this in mind and choose a correct integration scheme when Eqs.(5.11) and (5.12) are integrated numerically. To calculate the Lyapunov exponent analytically, we need to know the probability distribution of $\Delta\tilde{\Phi}$ and the averages $\langle \cos\tilde{\Phi}_1 \eta_1(t) \rangle$, $\langle \sin\tilde{\Phi}_1 \eta_2(t) \rangle$. First, we write a two-dimensional Fokker-Planck equation for $\tilde{\Phi}_1$ and $\Delta\tilde{\Phi}$ corresponding to the Langevin equations (5.11) under Stratonovich interpretation [HT82] as follows. The 2 SDEs are

$$\begin{aligned} \dot{\tilde{\Phi}}_1 &= p_1 \sin\alpha + p_2 \sin(\Delta\tilde{\Phi} + \alpha) + \sigma \sin\tilde{\Phi}_1 \eta_1(t) + \sigma \cos\tilde{\Phi}_1 \eta_2(t) \\ \Delta\dot{\tilde{\Phi}} &= (p_2 - p_1) \sin\alpha (1 - \cos\Delta\tilde{\Phi}) - \cos\alpha \sin\Delta\tilde{\Phi} + \sigma[\sin(\tilde{\Phi}_1 + \Delta\tilde{\Phi}) - \sin\tilde{\Phi}_1]\eta_1(t) \\ &\quad + \sigma[\cos(\tilde{\Phi}_1 + \Delta\tilde{\Phi}) - \cos\tilde{\Phi}_1]\eta_2(t) \ . \end{aligned} \tag{5.14}$$

Rewrite them in this short form

$$\begin{aligned} \dot{\tilde{\Phi}}_1 &= \bar{h}_1(\Delta\tilde{\Phi}) + \bar{g}_{11}(\tilde{\Phi}_1)\eta_1(t) + \bar{g}_{12}(\tilde{\Phi}_1)\eta_2(t) \\ \Delta\dot{\tilde{\Phi}} &= \bar{h}_2(\Delta\tilde{\Phi}) + \bar{g}_{21}(\Delta\tilde{\Phi}, \tilde{\Phi}_1)\eta_1(t) + \bar{g}_{22}(\Delta\tilde{\Phi}, \tilde{\Phi}_1)\eta_2(t) \ , \end{aligned} \tag{5.15}$$

where $\bar{h}, \bar{g}$ are functions expressed in Eq. (5.14). $\bar{h}$ is to be distinguished from the time step parameter h. $\bar{g}$ is to be distinguished from the frequency distribution g. According to the formula in the introductory section Eq. (2.18), the Fokker-Planck equation is [2]

$$\begin{aligned} \frac{\partial W(\tilde{\Phi}_1, \Delta\tilde{\Phi}, t)}{\partial t} =& -\frac{\partial}{\partial\tilde{\Phi}_1}(\bar{h}_1 W) - \frac{\partial}{\partial\Delta\tilde{\Phi}}(\bar{h}_2 W) \\ &+ \frac{1}{2}\frac{\partial}{\partial\tilde{\Phi}_1}\left\{\bar{g}_{11}[\frac{\partial}{\partial\tilde{\Phi}_1}(\bar{g}_{11} W) + \frac{\partial}{\partial\Delta\tilde{\Phi}}(\bar{g}_{21} W)]\right\} \\ &+ \frac{1}{2}\frac{\partial}{\partial\tilde{\Phi}_1}\left\{\bar{g}_{12}[\frac{\partial}{\partial\tilde{\Phi}_1}(\bar{g}_{12} W) + \frac{\partial}{\partial\Delta\tilde{\Phi}}(\bar{g}_{22} W)]\right\} \\ &+ \frac{1}{2}\frac{\partial}{\partial\Delta\tilde{\Phi}}\left\{\bar{g}_{21}[\frac{\partial}{\partial\tilde{\Phi}_1}(\bar{g}_{11} W) + \frac{\partial}{\partial\Delta\tilde{\Phi}}(\bar{g}_{21} W)]\right\} \\ &+ \frac{1}{2}\frac{\partial}{\partial\Delta\tilde{\Phi}}\left\{\bar{g}_{22}[\frac{\partial}{\partial\tilde{\Phi}_1}(\bar{g}_{12} W) + \frac{\partial}{\partial\Delta\tilde{\Phi}}(\bar{g}_{22} W)]\right\} \ . \end{aligned} \tag{5.16}$$

where $W(\tilde{\Phi}_1, \Delta\tilde{\Phi}, t)$ is the time-varying joint probability density of $\tilde{\Phi}_1$ and $\Delta\tilde{\Phi}$.

Then, when integrating the joint probability distribution $W(\tilde{\Phi}_1, \Delta\tilde{\Phi}, t)$ over the slow variable $\tilde{\Phi}_1$ to obtain the probability distribution $P(\Delta\tilde{\Phi})$, we use the fact that

[2] Note that our definition of noise intensity is different from that in Gil et al. [GKM09]. Our definition for the Gaussian noise has noise intensity 1, i.e. $\langle \eta_m(t)\eta_{m'}(t') \rangle = \delta_{mm'}\delta(t - t')$, instead of $\langle \eta_m(t)\eta_{m'}(t') \rangle = 2\delta_{mm'}\delta(t - t')$. So in Eq. (5.16), for terms containing products of two noise terms, we do not need to multiply it by 2.

the probability distribution of $\tilde{\Phi}_1$ is rotationally symmetric, which means all partials with respect to $\tilde{\Phi}_1$ vanish[3]

$$\begin{aligned}\frac{\partial P(\Delta\tilde{\Phi})}{\partial t} &= \int_0^{2\pi} W(\tilde{\Phi}_1, \Delta\tilde{\Phi}) d\tilde{\Phi}_1 \\ &= \int_0^{2\pi} \Big\{ -\frac{\partial\left(\bar{h}_2\, W\right)}{\partial\Delta\tilde{\Phi}} + \frac{1}{2}\frac{\partial}{\partial\Delta\tilde{\Phi}}\left[-\bar{g}_{21}\, W \frac{\partial\bar{g}_{21}}{\partial\Delta\tilde{\Phi}} + \bar{g}_{21} W \frac{\partial\bar{g}_{11}}{\partial\tilde{\Phi}_1} + \bar{g}_{21}\bar{g}_{11}\frac{\partial W}{\partial\tilde{\Phi}_1}\right] \\ &\quad + \frac{1}{2}\frac{\partial}{\partial\Delta\tilde{\Phi}}\left[-\bar{g}_{22}\, W \frac{\partial\bar{g}_{22}}{\partial\Delta\tilde{\Phi}} + \bar{g}_{22} W \frac{\partial\bar{g}_{12}}{\partial\tilde{\Phi}_1} + \bar{g}_{22}\bar{g}_{12}\frac{\partial W}{\partial\tilde{\Phi}_1}\right] \Big\} d\tilde{\Phi}_1 \\ &\quad + \frac{1}{2}\frac{\partial^2}{\partial\Delta\tilde{\Phi}^2}\left[\int_0^{2\pi} (\bar{g}_{21}^2 + \bar{g}_{22}^2) W d\tilde{\Phi}_1\right]\end{aligned} \tag{5.17}$$

After straightforward differentiation, finally, we obtain a closed-form equation for the probability distribution $P(\Delta\tilde{\Phi})$ of the phase difference

$$\begin{aligned}\frac{\partial P(\Delta\tilde{\Phi})}{\partial t} = &-\frac{\partial}{\partial\Delta\tilde{\Phi}}\left\{\left[(p_2 - p_1)\sin\alpha(1 - \cos\Delta\tilde{\Phi}) - \cos\alpha\sin\Delta\tilde{\Phi}\right] P\right\} \\ &+ \sigma^2 \frac{\partial^2}{\partial\Delta\tilde{\Phi}^2}\left[(1 - \cos\Delta\tilde{\Phi}) P\right] .\end{aligned} \tag{5.18}$$

Note that this probability density function is defined and restricted on the open interval $(0, 2\pi)$ since the two clusters cannot cross each other. We then find the stationary solution [Ris96] to the above Fokker-Planck equation. The solution is stationary when r.h.s. of Eq. (5.18) is zero, i.e., when the probability flux is constant. However, due to rotational invariance, the probability current can be set to 0, because if the probability current vanishes at some $\Delta\tilde{\Phi}$ the current must be zero for any $\Delta\tilde{\Phi}$. The flux (r.h.s. of Eq. (5.18)) does vanish at value $\Delta\tilde{\Phi} = 0$. So for a general Fokker-Planck equation of the form

$$J(x) := \frac{\partial P(x)}{\partial t} = -\frac{\partial}{\partial x}\bar{f}_1 P + \frac{\partial^2}{\partial x^2}\bar{f}_2 P, \tag{5.19}$$

the stationary probability distribution P_{st} ($J = 0$), i.e. the zero-flux solution, satisfies

$$\bar{f}_1(x) P_{st} = \frac{\partial}{\partial x}\bar{f}_2(x) P_{st} . \tag{5.20}$$

After integration, the stationary solution has the form

$$P_{st}(\Delta\tilde{\Phi}) = N_0 \exp\left[\frac{\Delta\tilde{\Phi}(p_2 - p_1)\sin\alpha}{\sigma^2}\right] \left|\sin\frac{\Delta\tilde{\Phi}}{2}\right|^{-2\left(\frac{\cos\alpha}{\sigma^2}+1\right)} . \tag{5.21}$$

A closed-form expression for the normalized probability density is possible when $\alpha = \pi$, i.e., the repulsion between the oscillators is maximal. In this case,

$$P_{st}(\Delta\tilde{\Phi}) = \frac{1}{2B\left(\frac{1}{\sigma^2} - \frac{1}{2}, \frac{1}{2}\right)} \left|\sin\frac{\Delta\tilde{\Phi}}{2}\right|^{-2\left(1-\frac{1}{\sigma^2}\right)} , \tag{5.22}$$

[3]Note $\bar{g}_{21}\frac{\partial(\bar{g}_{11}\, W)}{\partial\tilde{\Phi}_1}$ and $\bar{g}_{22}\frac{\partial(\bar{g}_{12}\, W)}{\partial\tilde{\Phi}_1}$ do not vanish, for the reason that they are multiplied with $\bar{g}_{11}$ or $\bar{g}_{12}$ which when integrating over $\tilde{\Phi}_1$ isn't 0.

where $B(x, y)$ is the beta function. The shape of the probability density function in the general case Eq. (5.21) is shown in Fig. 5.2.

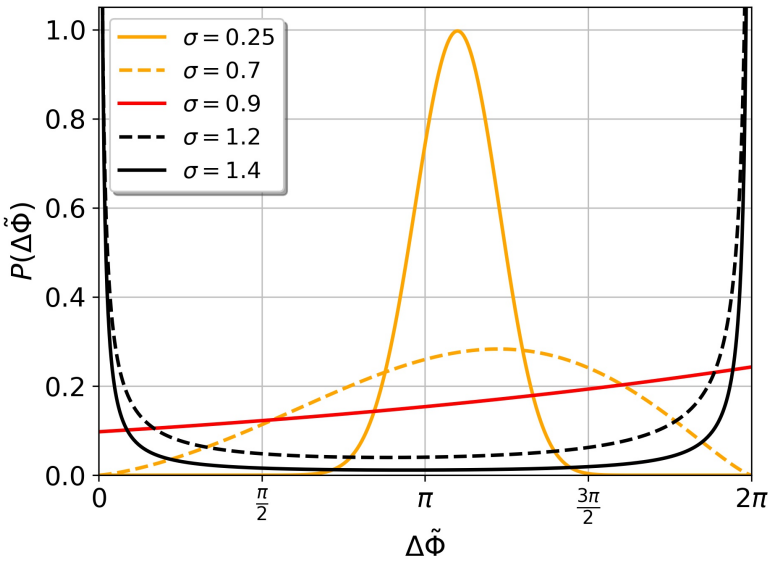

FIGURE 5.2: Probability density function Eq. (5.21), when $p_1 = 0.4$, $\alpha = 0.8\pi$ and the noise strength takes on various values (see legend). When the exponent of $\left|\sin\frac{\Delta\tilde{\Phi}}{2}\right|$ is positive, the function peaks asymmetrically at values larger than π (orange lines, solid and dashed); when the exponent is 0, it is an exponential distribution (red), and when it's negative, the distribution has an asymmetrical singularity at 0 (black lines, dashed and solid). The function will become a Dirac delta function when the exponent is -1 (not shown here). Figure reprinted with permission from [Gon+19].

In the expression Eq. (5.21), a nonzero phase shift parameter α introduces a curious asymmetry in form of the exponential factor which is not a periodic function, i.e., when we consider the distribution on $(0, 2\pi)$ wrapped around the circle, the derivative is not continuous at the singular absorbing point $\Delta\tilde{\Phi} = 0 = 2\pi$. The critical noise strength σ_{cr} beyond which the two clusters are synchronized to become one cluster, corresponds to the case where $P_{st}(\Delta\tilde{\Phi})$ becomes the delta distribution $P(\Delta\tilde{\Phi}) = \delta(\Delta\tilde{\Phi})$. Formally, this corresponds to divergence of the integral of the probability density Eq. (5.21). This happens if the exponent of $|\sin(\Delta\tilde{\Phi}/2)|$ is smaller than -1, and from this we can calculate the critical noise strength to be $\sigma_{cr}^2/2 = -\cos\alpha$.

In addition to the distribution of the phase difference $\Delta\tilde{\Phi}$, one needs to calculate the averages $\langle\cos\tilde{\Phi}_1\eta_1(t)\rangle$ and $\langle\sin\tilde{\Phi}_1\eta_2(t)\rangle$ to evaluate Eq. (5.13). Since $\eta_1(t)$ and $\eta_2(t)$ are independent Gaussian white noise processes and $\tilde{\Phi}_1$ is a functional of both η_1 and η_2 this can be accomplished by virtue of the Furutsu-Novikov formula [Fur63; Nov64]

$$\langle\sin\tilde{\Phi}_1\eta_2(t)\rangle = \int \delta(t-t')\left\langle\frac{\delta\sin\tilde{\Phi}_1}{\delta\eta_2}\right\rangle dt' = \left\langle\frac{d(\sin\tilde{\Phi}_1)}{d\tilde{\Phi}_1}\frac{\delta\tilde{\Phi}_1}{\delta\eta_2}\right\rangle = \left\langle\frac{1}{2}\sigma\cos^2\tilde{\Phi}_1\right\rangle = \frac{\sigma}{4}\,, \tag{5.23}$$

where $\frac{\delta}{\delta}$ is the functional derivative operator. Similarly, $\langle\eta_1(t)\cos\tilde{\Phi}_1\rangle = -\frac{\sigma}{4}$. A general expression for the Lyapunov exponent $\bar{\lambda}_1$, which describes the stability of the

cluster 1, is therefore

$$\bar{\lambda}_1 = -p_1 \cos\alpha - (1-p_1)\int_0^{2\pi} \cos(\Delta\tilde{\Phi}+\alpha)P(\Delta\tilde{\Phi})d\Delta\tilde{\Phi} - \frac{\sigma^2}{2}\,. \tag{5.24}$$

Lyapunov exponent Eq. (5.24) can even be analytically represented for the case $\alpha = \pi$

$$\bar{\lambda}_1 = \begin{cases} p_1 + p_2(\sigma^2-1) - \frac{\sigma^2}{2}, & \sigma^2 < 2\,; \\ 1 - \frac{\sigma^2}{2}, & \sigma^2 \geq 2\,. \end{cases} \tag{5.25}$$

Exchanging p_1 and p_2, we obtain the Lyapunov exponent $\bar{\lambda}_2$ of the other cluster. From this special case one can easily see that when $\sigma^2 < 2$, i.e., when a fully synchronized one-cluster state is unstable and the two-cluster Lyapunov exponents are well defined, they satisfy $\bar{\lambda}_1 + \bar{\lambda}_2 = 0$.

Through direct numerical evaluation of the Lyapunov exponent $\bar{\lambda}_1$ in Fig. 5.3 , we obtain a confirmation of the above analytical result.

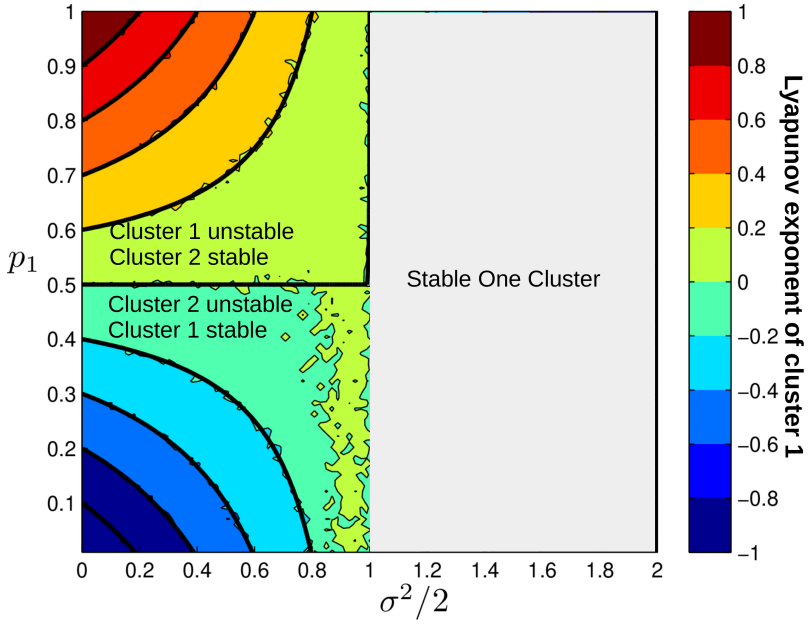

FIGURE 5.3: Diagram for linear stability of one of the two clusters indicated by its Lyapunov exponent, for phase shift $\alpha = \pi$ (maximal repulsion), in the plane of parameters p_1, the relative size of cluster 1, and the noise strength $\sigma^2/2$. Bold solid lines: theoretical result Eq. (5.25) obtained by Fokker-Planck formulation. Contour lines/color: by direct simulation of Eqs. (5.11)-(5.13) via Euler-Heun scheme. The Lyapunov exponent for cluster 1 below the critical noise strength $\sigma^2_{cr}/2 = 1$ is shown in color gradient. Above the critical noise strength one cluster is formed. The diagram is symmetric with respect to the line $p_1 = 0.5$ (except for very small positive exponents for $p_1 < 0$ and $\sigma^2 \approx 2$, which can be attributed to finite averaging time), indicating that together with the second cluster Lyapunov exponent $\bar{\lambda}_1 + \bar{\lambda}_2 = 0$. Figure reprinted with permission from Ref. [Gon+19].

For the case of the Kuramoto-Sakaguchi model with general phase shift parameter α, using Eq. (5.13) and the corresponding expression for $\bar{\lambda}_2$, we obtain for the sum

$$\begin{aligned}\bar{\lambda}_1 + \bar{\lambda}_2 = &- \cos\alpha - \sigma^2 - \cos\alpha \int_0^{2\pi} \cos\Delta\tilde{\Phi} P(\Delta\tilde{\Phi}) d\Delta\tilde{\Phi} \\ &+ (p_2 - p_1)\sin\alpha \int_0^{2\pi} \sin\Delta\tilde{\Phi} P(\Delta\tilde{\Phi}) d\Delta\tilde{\Phi}\end{aligned} \tag{5.26}$$

After applying integration by parts for the product of three functions[4], $\langle \sin\Delta\tilde{\Phi}\rangle$ can be written in terms of $\langle \cos^2(\Delta\tilde{\Phi}/2)\rangle$ and $\langle \cos\Delta\tilde{\Phi}\rangle$ in the following way

$$\begin{aligned}&\int_0^{2\pi} \sin\Delta\tilde{\Phi} P(\Delta\tilde{\Phi}) d\Delta\tilde{\Phi} \\ &= \int_0^{2\pi} \sin\Delta\tilde{\Phi} N_0 \exp\Big\{\frac{(p_2-p_1)\sin\alpha\Delta\tilde{\Phi}}{\sigma^2}\Big\} |\sin\frac{\Delta\tilde{\Phi}}{2}|^{-(\frac{2\cos\alpha}{\sigma^2}+2)} d\Delta\tilde{\Phi} \\ &= N_0\Big[\frac{\sigma^2}{(p_2-p_1)\sin\alpha}(\frac{\cos\alpha}{\sigma^2}+1)\int_0^{2\pi} \frac{\sin\Delta\tilde{\Phi}\cos\frac{\Delta\tilde{\Phi}}{2}}{\sin\frac{\Delta\tilde{\Phi}}{2}} P(\Delta\tilde{\Phi}) d\Delta\tilde{\Phi} \\ &- \frac{\sigma^2}{(p_2-p_1)\sin\alpha}\int_0^{2\pi} (\cos\Delta\tilde{\Phi}) P(\Delta\tilde{\Phi}) d\Delta\tilde{\Phi}\Big] \\ &= N_0\Big[\frac{\sigma^2}{(p_2-p_1)\sin\alpha}(\frac{\cos\alpha}{\sigma^2}+1)\langle 2\cos^2\frac{\Delta\tilde{\Phi}}{2}\rangle - \frac{\sigma^2}{(p_2-p_1)\sin\alpha}\langle\cos\Delta\tilde{\Phi}\rangle\Big]\end{aligned} \tag{5.27}$$

With the help of simple algebra, the relation $\bar{\lambda}_1 + \bar{\lambda}_2 = 0$ for the generic Kuramoto-Sakaguchi model can be shown. This means that for two narrowly distributed groups of repulsively coupled oscillators with common multiplicative noise, the larger group will dissolve while the smaller group is attractive (Fig. 5.3). Simultaneous attraction into two clusters is not possible.

5.4 Deterministic Evolution

We first explore how well the WS integrability is preserved in numerical simulation of deterministic equations. Here the original Kuramoto-Sakaguchi model is not optimal. After a short initial transient, the evolution of $R_1 = |Z_1|$ effectively comes to a halt as soon as a steady state is reached, i.e., $R_1 = |Z_1|$ is zero for repulsive coupling or unity for attractive coupling. Instead, we integrate a model of type Eq. (3.1) with a prescribed modulated time-dependent forcing $\omega(t) = 0.2\sin(1.752t)$, $H(t) = 0.4\cos(2.33t)\cdot Z$, and $N = 10$, designed to ensure the state remains nontrivial (see Fig. 5.4). Integrating this deterministic equation, we use the standard Runge-Kutta method of 4th order (RK4) and the first-order Euler method.

First, comparing Fig. 5.4 panels (a) and (b), where the two methods Eq. (5.8) and Eq. (5.9) of determining the constants of motion are used, we can conclude that, while the errors in the constants of motion are similar for large steps, the calculation

[4]Integration by parts of three functions

$$\int_{\tilde{b}}^{\tilde{a}} \bar{u}\bar{v}d\bar{w} = [\bar{u}\bar{v}\bar{w}]_{\tilde{b}}^{\tilde{a}} - \int_{\tilde{b}}^{\tilde{a}} \bar{u}\bar{w}d\bar{v} - \int_{\tilde{b}}^{\tilde{a}} \bar{v}\bar{w}d\bar{u} \tag{5.28}$$

where $d\bar{w} = e^{\frac{(p_2-p_1)\sin\alpha}{\sigma^2}\Delta\tilde{\Phi}} d\Delta\tilde{\Phi}$, $\bar{w} = \frac{\sigma^2}{(p_2-p_1)\sin\alpha} e^{\frac{(p_2-p_1)\sin\alpha}{\sigma^2}\Delta\tilde{\Phi}}$, $\bar{u} = \sin\Delta\tilde{\Phi}$, $d\bar{u} = \cos\Delta\tilde{\Phi} d\Delta\tilde{\Phi}$ and $\bar{v} = (\sin\frac{\Delta\tilde{\Phi}}{2})^{-(\frac{2\cos\alpha}{\sigma^2}+2)}$, $d\bar{v} = -\frac{1}{2}(\frac{2\cos\alpha}{\sigma^2}+2)(\sin\frac{\Delta\tilde{\Phi}}{2})^{-(\frac{2\cos\alpha}{\sigma^2}+3)}\cos\frac{\Delta\tilde{\Phi}}{2} d\Delta\tilde{\Phi}$. And $[\bar{u}\bar{v}\bar{w}]_{\tilde{b}}^{\tilde{a}}$ vanishes in this case due to periodicity in $\bar{v}$.

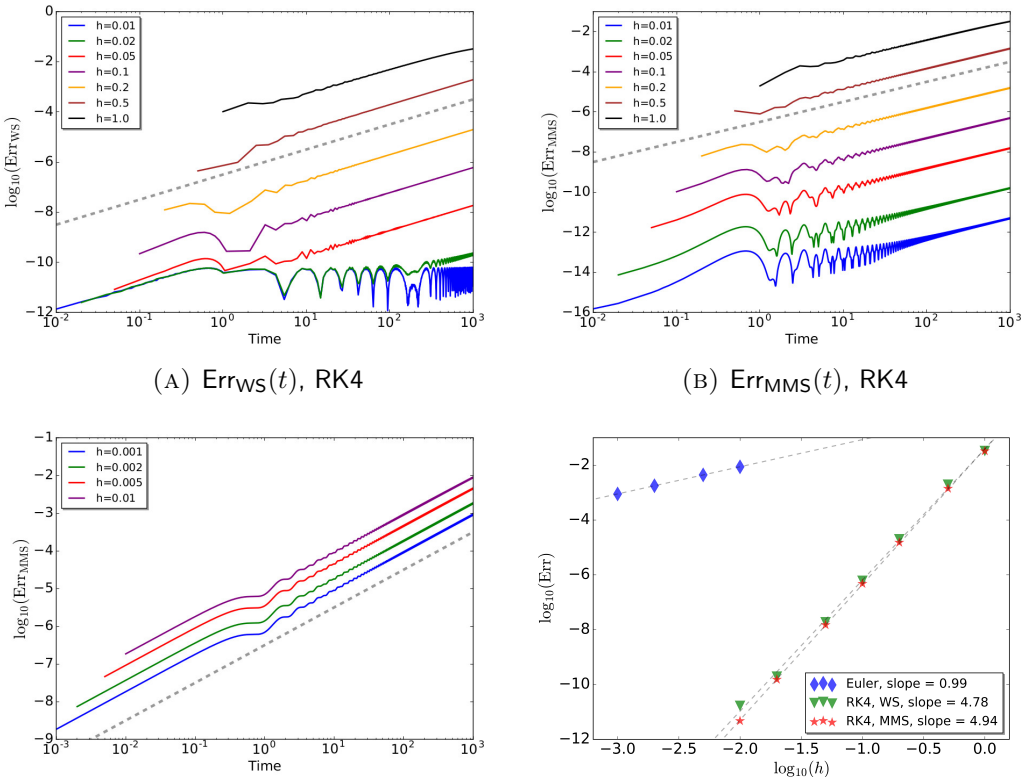

(A) $\mathrm{Err}_{\mathrm{WS}}(t)$, RK4 (B) $\mathrm{Err}_{\mathrm{MMS}}(t)$, RK4

(C) $\mathrm{Err}_{\mathrm{MMS}}(t)$, Euler (D) $\log_{10}\mathrm{Err}(T)$ vs. $\log_{10} h$

FIGURE 5.4: Time evolution of discretization errors as calculated from the drift in the constants of motion (Eq. 5.9), with RK4 (A-B) and Euler scheme (C), of a deterministic Kuramoto model, which was designed to ensure the state remains nontrivial. Dashed lines in (A-C) have slope = 1 in log10-log10 plot. (D) shows the numerical errors at end time $T_{\mathrm{int}} = 1000$ vs. time step h, as well as their linear fits (shown in legend). Figure reprinted with permission from Ref. [Gon+19].

of the errors via $\mathrm{Err}_{\mathrm{WS}}$ Eq. (5.8) does not allow for a proper estimation of very small errors, due to the necessity of a minimization procedure which can be performed only with finite precision. Therefore, for the rest of the section we calculate the errors using only $\mathrm{Err}_{\mathrm{MMS}}$ Eq. (5.9).

The second observation is that in all the cases the errors grow roughly linearly in time, with prefactors depending on the integration step h: $\mathrm{Err}_{\mathrm{MMS,RK4}} \sim h^{4.94}t$ for the RK4 method, and $\mathrm{Err}_{\mathrm{Euler}} \sim h^{0.99}t$ for the Euler method, indicating a drift of the constants of motion. This is consistent with the known fact that the numerical error per time step is h^5 for RK4, and h for Euler.

In Fig. 5.5 we present the results for the integration of the deterministic equation Eq. (5.3) with $\omega_0 = \sigma = 0$, $N = 100$ and $\alpha = 0.54\pi$ (slightly repulsive). Here we use rather large integration steps to make the clustering effect visible during a relatively short transient time interval, before the main order parameter becomes very small and the dynamics stops. One can see that for $h > 0.6$ the order parameter R_2, which measures formation of a two-cluster state, grows to macroscopic values.

For instructive purposes, we explore here which type of perturbations are introduced by the numerical integration methods to the original dynamics Eq. (5.3) when noise is not present. The simplest case is to estimate the perturbations introduced by the Euler method. The Euler method models a continuous-time dynamical system $\dot{\varphi}_j = \bar{f}_j(\vec{\varphi})$ up to the order h as a map $\varphi_j(t+h) = \varphi_j(t) + h\bar{f}_j[\vec{\varphi}(t)]$. Then we might

ask, what continuous equation is integrated by the same map correctly up to the order h^2. Looking for this equation in the form of $\dot{\varphi}_j = \bar{f}_j(\vec{\varphi}) + h\bar{g}_j(\vec{\varphi})$, we find

$$\bar{g}_j(\vec{\varphi}) = -\frac{1}{2}\sum_k \bar{f}_k(\vec{\varphi})\frac{\partial}{\partial\varphi_k}\bar{f}_j(\vec{\varphi}) \ .$$

Substituting for the Kuramoto-Sakaguchi model $\bar{f}_j = \omega_0 + \mathrm{Im}\left[Ze^{i(\alpha-\varphi_j)}\right]$ (details and result to h^3 order are presented in Appendix D), we obtain a modified equation where the error in the Euler integration is part of the dynamics

$$\dot{\varphi}_j \quad = \quad \omega_0 + \mathrm{Im}\left[Ze^{i(\alpha-\varphi_j)}\right] - \frac{\epsilon}{4}\mathrm{Im}\left[Ze^{i(2\alpha-\varphi_j)} + ZZ_2^*e^{i\varphi_j} - Z^2e^{i2(\alpha-\varphi_j)}\right] \quad (5.29)$$

Here $Z_2 = \langle \exp(2i\varphi_k)\rangle_k$ is the second Kuramoto-Daido mean-field. One can see, that in addition to the new coupling terms proportional to $\sin\varphi$ or $\cos\varphi$, which do not violate the WS integrability, terms proportional to $\sin 2\varphi$, $\cos 2\varphi$ appear, which violate the WS integrability and may result in the formation of two clusters. Clusters of the third order can presumably be attributed to terms $\sim \sin 3\varphi$ etc. appearing in the third order errors in h.

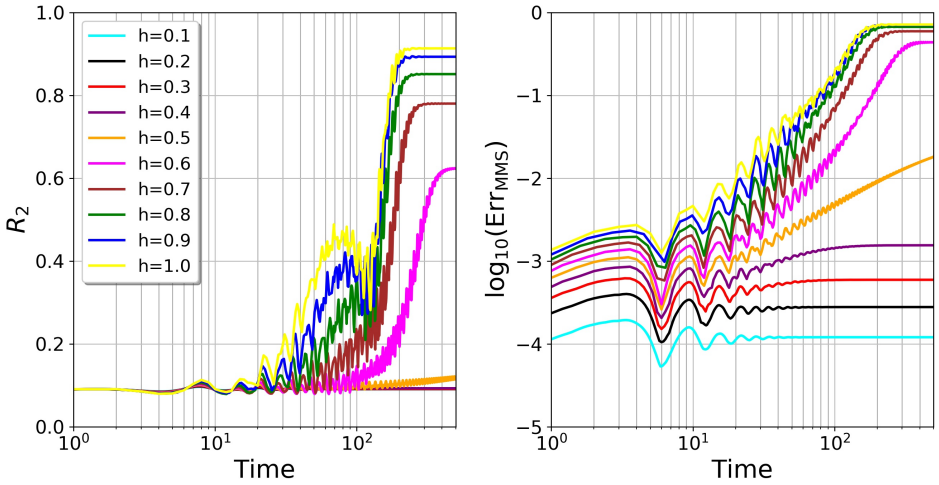

FIGURE 5.5: Main model Eq. (5.3) with $\omega_0 = \sigma = 0$ (no noise), $N = 100$ and $\alpha = 0.54\pi$ are integrated using the Euler method. Clustering, indicated by the second Kuramoto-Daido order parameter R_2 (Eq. 2.11) (left) and errors deviating from the partial integrability (Eq. 5.9) (right) grow together in time. The time series are averaged over 10 random initial conditions of phases drawn from a uniform distribution on the unit circle. Cluster formation on the left always corresponds to poor conservation of the constants on the right. Figure reprinted with permission from Ref. [Gon+19].

5.5 Numerical Evaluation of Clustering

In numerical simulations of model Eq. (5.3) (details shall be outlined below) we may observe different clustered states, illustrated in Fig. 5.6.

We quantify the formation of synchronized clusters with the help of the Kuramoto-Daido mean-fields Eq. (2.11).

After long integration time, the first-order mean-field Z_1 for repulsive coupling is either small if noise is present, or vanishes completely in the deterministic case. The second-order parameter $R_2 = |Z_2|$ is maximal and equal to 1 for two fully synchronized

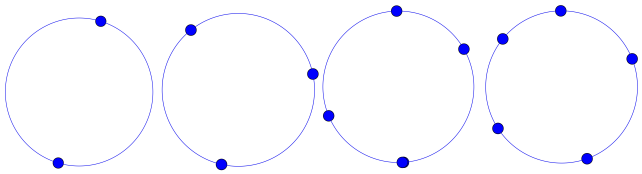

FIGURE 5.6: Besides 2-cluster and 3-cluster states discovered by Gil et al., 4 or 5 clusters can also be found for large integration steps. Shown here are the multiclusters, formed under model Eq. (5.3), from the same set of initial conditions of 100 Kuramoto phase oscillators, drawn randomly from a uniform distribution, with coupling phase shift $\alpha \in (\pi/2, \pi)$ (repulsive coupling regime), various integration step sizes h and noise strength σ, after an integration time of T_{int}. (a): $\sigma = 0.01$, $\alpha = 0.3$, $h = 1.0$, $T_{\text{int}} = 220,000$; (b): $\sigma = 0.1$, $\alpha = 0.4$, $h = 1.5$, $T_{\text{int}} = 225,000$; (c): $\sigma = 0.1$, $\alpha = 0.4$, $h = 2.0$, $T_{\text{int}} = 100,000$; (d): $\sigma = 0.1$, $\alpha = 0.45$, $h = 2.0$, $T_{\text{int}} = 100,000$. In most cases the final distributions of clusters are close to equipartition; in some cases the dynamics is quite complex, with switchings between different nearly-clustered states. Figure reprinted with permission from Ref. [Gon+19].

clusters of arbitrary sizes with phase difference π between them. Altogether, the degree of the formation of two clusters can be measured by a growth of R_2 approaching values close to one. We will henceforth use the evolution of R_2 as an indication for a two-cluster state.

5.6 Stochastic Evolution

Throughout this section we interpret the stochastic system Eq. (5.3) in the Stratonovich sense. However, the additional drift term needed to transform it into Itô interpretation vanishes in the case where the two noise terms correspond to complex isotropic noise term, i.e., $\sigma_1 = \sigma_2$ in Eq. (5.3). Therefore, the numerical schemes for both Stratonovich and Itô interpretations can be used to integrate the phases in the case of two noise terms of equal strength. On the other hand, the two noise terms in Eq. (5.3) do not commute according to commutativity condition (8.10), because $\sum_j \cos\varphi_j \frac{\partial \sin\varphi_{j'}}{\partial\varphi_j} \neq \sum_j \sin\varphi_j \frac{\partial \cos\varphi_{j'}}{\partial\varphi_j}$. Therefore it is sensible for us to only use lower-order integration schemes (see Appendix A and Appendix E). Only in the case of noise in a single direction (i.e., $\sigma_1 \neq 0$, $\sigma_2 = 0$), higher-order methods like the stochastic Runge-Kutta method [Bur98] are used.

In Fig. 5.7 we show the results in the case of two relatively strong noise terms $\sigma_1 = \sigma_2 = 0.1$. The integration is performed with the Euler-Heun scheme for various time steps h. Due to the rotational invariance preserved by two noise terms of equal strength, we have set $\omega_0 = 0$. One can clearly see the formation of two clusters, indicated by values of R_2 growing close to one, on a time scale $\sim h^{-1}$. For a weaker noise $\sigma = 0.01$, clustering appears much slower. This dependence of the clustering time scale on the integration step size demonstrates that clustering in this system is a numerical artefact. In fact, when we break WS integrability by adding a term to the stochastic dynamics Eq. (5.3) which is proportional to the error in the deterministic integration scheme as in Eq.(5.29), namely

$$\dot{\varphi}_j = \omega_0 + \text{Im}\left\{\left[Ze^{i\alpha} + \sigma\xi - \frac{\epsilon}{4}\left(Ze^{2i\alpha} + ZZ_2^* e^{2i\varphi_j} - Z^2 e^{2i\alpha}\right)\right] e^{-i\varphi_j}\right\} , \qquad (5.30)$$

we observe a robust clustering of two synchronized subgroups under dynamics Eq. (5.30) at a similar time scale as in the original system Eq. (5.3) for an integration time step

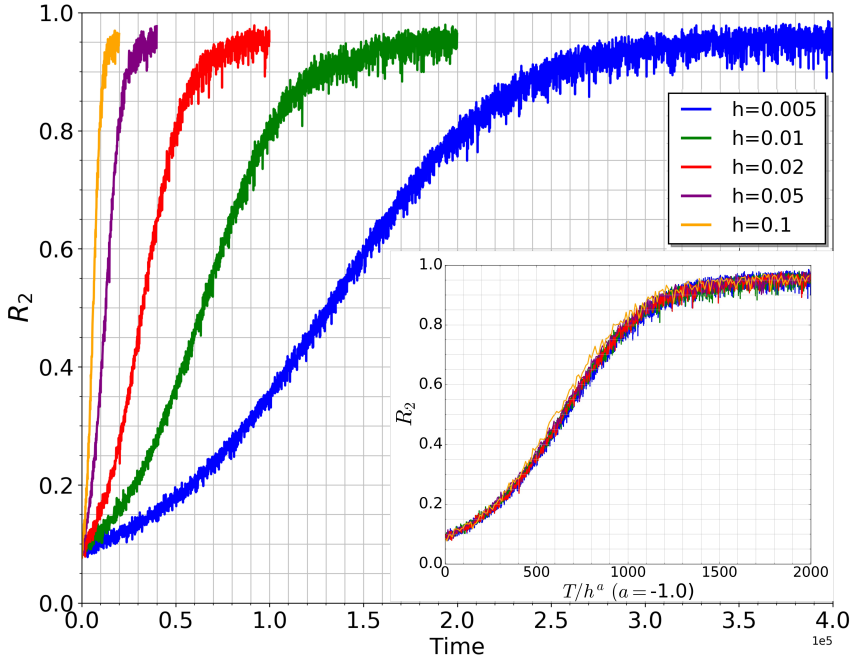

FIGURE 5.7: Evolution of the second Kuramoto-Daido order parameter R_2 under integration of Eq. (5.3) with strong noise. using Euler-Heun scheme for different step sizes h. Inset: collapse of the curves when plotted as functions of ht. The data is averaged over simulations with 10 different sets of initial conditions. System parameters: system size $N = 100$, intrinsic frequency $\omega_0 = 0$, noise strength $\sigma = 0.1$, phase shift $\alpha = 0.6\pi$. Figure reprinted with permission from Ref. [Gon+19].

of $h = \epsilon$ (see Fig.5.8).

In Fig. 5.9, we compare different integration schemes applied to models with one or two noise terms. Here for the cases of two noise terms (like in Fig. 5.7) and of one noise term (where we set $\omega_0 = 10$ because the rotational symmetry is broken), we present results for the Euler-Heun scheme, suitable for the Stratonovich interpretation of the SDE. Additionally, we show the results of the stochastic Runge-Kutta scheme 4th-order (sRK4), which is suitable for the one-noise term case only, because of the non-commutativity of the two noise terms mentioned above. One can see that all plots are qualitatively similar, with only some quantitative differences. As one would expect, the conservation of the constants of motion under the sRK4 scheme is the best, and here also the growth of the second Kuramoto-Daido order parameter is rather weak on the chosen time interval $t < 2 \times 10^5$. Additionally, we performed simulations with the Euler-Maruyama scheme with Stratonovich shift for the model Eq. (5.3) in the Stratonovich interpretation, both with one noise term and with two noise terms (where the Stratonovich shift is zero), all of which yield quantitatively identical results to the Euler-Heun scheme and are therefore not shown.

We can conclude this section by stating that in general, numerical schemes do not conserve the integrals of motion of the system, and eventually may lead to formation of clusters. Because the numerical methods for integrating SDE typically have lower order than the deterministic ones, the clusters may be more easily observed in the integration of noisy equations. In the deterministic case, clustering may not be observed at all if a zero mean-field steady state is reached first. The presence of noise can prolong the time within which the constants of motion continue to drift and their deviation from their initial values continues to grow until at some point fully synchronized multiclusters are formed.

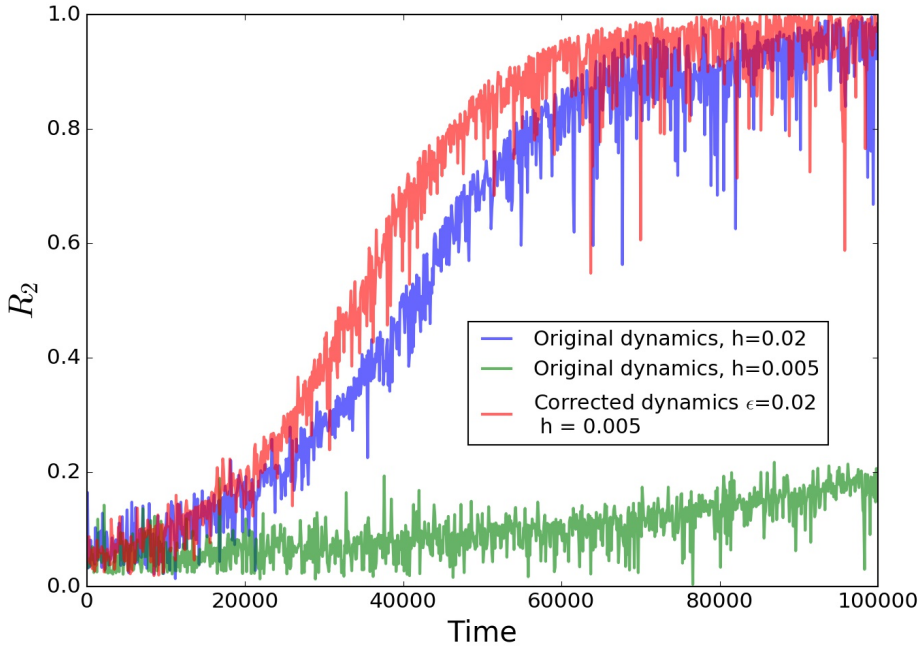

FIGURE 5.8: Three Euler-Heun integrations of identical initial conditions showing the time series for the 2-cluster order parameter R_2. Blue and green: under the original model Eq. (5.3) with 2 equal noise terms, with time step $h_0 = 0.02$ and $h_1 = 0.005$, respectively. Red: under the modified dynamics Eq. (5.30) with the perturbation amplitude $\epsilon = h_0$ in the modified dynamics and time steps $h = h_1$. The time scales at which the 2 clusters build up for the blue and red time series are comparable, supporting the hypothesis that the Fourier terms of second order in the discretization errors of the integration scheme are responsible for the formation of two clusters. Figure reprinted with permission from Ref. [Gon+19].

As mentioned in Sec. 5.2, the best way to avoid the numerical artefacts of clustering is to integrate the Watanabe-Strogatz equations Eq. (3.4). However, in order to accomplish this, one has to perform multiple Möbius transforms at each time step for a full time series of the mean-field, which may be quite computationally expensive. [5] Furthermore, discretization errors will still be present in integrating the low-dimensional dynamics of the Möbius group parameters. Only multicluster formation would be guaranteed to no longer occur.

5.7 Van der Pol Oscillators: Oscillators with Naturally Occurring Clusters Under Repulsive Coupling and Common Noise

Unlike the Kuramoto model, more realistic oscillator models such as Van der Pol oscillators have limit cycles which intrinsically contain higher-order Fourier terms and additional amplitude dynamics. Under common additive noise and repulsive coupling, formation of multiclusters is no longer forbidden and could now naturally occur. We consider N identical repulsively all-to-all coupled Van der Pol oscillators subject to

[5] However, it should be noted that the method via iterated Möbius Map introduced in Ch. 4 would be a better alternative. It is faster than integrating WS equations, and it preserves the constants of motion.

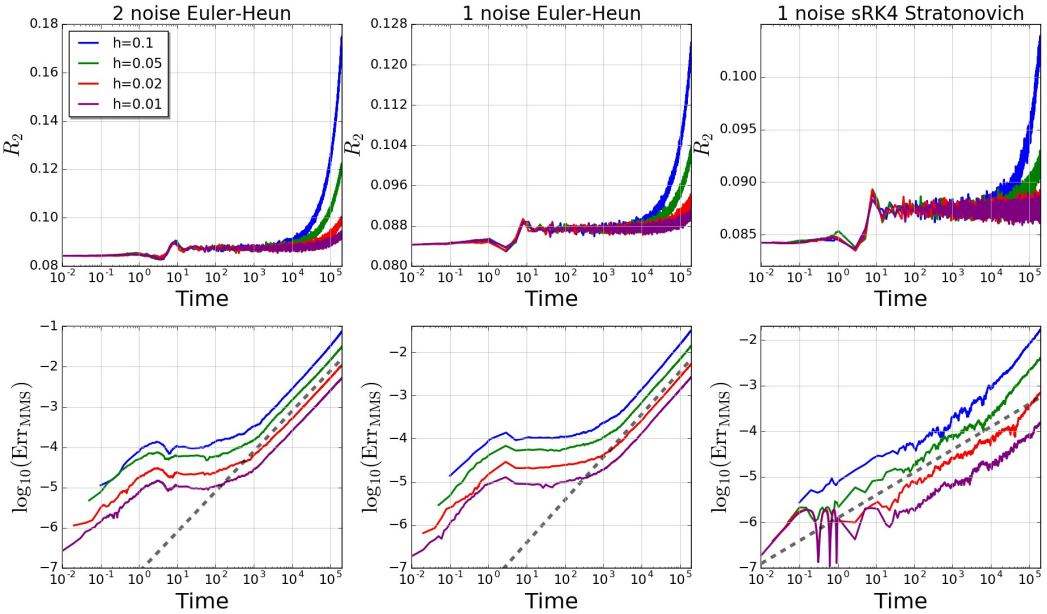

FIGURE 5.9: Simulations of Eq. (5.2) with 1 and 2 noise terms. We show R_2 (top panels) and numerical errors (bottom panels) as functions of time, for the Euler-Heun and sRK4 order methods. Constant parameters: $N = 100$, noise strength $\sigma = 0.01$, phase shift $\alpha = 0.6\pi$. Intrinsic frequency $\omega_0 = 0$ for 2 noise terms, and $\omega_0 = 10$ for one noise term. Resulting evolution is averaged over 8 different initial conditions (same for all experiments). The dashed lines in the left and middle columns (Euler-Heun method) have slopes equal to 1, whereas in the right column the slope is 0.5, showing the superiority of the sRK4 method of integration. Figure reprinted with permission from Ref. [Gon+19].

additive common Gaussian white noise in the y direction

$$\begin{aligned}\dot{x}_j &= y_j \\ \dot{y}_j &= \bar{a}(1-x_j^2)y_j - x_j - \bar{b}\frac{1}{N}\sum_{k=1}^{N}(y_k - y_j) + \sigma\eta(t)\ .\end{aligned} \tag{5.31}$$

Here $\bar{b} > 0$ is the repulsive coupling strength, $\bar{a}$ parametrizes the nonlinearity of the Van der Pol oscillators, σ is the noise strength, and $\eta(t)$ is a scalar random Gaussian variable. To distinguish from later use of a and b in Ch. 6, we use $\bar{a}$ and $\bar{b}$ here. Using phase reduction [Win67; PD19] the additive noise term will become multiplicative with the linear phase response function as a factor.

With a similar approach to that of Sec. 5.3, one can determine the Lyapunov exponents for the two-cluster state in Eqs. (5.31) numerically by integrating a perturbation from one of the clusters in the linearized dynamics of the two-cluster system. Contrary to the case of the Kuramoto model, presented in Fig. 5.3, now in Fig. 5.10 we see that the two-cluster state with $p_1 \approx p_2$ is locally stable, which is confirmed in Fig. 5.11 by direct simulations of Eqs. (5.31). Here, we defined the Kuramoto order parameter R using the phases defined by virtue of Poincaré sections (see also Ref. [PRK01]). One oscillator has been chosen as a reference, and the moments of time $\bar{t}^{(1)}, \bar{t}^{(2)}, \ldots$ at which it crosses half-line $(x > 0, y = 0)$ have been determined. Then the phase differences of all other oscillators to the reference oscillator at time $\bar{t}^{(n)}$ are defined as $2\pi(t_j^{(n)} - \bar{t}^{(n)})/(\bar{t}^{(n+1)} - \bar{t}^{(n)})$. Here $t_j^{(n)} - \bar{t}^{(n)}$ is the time needed for the j-th oscillator to reach the Poincaré section (positive half-line) from its position at time $\bar{t}^{(n)}$.

In general, clustering strongly depends on the level of nonlinearity of the Van der

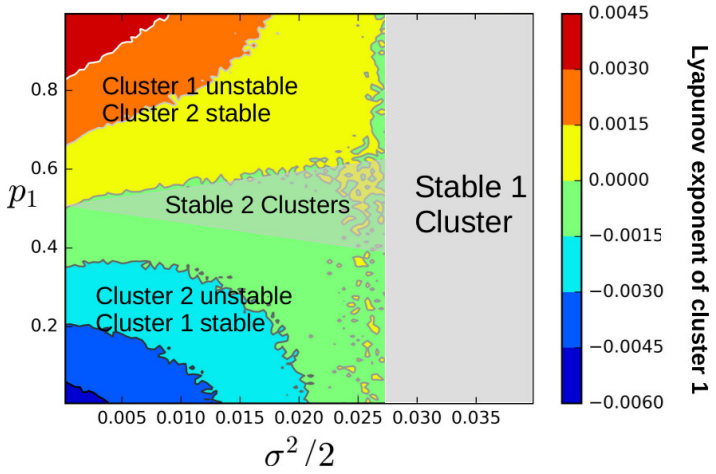

FIGURE 5.10: Contour plot of the Lyapunov exponent for one of the two clusters of repulsively coupled Van der Pol oscillators with additive noise in one direction, similar to Fig. 5.3. Contour plot of the Lyapunov exponent of cluster 1 is obtained by numerical integration of the linearized equations of Eqs. (5.31) for two clusters of relative sizes p_1 and $p_2 = 1-p_1$. Constant system parameters: $\bar{a} = 1$ and $\bar{b} = 0.01$ correspond to a highly nonlinear regime of the Van der Pol oscillator limit cycle. The numerical integration uses the Euler-Maruyama scheme with step size $h = 0.005$. Unlike in Fig. 5.3, an analytical expression for critical noise strength is hard to obtain. From the simulations we found it to be $\sigma_{cr}^2/2 \approx 0.027$ for Van der Pol oscillators. The gray region beyond the critical noise strength therefore corresponds to the formation of one cluster under strong noise. Compared to the Kuramoto-Sakaguchi model in Fig.5.3, a previously forbidden region of 2 stable clusters appears in the domain $p_1 \approx p_2$ below the critical noise strength. As the noise strength increases, the region with a negative Lyapunov exponent becomes larger, and it is evident that the common noise stabilizes both clusters. Figure reprinted with permission from Ref. [Gon+19].

Pol oscillators, described by $\bar{a}$. For large $\bar{a}$ ($\bar{a} = 1$, $\bar{b} = 0.01$), in the deterministic case three clusters can be observed. In the presence of noise, the picture is not so clear as several different cluster states may appear depending on the realization of initial conditions and of the noise, but at least a tendency toward temporal formation of clusters can clearly be observed. For small values of nonlinearity parameter $\bar{a}$, typically, non-clustered states are observed both with and without noise. This is to be expected, since the Van der Pol oscillators with a weakly anharmonic limit cycle have comparably much smaller amplitude for the higher-order Fourier terms in their phase response functions. In general, the dynamic complexity of systems like Eq. (5.31) with non-negligible amplitude dynamics can be very high, with chimera-like states becoming possible (i.e., where clusters coexist with dispersed elements), and a full characterization is beyond the scope of this thesis.

From the above observation we can therefore conclude that there exists a qualitative difference between the dynamics of the phase oscillator model (e.g., Fig. 5.3), and that of the more general oscillator model with additional amplitude dynamics (e.g., Fig. 5.10), specifically under a repulsive coupling and common noise: while under the Kuramoto-Sakaguchi model clusters are not able to form, under the Van der Pol model they are naturally forming and are stablized by the common stochastic forces.

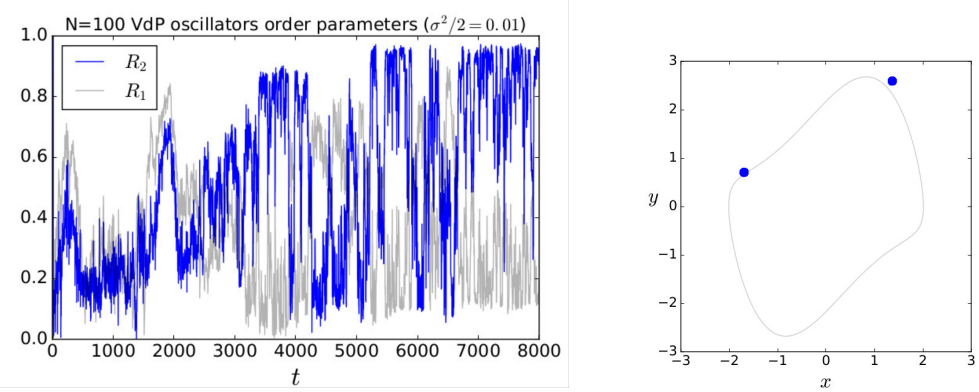

FIGURE 5.11: Direct simulation of Van der Pol oscillator ensemble of size $N = 100$ under weak common additive noise and repulsive coupling results in stable two clusters with relative sizes $p_1 = 53\%$ and $p_2 = 47\%$ after a transient. Left: time series for order parameters R_1 and R_2 during the initial transient from normal Gaussian random initial conditions in the (x, y) plane. Right: snap shot of two stable clusters formed after integration time $T_{\text{int}} = 33000$. System parameters are $\bar{a} = 1.0$, $\bar{b} = 0.01$ and $\sigma^2/2 = 0.01$. Euler-Maruyama integration scheme with $h = 0.001$ is used. This is consistent with the negative evaporation Lyapunov exponents for both clusters within the triangular parameter region in Fig. 5.10. Figure reprinted with permission from Ref. [Gon+19].

5.8 Conclusion

In this chapter, we apply WS theory to the Kuramoto-Sakaguchi model of repulsively coupled phase oscillators under common noise, studied previously in Ref. [GKM09] . Although both WS theory and the stability analysis of clustered states exclude the possibility for an appearance of clusters as observed in Ref. [GKM09], the numerical observations of clustering can be generally explained as artefacts from the discretization of numerical simulations. The correct long term behavior for repulsively coupled phase oscillators under common noise is either an incoherent state with no clustering (when the common noise has weaker effect compared to coupling forces) or a completely coherent state (when the common noise has a stronger effect compared to coupling forces). We study the numerical errors of different deterministic and stochastic schemes by monitoring the evolution of the constants of motion which must be conserved under the exact dynamics.

It should be stressed that the conclusions of WS theory only apply to a restricted class of phase oscillators which approximate weakly coupled, weakly nonlinear limit cycle oscillators. Violation of WS integrability occurs naturally in general coupled oscillator systems. We show that in the case of repulsively coupled Van der Pol oscillators noise-induced or deterministic clustering can indeed be easily observed in regimes of larger nonlinearity.

Due to the limitation of the Kuramoto-Sakaguchi system in describing real-world oscillator models or even more complicated coupled systems of differential equations, in terms of numerics, this chapter presents only a cautionary tale. For most types of high-dimensional coupled differential equations, a hidden low-dimensional dynamics such as present in Kuramoto-type systems is not available, nor do there often exist integrals of motion. For these systems, often the only way to measure or to gauge numerical errors is by using integration steps which are as small as possible, and to compare results under various degrees of numerical accuracy.

Chapter 6

Finite-Size Induced Cross-Correlation in Non-Identical Populations

Despite the mathematical simplicity of the Kuramoto model, the ground-breaking theoretical treatments which simplify the original high-dimensional dynamics frequently face the limitation that they are derived at the thermodynamic limit. Specifically, the critical synchronization transition, as solved by Kuramoto, was derived under the assumption of the thermodynamic limit, in order for the assumption of the constant mean-field to be valid. The latter is necessary for the self-consistency equation to be applied. The Ott-Antonsen theory of the mean-field evolutionary equation was similarly derived at the thermodynamic limit. However, one important real-world phenomenon that is missing from these descriptions is the fluctuating mean-field of the ensemble when the ensemble is finite.

As mentioned in the introduction (Sec. 2.2.3), a system of infinite number of Kuramoto oscillators at the supercritial state (i.e. beyond the synchronization transition) exhibit the coexistence of two subgroups. One subgroup is completely synchronous, with their natural frequency band located at the central bulge of the frequency distribution. In the synchronous subgroup, the oscillators are frequency- and phase-locked by the constant mean-field. A second subgroup is completely asynchronous, and with their natural frequencies flanking either side of the central bulge of the frequency distribution. In the asynchronous subgroup, the oscillators are not locked to the mean-field, and instead rotate incoherently at their own natural frequencies. When the coupling strength increases, the synchronous group recruits more and more oscillators from outside the central bulge of the frequency distribution, and more and more oscillators are locked by the increasing mean-field.

For a finite-sized ensemble, this picture is qualitatively similar, except that the Kuramoto mean-field now fluctuates continuously with an amplitude which depends on the ensemble size N in a nontrivial way [Dai87; Hon+07; Hon+15; PP18]. Intriguingly, the persistent fluctuations of the mean-field are most pronounced close to the critical transition, and can be attributed to the weak chaoticity of the finite-population dynamics [Bar13; PP16].

In this chapter, we investigate the effect of the mean-field of a finite-sized Kuramoto oscillator ensemble. Specifically, how does the fluctuation of the mean-field of a finite ensemble act on the oscillators that compose it? To answer that, we approximate the fluctuating mean-field with Gaussian white noise, effectively returning the finite-sized model to an earlier model, namely the Kuramoto-Sakaguchi model under common multiplicative noise (Eq. 5.3 in Ch. 5), which corresponds to adding an externally imposed noise on the mean-field. The difference from the setup of model

Eq. 5.3 is that here we consider non-identical oscillators and attractive coupling under infinite system-size limit — the classic Kuramoto setup.

Considering the well known effect of noise-induced synchronization (Sec. 2.3.1), we calculate the induced ordering effect by the fluctuating mean-field, first analytically via the Fokker-Planck formulation, then numerically of the induced cross-correlation between pairs of oscillators of different intrinsic frequencies. As expected, there are discrepancies between the analytical approach and the measurement in numerical experiments due to the fact that the fluctuating mean-field is qualitatively different from the approximate mean-field; nevertheless, the two approaches present qualitatively similar results.

Due to the limited space and the scope of the author's own contribution to the whole of this collaborative project, only analytical results are presented here. We refer the reader to the publication [PGP19] for a detailed presentation of the numerical results.

We find it instructive to begin the analytical approach with a Kuramoto model at the thermodynamic limit under external Gaussian white noise in the complex plane. We will in the end analytically derive the cross-correlation of a pair of oscillators outside the synchronous region as a function of system parameters — noise strength, system size, and the difference of the intrinsic frequencies of the pair.

6.1 Analytical Derivation for the Deterministic Case

As a first step of the derivation, we calculate the pair-wise correlation under a purely deterministic setup, i.e., under the classic, i.e. infinite-sized Kuramoto model

$$\dot{\varphi} = \omega + \varepsilon R \,\mathrm{Im}[e^{i(\Theta-\varphi)}] \,, \tag{6.1}$$

where the complex mean-field is $Z := R\exp(i\Theta) = \int_0^{2\pi} d\varphi \int_{-\infty}^{\infty} d\omega P(\varphi|\omega) g(\omega) e^{i\varphi}$. (See Sec. 2.2.3 for the finite-sized model.) ω is the non-identical intrinsic frequency of the oscillator, which has a continuous distribution $g(\omega)$. Here $g(\omega)$ can have an infinite support. ε is the coupling strength. $P(\varphi|\omega)$ is the conditional probability distribution of the oscillator phase φ given intrinsic frequency ω.

We define a mean-field frequency by $\bar{\omega} := \dot{\Theta}$, then go into its co-rotating frame by redefining phase $\varphi = \bar{\omega}t + \tilde{\varphi}$ and obtain

$$\dot{\tilde{\varphi}} = \omega - \bar{\omega} - \varepsilon R \sin\tilde{\varphi} \tag{6.2}$$

For a given frequency ω the probability density of the phase is:

$$P(\tilde{\varphi}, \omega) \sim \frac{1}{|\dot{\tilde{\varphi}}|} \tag{6.3}$$

since the probability of observing a value $\tilde{\varphi}$ is inversely proportional to the rotational speed at this point $|\dot{\tilde{\varphi}}|$. With normalization constraint

$$P(\tilde{\varphi}, \omega) = (|\omega - \bar{\omega} - \varepsilon R \sin\tilde{\varphi}| C_0)^{-1} \,, \tag{6.4}$$

where $C_0 = \int_0^{2\pi} (1/|\omega - \bar{\omega} - \varepsilon R \sin\tilde{\varphi}|) d\tilde{\varphi}$ is the normalization constant. Using a change of variable

$$\sin\tilde{\varphi} = \frac{z - z^{-1}}{2i}, d\tilde{\varphi} = -\frac{idz}{z} \,, \tag{6.5}$$

where $z = \exp(i\tilde{\varphi})$, and defining $\lambda = (\bar{\omega} - \omega)/\varepsilon R$, when $\lambda > 1$

$$\begin{aligned} C_0 &= \frac{2}{\varepsilon R} \oint_{C:|z|=1} \frac{1}{(z - z_+)(z - z_-)} dz \\ z_+ &= i(-\lambda + \sqrt{\lambda^2 - 1}); z_- = i(-\lambda - \sqrt{\lambda^2 - 1}) \ . \end{aligned} \tag{6.6}$$

In order to quickly determine the position of the poles in relation to the contour $\mathcal{C} : |z| = 1$, we check the modulus of $z_\pm$ by letting $\lambda = 1$, which means $z_\pm = -i$. Letting $\lambda \to \infty$, we find $z_+ \to 0$ and $z_- \to -\infty$, so $|z_+| < 1$ and $|z_-| > 1$, only z_+ is inside the contour. We do this similarly for $\lambda < -1$. Using the residue theorem, we obtain

$$C_0 = \frac{2\pi}{\varepsilon R\sqrt{\lambda^2 - 1}} \tag{6.7}$$

for both $\lambda > 1$ and $\lambda < -1$. Therefore the joint probability density function of phase (in co-rotating frame of the ensemble mean-field) and frequency is

$$P(\tilde{\varphi}, \omega) = \frac{\sqrt{(\bar{\omega} - \omega)^2 - (\varepsilon R)^2}}{|\omega - \bar{\omega} + \varepsilon R \sin\tilde{\varphi}| 2\pi} \ . \tag{6.8}$$

Because both $\cos(\tilde{\varphi})$ and $P(\tilde{\varphi}, \omega)$ are even functions, integrating over their product we get 0: $< \cos\tilde{\varphi} >= \int_0^{2\pi} \cos\tilde{\varphi} P(\tilde{\varphi}, \omega) d\tilde{\varphi} = 0$. With $< \sin\tilde{\varphi} >= \lambda\sqrt{1 - (1/\lambda^2)} - \lambda$, the expectation value of the first-order harmonics $\bar{Z}$ (averaged over phase) for a given intrinsic frequency ω is

$$\bar{Z}(\omega) =< e^{i\tilde{\varphi}} >= 0 + i < \sin\tilde{\varphi} >= i\lambda(\omega)\sqrt{1 - \frac{1}{\lambda(\omega)^2}} - i\lambda(\omega) \ . \tag{6.9}$$

The phases with the same intrinsic frequency clearly do not distribute uniformly along the circle, according to Eq. (6.8). But we can apply Möbius transform

$$e^{i\tilde{\psi}} = \frac{e^{i\tilde{\varphi}} - \bar{Z}}{1 - \bar{Z}^* e^{i\tilde{\varphi}}} \ , \tag{6.10}$$

on the distribution of $\tilde{\varphi}$ such that the transformed phases $\tilde{\psi}$ distribute uniformly on the circle. Taking the time derivative on both sides of Eq. (6.10), and with straightforward algebraic manipulations, we obtain the observed frequency of the transformed angles $\tilde{\psi}$

$$\nu(\omega) := \dot{\tilde{\psi}} = -\varepsilon R\lambda(\omega)\sqrt{1 - \frac{1}{\lambda(\omega)^2}} \ . \tag{6.11}$$

Since in the Kuramoto model R is constant in time for a given coupling strength ε in the thermodynamic limit, the observed frequency ν is also constant in time, only depending on the intrinsic parameter ω. So after the transformation, the phase angles in the asynchronous regions of the ensemble rotate at their own constant frequency $\nu(\omega)$ and grow linearly in time. With different frequency $\nu(\omega)$, the phases have zero pair-wise correlation, as defined by

$$\gamma_{12} = |e^{i(\tilde{\psi}_2 - \tilde{\psi}_1)}| \ . \tag{6.12}$$

The correlation equals to 1 only when the two oscillators share the same observed frequency. That is, either they are in the synchronous subgroup (the bulk of the frequency distribution), or they are in the asynchronous subgroup (flanking either

side of the frequency distribution) but share the same intrinsic frequency and initial phase. This shows that under the Möbius transformation, for non-identical oscillators, the asynchronous group has exactly pair-wise correlation 0 among their oscillators, whereas the synchronous group has exactly pair-wise correlation 1. This result will be different for both the noisy infinite-sized case and the deterministic finite-sized case below, since for what was before the asynchronous region, there will be a small correlation that arises from the fact that the mean-field is no longer constant but fluctuating in time.

6.2 Analytical Derivation for the Case with External Gaussian Noise

In this section, we approximate the fluctuation of the mean-field in a finite Kuramoto ensemble with an externally imposed Gaussian white noise. We add complex Gaussian noise to the constant Kuramoto mean-field, namely $Z := R\exp(i\bar{\omega}t)+\sigma\xi(t)$, where $\xi = -\eta_1+i\eta_2$ is complex Gaussian white noise, with η_1 and η_2 both scalar random Gaussian variables, $\langle\eta_m(t)\rangle = 0$, $\langle\eta_m(t)\eta_{m'}(t')\rangle = 2\delta_{mm'}\delta(t-t')$. A necessary assumption must be made for the noise strength to be weak, such that the intrinsic oscillator dynamics as well as the distribution function of their microscopic density of state remains the same, i.e., a wrapped Cauchy distribution (Eq. 6.8). We perform the same Möbius transform as before

$$e^{i\tilde{\vartheta}} = \frac{e^{i\tilde{\varphi}} - \bar{Z}}{1 - \bar{Z}^* e^{i\tilde{\varphi}}} \ , \tag{6.13}$$

this time using $\tilde{\vartheta}$ to denote the transformed phases. Under the weak noise limit, we can use the previously derived value $\bar{Z} = i\lambda\sqrt{1-\frac{1}{\lambda^2}} - i\lambda$, $\bar{Z}^* = -\bar{Z}$,

$$\cos\tilde{\vartheta} + i\sin\tilde{\vartheta} = \frac{(2-2i\lambda\bar{Z})\cos\tilde{\varphi}}{2i\lambda\bar{Z} + 2\bar{Z}i\sin\tilde{\varphi}} + i\frac{1+\lambda\sin\tilde{\varphi}}{\lambda+\sin\tilde{\varphi}} \ . \tag{6.14}$$

Noticing $\bar{Z}$ is purely imaginary, so the first term on the r.h.s. is real, we can match the two terms on either side

$$\cos\tilde{\vartheta} = \frac{(|\lambda|\sqrt{1-\lambda^{-2}})\cos\tilde{\varphi}}{\lambda+\sin\tilde{\varphi}} \ , \ \sin\tilde{\vartheta} = \frac{1+\lambda\sin\tilde{\varphi}}{\lambda+\sin\tilde{\varphi}} \ . \tag{6.15}$$

We can rewrite the second relation as

$$\frac{\sin\tilde{\varphi}}{\lambda+\sin\tilde{\varphi}} = \frac{\lambda\sin\tilde{\vartheta}-1}{\lambda^2-1} \ , \tag{6.16}$$

then the new observed rotational frequency of the transformed phases is

$$\begin{aligned}\tilde{\nu} := \dot{\tilde{\vartheta}} &= \nu + \varepsilon\mathrm{Im}\{[\sigma\eta_1(t) + i\sigma\eta_2(t)]e^{-i\tilde{\varphi}}\}\frac{\lambda\sqrt{1-\frac{1}{\lambda^2}}}{\lambda+\sin\tilde{\varphi}} \\ &= \nu + \varepsilon\left[-\sigma\eta_1(t)\frac{\lambda\sqrt{1-\frac{1}{\lambda^2}}\sin\tilde{\varphi}}{\lambda+\sin\tilde{\varphi}} + \sigma\eta_2(t)\frac{\lambda\sqrt{1-\frac{1}{\lambda^2}}\cos\tilde{\varphi}}{\lambda+\sin\tilde{\varphi}}\right] \ .\end{aligned} \tag{6.17}$$

We substitute the derived relations from Eqs. (6.15) and (6.16) and rearrange to obtain

$$\dot{\tilde{\vartheta}} = \nu + (\bar{A} + \bar{B}\sin\tilde{\vartheta})\eta_1(t) + \bar{C}\cos\tilde{\vartheta}\eta_2(t) \ . \tag{6.18}$$

$\bar{A} = -\sigma\varepsilon^2 R/\nu$, $\bar{B} = -\varepsilon\sigma(\omega - \bar{\omega})/\nu$ and $\bar{C} = \varepsilon\sigma$ are effective noise strengths. To distinguish from the Adler equation parameter A (Eq. (4.34)), we have used $\bar{A}$ here. ν is shown in Eq. (6.11).

We now assume two oscillators (in the asynchronous region at the thermodynamic limit) with very close intrinsic frequencies $\omega_1 \approx \omega_2$, and has a difference $\Delta\omega := \omega_1 - \omega_2 \ll \omega$ (this is valid since $|\omega|$ for supercritical states is far from zero). Because $\bar{A}, \bar{B} \sim 1/\nu$, and as before the observed frequencies ν depend on ω, $\nu = (\omega - \bar{\omega})\sqrt{1 - (\epsilon R)^2/(\bar{\omega} - \omega)^4}$, via Taylor expansion it is easy to establish $\nu \sim O(\omega)$ and $1/\nu \sim O(\omega)$. First we can define the difference between the observed frequencies $\Delta\nu$, such that we can write $\nu_2 = \nu_1 - \Delta\nu/2$, with $\Delta\nu \ll \nu_1$, while treating $\nu_2 \approx \nu_1$. Secondly, we can write $\bar{A}_1 \approx \bar{A}_2 := \bar{A}$ and $\bar{B}_1 \approx \bar{B}_2 := \bar{B}$.

To calculate the correlation function Eq. (6.12), we denote the Langevin equations for the difference and the sum of the two phases

$$a = \tilde{\vartheta}_1 - \tilde{\vartheta}_2 \qquad b = \tilde{\vartheta}_1 + \tilde{\vartheta}_2 \ , \tag{6.19}$$

whose differential equations are

$$\begin{aligned}
\dot{a} &= \Delta\nu + (\bar{A}_1 - \bar{A}_2)\eta_1(t) + \eta_1(t)(\bar{B}_1 \sin\tilde{\vartheta}_1 - \bar{B}_2 \sin\tilde{\vartheta}_2) + (\bar{C}_1 \cos\tilde{\vartheta}_1 - \bar{C}_2 \cos\tilde{\vartheta}_2)\eta_2(t) \\
\dot{b} &= 2\nu + (\bar{A}_1 + \bar{A}_2)\eta_1(t) + \eta_1(t)(\bar{B}_1 \sin\tilde{\vartheta}_1 + \bar{B}_2 \sin\tilde{\vartheta}_2) + (\bar{C}_1 \cos\tilde{\vartheta}_1 + \bar{C}_2 \cos\tilde{\vartheta}_2)\eta_2(t) \ .
\end{aligned} \tag{6.20}$$

Inserting identities

$$\begin{aligned}
\cos\tilde{\vartheta}_1 &= \cos\left(\frac{a+b}{2}\right) = \cos\frac{a}{2}\cos\frac{b}{2} - \sin\frac{a}{2}\sin\frac{b}{2} \\
\sin\tilde{\vartheta}_1 &= \sin\left(\frac{a+b}{2}\right) = \sin\frac{a}{2}\cos\frac{b}{2} + \cos\frac{a}{2}\sin\frac{b}{2} \\
\cos\tilde{\vartheta}_2 &= \cos\left(\frac{-a+b}{2}\right) = \cos\frac{a}{2}\cos\frac{b}{2} + \sin\frac{a}{2}\sin\frac{b}{2} \\
\sin\tilde{\vartheta}_2 &= \sin\left(\frac{-a+b}{2}\right) = \cos\frac{a}{2}\sin\frac{b}{2} - \sin\frac{a}{2}\cos\frac{b}{2} \ ,
\end{aligned}$$

and since $\bar{C}_1 = \bar{C}_2$, denoting $\bar{C}_1 = \bar{C}_2 = \bar{C}$, as well as $\bar{A}_1 = \bar{A}_2$ and $\bar{B}_1 = \bar{B}_2$, we obtain

$$\begin{aligned}
\dot{a} =& \Delta\nu + 2\bar{B}\,\sin\frac{a}{2}\cos\frac{b}{2}\,\eta_1(t) - 2\bar{C}\sin\frac{a}{2}\sin\frac{b}{2}\eta_2(t) \\
\dot{b} =& 2\nu + 2\bar{A}\eta_1(t) + 2\bar{B}\,\cos\frac{a}{2}\sin\frac{b}{2}\,\eta_1(t) + 2\bar{C}\cos\frac{a}{2}\cos\frac{b}{2}\eta_2(t) \ ,
\end{aligned}$$

and rewrite them in this short form

$$\begin{aligned}
\dot{a} &= \bar{h}_1 + \bar{g}_{11}(a,b)\eta_1(t) + \bar{g}_{12}(a,b)\eta_2(t) \\
\dot{b} &= \bar{h}_2 + \bar{g}_{21}(a,b)\eta_1(t) + \bar{g}_{22}(a,b)\eta_2(t) \ .
\end{aligned} \tag{6.21}$$

We use now a similar procedure at integrating over the fast variable as in Ref. [PDG19], or in the earlier part of this thesis Sec. 5.3, to obtain a Fokker-Planck equation for

the density of state of the slow variable a,

$$\frac{\partial P(a)}{\partial t} = \int_0^{2\pi} W(a,b)db \tag{6.22}$$

where $P(a)$ and $W(a,b)$ are probability density functions. Using the fact that b is rotationally invariant

$$\begin{aligned}\frac{\partial P(a)}{\partial t} &= \int_0^{2\pi} W(a,b)db \\ &= \int_0^{2\pi} \Big\{ -\bar{h}_1 \frac{\partial W}{\partial a} + \frac{\partial}{\partial a}\left[-\bar{g}_{11}\, W \frac{\partial \bar{g}_{11}}{\partial a} + \bar{g}_{11} W \frac{\partial \bar{g}_{21}}{\partial b}\right] \\ &+ \frac{\partial}{\partial a}\left[-\bar{g}_{12}\, W \frac{\partial \bar{g}_{12}}{\partial a} + \bar{g}_{12} W \frac{\partial \bar{g}_{22}}{\partial b}\right]\Big\} db + \frac{\partial^2}{\partial a^2}\Big(\int_0^{2\pi} (\bar{g}_{11}^2 + \bar{g}_{12}^2) W db\Big)\end{aligned} \tag{6.23}$$

Since $\frac{\partial \bar{g}_{11}}{\partial a} = \frac{\partial \bar{g}_{21}}{\partial b}$, $\frac{\partial \bar{g}_{12}}{\partial a} = \frac{\partial \bar{g}_{22}}{\partial b}$, above equation becomes

$$\frac{\partial P(a)}{\partial t} + \Delta\nu \frac{\partial P(a)}{\partial a} = \Big[\frac{(\bar{B}_1 + \bar{B}_2)^2}{4} + \bar{C}^2\Big] \frac{\partial^2}{\partial a^2}[P(a)(1-\cos a)] \tag{6.24}$$

The stationary solution of the 1D Fokker Planck equation (6.24) with flux $J = \Delta\nu/(2\pi)$[1]is

$$\Delta\nu P(a) - \left[\frac{(\bar{B}_1 + \bar{B}_2)^2}{4} + \bar{C}^2\right] \frac{\partial}{\partial a}[P(a)(1-\cos a)] = J = \frac{\Delta\nu}{2\pi} \tag{6.25}$$

Letting $(\bar{B}_1 + \bar{B}_2)^2/4 + \bar{C}^2 \approx \bar{B}^2 + \bar{C}^2 = \sigma_{\text{eff}}^2$ be an effective noise strength term for the (transformed) phase difference variable a, where σ_{eff} is the effective noise strength, we normalize the Eq. (6.25) as

$$KP - \frac{\partial}{\partial a}[(1-\cos a)P] = \tilde{J} \tag{6.26}$$

where

$$K = \frac{\Delta\nu}{\sigma_{\text{eff}}^2} \qquad \tilde{J} = \frac{J}{\sigma_{\text{eff}}^2}\ . \tag{6.27}$$

Integrating Eq. (6.26) from 0 to 2π yields

$$2\pi\tilde{J} = K. \tag{6.28}$$

With the two methods shown in Appendix F we solve for probability density function P that satisfies the stationary density flux equation

$$KP - \frac{\partial}{\partial a}[(1-\cos a)P] = \frac{K}{2\pi}\ . \tag{6.29}$$

The analytical result reads

$$\begin{aligned}\gamma_{12}^2 &= (\langle\cos a\rangle)^2 + (\langle\sin a\rangle)^2 \\ &= 1 + 4K^2[\mathrm{ci}^2(2K) + \mathrm{si}^2(2K)] - 4K[\mathrm{ci}(2K)\sin(2K) - \mathrm{si}(2K)\cos(2K)]\ .\end{aligned} \tag{6.30}$$

[1]The average frequency of a is $\Delta\nu$, hence $\langle\dot{a}\rangle_a = \Delta\nu, \int \frac{dP(a)}{dt} da = \Delta\nu, \int J da = \Delta\nu$, because $J = \frac{dP(a)}{dt}$, then $J = \frac{\Delta\nu}{2\pi}$.

In Fig. 6.1 we plot both the numerical approach via truncated series presented in Appendix F, as well as the analytical expression Eq. (6.30) above, and obtain visually the relation between the effective parameter difference K between two oscillators, given by Eq. (6.27), and their cross-correlation (synchronization index) γ_{12} under an idealized setup of an infinitely sized population with a mean-field biased by a common complex Gaussian white noise.

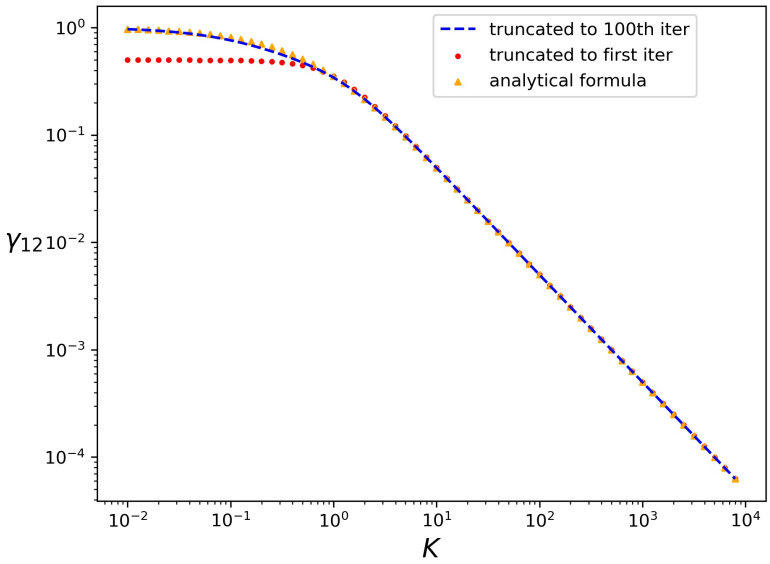

FIGURE 6.1: Synchronization index γ_{12} of two oscillators in the transformed frame as a function of their effective parameter difference K, $K = \Delta\nu/\sigma^2_{\text{eff}}$ (Eq. (6.27)), calculated by three methods: two approximate functions using numerical method listed in Appendix F up to two various degrees of truncation of the iterated series (Eq. 8.55 to first iteration and Eq. 8.53 to hundredth iteration, i.e., $1/r_{100} = 0$), one analytical function which is exact (Eq. 6.30).

6.3 Conclusion

In order to theoretically examine the effect that the finite-sized fluctuation of the Kuramoto mean-field in an ensemble of non-identical oscillators has on the population, we have turned to a model of a Kuramoto ensemble in the thermodynamic limit, whose mean-field has an externally imposed noisy component. Through analytical calculations, we have shown that the mean-field in the Kuramoto model with external noise leads to cross-correlation in the disordered part of the oscillator population. The size of the cross-correlations of an oscillator at a particular frequency depends only on the competition between the natural frequency mismatch from its neighbor, and the noise strength. This theoretical result is directly applicable to Kuramoto-type models, where the mean-field of a population is subject to external Gaussian noise.

Part III

SUMMARY AND DISCUSSION

Chapter 7

Conclusion and Future Work

In the world of complex interacting dynamics, the topic of this thesis only represents the tip of the iceberg. Most of the elementary dynamics of real-world coupled systems cannot be properly described as recurring or oscillatory. Similarly, most elementary oscillatory dynamics cannot be properly described by simple phase oscillators, i.e. Kuramoto oscillators. The complexity of real-world networks is also not to be underestimated. Nevertheless, studying simple elementary dynamics on simple connective topologies offer insights and understandings not obtainable via direct numerical simulations or experiments of more complex dynamical models. This can be shown especially through the main focus of this thesis, namely, the mean-field reduction approach of studying coupled one-dimensional phase oscillators. Specifically, the mean-field approach provides a framework for reducing high-dimensional systems to lower dimensions for the ease of mathematical analysis.

There exists a large body of literature dedicated to the study of phase synchronization under the framework of the Kuramoto model due to its simplicity and its ability to capture the essence of the synchronizing dynamics. While many oscillatory dynamics cannot be categorized as pure phase-coupled oscillators, there exist surprisingly complex systems whose elementary dynamics or emergent dynamics can be categorized as similar to that of phase oscillators. In these notable cases, the Kuramoto model can surpass its usual status as a toy model to qualify as a more realistic model. For systems such as groups of firing neurons and electric power grids, frequency or phase synchronization is crucial for the functioning and control of the system. The stability of the synchronized frequency of the grid is crucial in maintaining the stability of the whole network [NM15]. When a large network perturbation occurs, the synchronized state of the power grid is destroyed, leading to power failures that could results in high human and economic costs. Groups of neurons generate emergent oscillations that are slower than the individual neuronal firing. It has been postulated that different groups of neurons could communicate with the help of phase synchronization of these slower oscillations [Doe+09; FA11; Mal+15; SMC18]. When two groups of neurons are phase synchronized on a macroscopic scale, it can be seen as an opening of the communication channel, after which the individual neurons in the different groups can communicate. This two-stage communication mechanism could potentially help filter out noise or signals from other parts of the brain which are not phase locked [TSP10].

Comprised of four rather distinct problems, this thesis is centered on various extensions of the Kuramoto model, which is the canonical model for studying phase synchronization. The thesis can be divided into theoretical methods and numerical methods. In Ch. 3, we extend the theoretical method of Watanabe and Strogatz such that it can be applied to a wider range of models. In previous literature [WS94; MMS09], only first-order sinusoidally coupled identical phase oscillators have been

shown to have low-dimensional dynamics under identical coupling. Under higher-mode coupling, the theory wasn't shown to be applicable. We now have extended the theory to pure higher-mode coupling. Similar to the low-dimensional case, we apply a Möbius transformation — a non-linear coordinate transformation to reduce an arbitrarily high-dimensional system to 3 dimensions. To demonstrate that the theory is correct in practice, we carried out numerical simulations based on the reduced dynamical equations and see that the result matches that of the high-dimensional original equations.

Connecting the now extended theory to numerical simulations in earlier literature [KP15], we are able to explain, albeit partially, the asymmetric clustering observed in a second-mode coupled model. We exploit the fact that the unstable points that mark the boundaries of the basins of attraction under such a model correspond to the mathematical singularity in the Möbius transform at the final steady state. The main obstacle to an exact prediction of the final cluster distribution is the fact that the pole only appears in the Möbius transform at the synchronous steady state. The pole cannot be analytically obtained in a similar way at any other parameter values, despite that the unstable points are observed at all times in the dynamics. This fact gives us pause. Ideally, a map that transforms between the original phase dynamics and the low-dimensional dynamics should have pole(s) throughout the parameter range to correspond with the unstable points. Because analytical expression for the unstable points are missing everywhere except at the steady state, this might hint at the potential for a better theory. In addition, in numerical simulations, we have observed phenomena not yet observed in first-order models, namely, in the aforementioned second-mode coupled model, we observe that the system evolves to an unstable desynchronized state even though the coupling is positive, i.e. attractive.

Chapters 4 and 5 consist mostly of applying the theory of Watanabe and Strogatz to other methods and models. In Ch. 4 we devised a numerical method of modelling synchronizing phase dynamics using an iterated Möbius map. The Möbius map precisely evolves the dynamics of general sinusoidally coupled phase oscillators in discrete time, and can be seen as a discrete version of the well-known Adler equation. Using the derived Möbius map, we simulated dynamics under setups analogous to several continuous-time collective dynamics from previous literature, and recovered various known phenomena. These include the the synchronization transition in the Kuramoto-Sakaguchi model of non-identical oscillators, as well as chimera states under non-local coupling (chimera in two coupled populations of identical phase oscillators, and Kuramoto-Battogtokh chimeras on a ring). We also discovered new behavior under the discrete dynamics. For large coupling strengths, and in particular for large repulsive coupling, the discrete time dynamics can lead to new synchronization phenomena with continuous and discontinuous bifurcations to synchrony, which are not observed in the equivalent continuous-time models.

In Ch. 5, we apply the WS theory to the Kuramoto-Sakaguchi model of repulsively coupled phase oscillators under common noise, studied previously in Ref. [GKM09]. We were initially interested in the numerical findings of Ref. [GKM09], because they showed the model formed stationary clusters, which is directly at odds with the prediction from WS theory. Despite containing noise terms, the system in Ref. [GKM09] is integrable as shown by WS, which precludes the formation of clusters. The preclusion of stationary clusters is further confirmed by a stability analysis of the two-cluster states. Through detailed and systematic numerical analysis, we demonstrated that the observed clusters are actually artefacts stemming from the discretization of the numerical integration schemes.

In order to compare the result of phase oscillators to real-world oscillators, we

also studied Van der Pol oscillators under similar setup (repulsive coupling, under various noise strengths). Because the WS theory only applies to harmonic coupling of a single order, not to mixed orders, it naturally does not apply to amplitude coupled oscillators such as Van der Pol oscillators. Amplitude and phase coupled oscillators such as Van der Pol oscillators have a phase response function of more than one mode (or harmonic), so that the WS theory cannot be applied here. Under a similar setup as the phase oscillator model, Van der Pol oscillators therefore are allowed to form clusters, unrestrained by the WS theory.

Continuing with the theme of oscillators under common noise from Ch. 5, in the final part of the thesis (Ch. 6), we study the fluctuations of the Kuramoto mean-field in an ensemble of non-identical Kuramoto oscillators. Specifically, we are interested in how this fluctuation leads to cross-correlations of a pair of phase variables in the disordered subpopulations under super-critical condition. The disordered subpopulations consist of those oscillators with intrinsic frequencies either too slow or too fast compared to the population mean frequency to be synchronized. We approach the problem first by studying an infinitely-sized ensemble. By artificially imposing a white Gaussian noise as a source of fluctuation onto the ensemble mean-field, we approximate the fluctuation of the mean-field of a finite-sized population. For non-identical oscillators, this creates two competitive effects. On the one hand, the common fluctuating mean-field creates noise-induced synchronization on the sub-population, and on the other hand, the differences in the natural frequencies create a desynchronizing effect. Under such a setup using an infinite-sized population, we can derive an analytical formula for the pairwise phase cross-correlation of the disordered subpopulations.

In Ref. [PGP19], the above analytical result is then compared to the result from numerical experiments in actual finite-sized populations. Comparing the analytical result with numerical observations, we find similarities and differences. As confirmed by Ref. [PGP19], for either sub- or super-critical coupling strength there exist nearly periodic components in the mean-field. There are regions in the parameter space where phases are locked to these periodic components, corresponding to high pairwise cross-correlations. However, in between these special locked regions, the phases are largely incoherent due to frequency mismatch, and in such zones, we could obtain qualitative agreement with the analytical result, which is derived from an approximate setup using infinite populations.

7.1 Future Work and Outlook

We would like to highlight two directions into which the approaches of mean-field dynamics of coupled (phase) oscillators could be extended. The first is to extend existing mean-field theories (WS or OA theories) to include more varieties of coupling function and connection topology. Currently, both WS and OA formulations are limited to harmonic coupling of a single harmonic order. They are not applicable to mixed harmonic coupling. Besides this constraint on the form of the coupling, these mean-field approaches are restricted also by the connection topology and by the natural frequency distribution of the oscillators. In the first case, global coupling or simple topologies like star graphs [VZP14] or random networks are usually required. In the latter case, the frequency distribution must be a delta distribution in the case of WS theory, and a Cauchy distribution in the case of OA theory.

The second direction involves making further connections between the two mean-field theories, namely the WS and OA theories. There has been successful theoretical attempt at partially connecting the two [MMS09]. However, a complete picture is still lacking. The difficulty mainly lies in the fact that the OA equation is a special

solution on a sub-manifold for the Kuramoto mean-field Z, whereas the WS equation is a reduced equation of the coordinate transformation parameter (sometimes also known as WS order parameter) $\tilde{z}$, which at best can be only characterized as a quasi-mean-field. In almost all practical cases, $Z \neq \tilde{z}$. For WS theory, there exist attempts to extend it to non-identical oscillators: either at the thermodynamic limit [PR11], or a perturbation theory for almost but not completely identical oscillators [VRP16; Tyu+18]. However, there currently lacks a reduced mean-field dynamical theory for finite-sized fully non-identical oscillators.

In conclusion, the canonical Kuramoto model is a simple model that nevertheless captures the basic characteristics of synchronization. On a symmetrical network and with pure mode coupling, under certain frequency distributions, the complex N-body dynamics can be reduced analytically to simply the dynamics of the mean-field. This method might provide some basis for understanding more complex phenomena in numerical and real-world experiments. However, this is reduction is highly limited to symmetrical setups, and its significance to real-world application is still not quite clear. Therefore, in general, we should look for more applications of WS or OA theories in context where symmetry is not presumed, as well as a similar mean-field dynamical approach for general oscillators — those that are coupled with not only phases but also amplitudes.

Chapter 8

Appendix

A. Stratonovich Shift and the Two Interpretations of Stochastic Calculus

The two standard interpretations for stochastic differential equations are Itô and Stratonovich interpretations. The problem arises with multiplicative Langevin equation

$$\dot{x} = \bar{f}(X) + \bar{g}(x)\eta(t) \ , \tag{8.1}$$

where $\eta(t)$ is a Gaussian white noise, $\bar{f}$, $\bar{g}$ are generic functions. Equation 8.1 can be written as a Wiener process

$$dX = \bar{f}(X)dt + \bar{g}(X)dW(t) \ , \tag{8.2}$$

where $dW(t) = \eta(t)dt$.

An interpretation of the multiplicative term $\bar{g}(X)dW(t)$ needs to be provided, since due to the extreme randomness of the white noise, it is not clear what value of X should be used during an infinitesimal time-step dt. According to the Itô interpretation, the evaluation is the one before the beginning of the time step, i.e., $X = X(t)$. According to the Stratonovich interpretation, the evaluation is at the middle of the time step, $X = X(t + dt/2) = X(t) + dX(t)/2$. As shown in Ref. [Per+00], the evaluations at different time points have real implications when we consider for example the chain rule for taking the derivative of the product of two random processes

$$d(XY) = [(X + dX)(Y + dY)] - XY \ . \tag{8.3}$$

This expression can be written in many different ways. One possibility is to follow the Stratonovich interpretation

$$d(XY) = (X + \frac{dX}{2})dY + (Y + \frac{dY}{2})dX \ . \tag{8.4}$$

Another is to follow the Itô interpretation

$$d(XY) = XdY + YdX + dXdY \ . \tag{8.5}$$

Notice that under the Stratonovich interpretation, Eq. (8.4) obeys the ordinary differential calculus chain rule

$$d(XY) = X_S dY + Y_S dX \ , \tag{8.6}$$

whereas Eq. (8.5) does not obey such a rule, which means it represents a different

calculus from the ordinary differential calculus. This is also why the Stratonovich interpretation, as opposed to the Itô interpretation, is the more frequently used interpretation of statistical integrals in physics, because only under the Stratonovich interpretation, does the act of applying the standard calculus procedure for deriving the SDE remain valid.

However, in terms of numerical algorithms, most of the standard SDE integration schemes assume the Itô interpretation, such as the Euler-Maruyama, Milstein and stochastic Runge-Kutta schemes (there are exceptions such as the Euler-Heun scheme). Therefore to integrate an SDE under the Stratonovich interpretation using an algorithm assuming the Itô interpretation, one needs to add an additional Stratonovich shift to the SDE which is to be integrated. The correspondence between the equation and the algorithm is as follows. To integrate an equation of Stratonovich interpretation

$$d\mathbf{X} = \bar{\boldsymbol{f}}(\mathbf{X}(t), t)dt + \sum_m \bar{\boldsymbol{g}}_{\boldsymbol{m}}(\mathbf{X}(t), t)\, dW_m(t) \ , \tag{8.7}$$

using an algorithm assuming Itô interpretation, one should instead integrate the following equation

$$d\mathbf{X} = [\bar{\boldsymbol{f}}(\mathbf{X}(t), t) + \mathbf{S}(\mathbf{X}(t))]dt + \sum_m \bar{\boldsymbol{g}}_{\boldsymbol{m}}(\mathbf{X}(t), t)dW_m(t) \ , \tag{8.8}$$

where the Stratonovich shift $\mathbf{S}$ is

$$S_j = \frac{1}{2}\sum_{m,k} \bar{g}_{mk}\frac{\partial \bar{g}_{mj}}{\partial X_k}, \qquad X = \{X_1, ...X_j..., X_N\} \ . \tag{8.9}$$

In other words, the solutions provided by the numerical integration of Eq. (8.8) is equivalent to that of Eq. (8.7) under their corresponding interpretations.

On a related note, the commutativity condition

$$\sum_k \bar{g}_{mk}\frac{\partial \bar{g}_{m'k'}}{\partial X_k} = \sum_k \bar{g}_{m'k}\frac{\partial \bar{g}_{mk'}}{\partial X_k} \tag{8.10}$$

needs to be satisfied for stochastic schemes of higher-order to be used to an advantage. It has been shown, e.g., in Refs. [Bur98; BB98; BBT04], that the strong order of convergence of all higher-order integration methods for SDEs with non-commutative noise cannot be higher than 0.5. Strong order of convergence is defined by the average error made by the time-discretized approximation of the stochastic integration scheme in approximating each individual path of the continuous-time process. Therefore for non-commutative noise terms it would be sufficient to restrict ourselves to using only low-order integration schemes, such as Euler-Heun or other Euler based schemes.

B. Numerical Procedure for Integrating the Z^2-Mean-Field Model via WS Formulation

The numerical procedure of integrating the system Eq. (3.20) via the WS formulation is summarized as follows.

1. Transform the original phases $\{\varphi_j^0\}$ into the space of the constants of motion ψ via $\mathcal{M}_2^{-1}$, using the recommended initial conditions $\zeta(0) = H(0) = Z^2(0)$ and $\tilde{\beta}(0) = 0$.

2. Integrate the WS equations (3.22) using a standard algorithm such as the Euler scheme to obtain the new values of $\zeta(t^{(n+1)})$ and $\tilde{\beta}(t^{(n+1)})$. Higher order schemes cannot be used here, since H cannot be calculated at several points within one integration step. Combined with the constants ψ_j we carry out the transform $\mathcal{M}_2$ (Eq. (3.15)) to obtain N values between 0 and π: $\bar{\varphi}_1^{(n+1)}, \bar{\varphi}_2^{(n+1)}, \ldots, \bar{\varphi}_N^{(n+1)}$. Given $\varphi_j^{(n+1)}$ which is the true new values of φ_j at step $n+1$, array $\{\bar{\varphi}_j^{(n+1)}\}$ will contain some unknown numbers of $\bar{\varphi}_j^{(n+1)}$ that are equal to $\varphi_j^{(n+1)} + \pi$ instead of to the true $\varphi_j^{(n+1)}$ due to the non-uniqueness of the mapping $\mathcal{M}_2$.

3. We denote the result of step (2) $\{\bar{\varphi}_j^{(n+1)}\} =: \{\bar{\varphi}_j^{n+1,0}\}$, and create a second array of phases shifted by π $\{\bar{\varphi}_j^{n+1,1}\} := \{\bar{\varphi}_j^{n+1,0} + \pi\}$. Then the j-th element of the correct phase array at time step $n+1$ is

$$\varphi_j^{(n+1)} = \underset{\tilde{w}=0,1}{\arg\min} |\bar{\varphi}_j^{n+1,\tilde{w}} - \varphi_j^{(n)}| \,, \tag{8.11}$$

where $\{\varphi_j^{(n)}\}$ are the phases at step n. This chooses the correct result from mapping $\mathcal{M}_2$, which guarantees the continuity of the flow of the variable phases.

4. The new phases $\{\varphi_j^{(n+1)}\}$ found at step $n+1$ give the new value for the global field $H(t^{(n+1)}) = Z(\vec{\varphi}^{(n+1)})^2$. Repeat steps (2)-(4) until a steady state is reached.

It is clear from the procedure, that because at every step a transform back to the original space is needed, numerically integrating the reduced WS equations does not save computational time. However, it does by default preserve the constants of motion, which the numerical integration of the original phase equations will not guarantee (see e.g., Ref. [Gon+19]).

C. Derivation of the Möbius Maps Solution for Adler Equation

We derive the following formula for the proposed Möbius map

$$\mathcal{K}_{\lambda,V,\beta}(z) = \frac{(\sigma + i\lambda\Gamma)z + e^{i\beta}\Gamma}{(\sigma - i\lambda\Gamma) + ze^{-i\beta}\Gamma} \tag{8.12}$$

where

$$\sigma = \sqrt{1-\lambda^2}, \quad \Gamma = \tanh\left(\frac{A\tau}{2}\sigma\right) \,. \tag{8.13}$$

Equation (8.12) (Eq. 4.36 in the main text) is the solution of the dynamics under Adler equation Eq. (4.34), $z^{(n+1)} = \mathcal{K}_{\lambda,V,\beta}\left(z^{(n)}\right)$. Before doing so, we first address the meaning of the parameter λ in the main Adler equation, which aids in the derivation later.

Geometric Meaning of the Parameter λ

The meaning of parameter λ is of a geometrical nature and is clear by observing the fixed points z_{FP} of the map $\mathcal{K}_{\lambda,V,0}$ when there is no rotation $\beta = 0$, obtained by letting $z^{(n+1)} = z^{(n)}$

$$z_{\mathrm{FP}} = i\lambda \pm \sigma. \tag{8.14}$$

When $|\lambda| < 1$, there are two fixed points on the unit circle: $z_{\mathrm{FP}}^{1,2} = i \sin\tilde{\vartheta} \pm |\cos\tilde{\vartheta}|$, where λ takes on the geometric meaning of $\sin\tilde{\vartheta}$, where $\tilde{\vartheta}$ is angular position of the fixed point. When V is furthermore positive, the fixed point at $\tilde{\vartheta}$ is stable and the one at $\pi - \tilde{\vartheta}$ is unstable (see Fig. 8.1(a)).

When $|\lambda| > 1$, there are no fixed points on the unit circle. Instead, two neutrally stable fixed points (i.e., centers) are inside and outside the circle: $z_{\mathrm{FP}}^{3,4} = i\lambda \pm i\sqrt{\lambda^2 - 1}$, and the phases merely rotate around the center inside the circle.

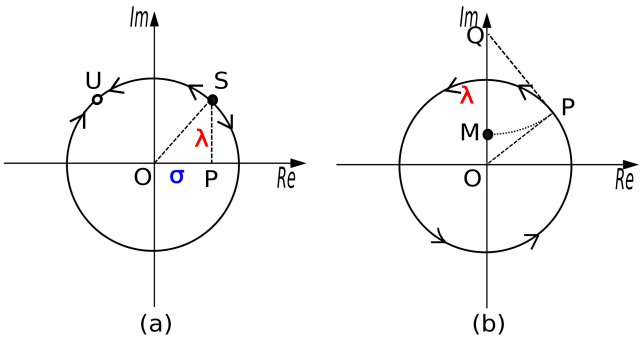

FIGURE 8.1: Significance of parameter λ in terms of the fixed points of a simplified Möbius map $\mathcal{K}_{\lambda,V,0}$. For simplicity, rotational parameter β in the map is set to zero. (a) $|\lambda| < 1$. When $V > 0$, the stable fixed point is S with angle $\tilde{\vartheta}$, and the unstable fixed point is U. $\lambda = \sqrt{1-\lambda^2}$ is the distance SP, and σ is hence OP. When $V < 0$, the positions of stable and unstable fixed points are switched. (b) $|\lambda| > 1$. The center M is inside the circle, and another center N is outside the circle (not shown). All other points rotate around M. The length of OQ is now λ. With the right triangle OPQ, the length of PQ is equal to the magnitude of σ, where $\sigma = i\sqrt{\lambda^2 - 1}$. The position of the center M can be determined geometrically by the length of PQ from Q, as shown by the arc.

When $\lambda = 0$, the stable and unstable fixed points are at 0 and π, respectively.

Now we are ready to derive the Möbius map Eq. (8.12).

To simplify the derivation, we first ignore the rotation parameter by letting $\beta = 0$, i.e., the Adler equation (4.34) becomes

$$\dot{\varphi} = A(t)(\lambda - \sin\varphi) \ . \tag{8.15}$$

Also for simplicity, we let the forcing amplitude $A(t)$ be a delta kick, $A(t) = A\delta(t - t_0)$, where t_0 is the kick time instance.

The kick map $\mathcal{K}_{\lambda,V,0}$, where $V = \int_0^\tau A(t)dt = A\tau$, τ the kick duration, is derived as a composition of four Möbius maps. First, a map $\overline{\mathcal{M}}$ which removes the bias term λ in the phase response function of the Adler equation; second, a map $\mathcal{G}$ which transforms the WS parameter from before the delta kick to after the kick; third, $\mathcal{M}$ which contracts the phase coordinate (result of $\overline{\mathcal{M}}$, with bias removed) according to the WS parameter after the kick (result of $\mathcal{G}$); and fourth, the inverse map $\overline{\mathcal{M}}^{-1}$ which transforms the coordinate back to the original coordinate with the bias.

Removal of bias in the phase response function via $\overline{\mathcal{M}}$

Consider the Adler equation (8.15), which we can write in terms of a unit-length vector z in the complex plane

$$\dot{z} = \frac{A(t)}{2}(2i\lambda z - z^2 + 1) \ , \tag{8.16}$$

where $A(t) = A\delta(t - t_0)$, and z is the complex exponential of the phase $z = \exp(i\varphi)$.

We make a first transformation which removes the bias term $(\lambda - \sin\varphi) \to (-\sin\varphi)$ in (8.15). We use a Möbius map $\overline{\mathcal{M}} = \mathcal{C}_{i\Delta}$ ($\mathcal{C}$ defined in Sec. 4.1)

$$\overline{\mathcal{M}} \ : \ z \to s, \quad s = \mathcal{C}_{i\Delta}(z) = \frac{i\Delta + z}{1 - i\Delta z} \ , \tag{8.17}$$

where the value of Δ $(0 \leq |\Delta| < 1)$, $\Delta \in \mathbb{C}$ as a transformation parameter is to be determined, and the factor i represents the fact that we are contracting the coordinates along the direction of the imaginary axis. This makes geometric sense especially when considering the case where $\lambda < 1$, namely we want to contract the points U and S to -1 and $+1$ respectively (see Fig. 8.1 (a)), which corresponds to having no bias term in the phase response function. Effectively, we are removing the first-order term from Eq. (8.16) via this first coordinate transform $\overline{\mathcal{M}}$.

Plug Eq. (8.17) into Eq. (8.16), we obtain the value for Δ by letting the term proportional to s be 0, and it is

$$\Delta = -\frac{1 - \sqrt{1 - \lambda^2}}{\lambda} \ . \tag{8.18}$$

After the transformation $\overline{\mathcal{M}}$, we obtain for s

$$\dot{s} = \frac{A(t)}{2}\sqrt{1 - \lambda^2}(1 - s^2) \ , \tag{8.19}$$

where s now stands for the first harmonic complex exponential of the original phases in a transformed coordinate system where the bias term in the phase response function is zero.

Delta Kick of the WS Parameter via $\mathcal{G}$

We now derive the second map $\mathcal{G}$ which corresponds to a kick of the WS group parameter $\tilde{z}^- \to \tilde{z}^+$, such that the phase variable s can be contracted according to $\tilde{z}^+$ via a third transform $\mathcal{M}$. Because at the continuous limit, the WS parameter $\tilde{z}$ is advanced according to the WS equation, we will first transform the WS equation.

Given the real function $A(t)$, the WS equation (Eq. (3.4)) for advancing $\tilde{z}$ is

$$\dot{\tilde{z}} = \frac{A(t)}{2}\sqrt{1 - \lambda^2}(1 - \tilde{z}^2) \ . \tag{8.20}$$

According to Eq. (8.20), if $\tilde{z}$ is real-valued before the kick, it will stay real-valued after the kick. In other words, the kick only shifts the value of $\tilde{z}$ along the real axis. This is because that before the kick, $\mathcal{G}$ is precisely the identity transform $\mathcal{I}$ since the variable $\tilde{z}$ is not under any force and therefore unchanged. To satisfy $\mathcal{G} = \mathcal{I}$, it must be that $\tilde{z}^- = 0$. Applying the map to $\tilde{z}^-$, it is clear that after the kick we can treat $\tilde{z}^+$ as a real parameter.

To write Eq. (8.20) as a map, we use an ansatz for $\mathcal{G}$ derived as follows. Generally, we want to rewrite an ODE

$$\dot{x} = \bar{f}(x) + \epsilon\bar{g}(x)\delta(t - t_0) \tag{8.21}$$

as a composite transform of three steps. Given $\mathcal{G}$ as the desired Möbius map: (1) transformation $\mathcal{G} : x(t_0^-) \to \mathcal{G}(x(t_0^-))$, (2) linearly shift the variable proportional the kick amplitude: $\mathcal{G}(x(t_0^-)) + \epsilon$, and (3) carry out the inverse transform $\mathcal{G}^{-1}$. So the

composite transform is summarized as

$$x(t_0^+) = \mathcal{G}^{-1}(\mathcal{G}(x(t_0^-)) + \epsilon) \ . \tag{8.22}$$

Defining a transformed variable $y := \mathcal{G}(x)$, $y(t_0^+) = y(t_0^-) + \epsilon$. We use an ansatz for $\mathcal{G}$

$$y = \mathcal{G}(x) = \int_x \frac{1}{\bar{g}(\bar{r})} d\bar{r} \ . \tag{8.23}$$

This ansatz is justified when we look at its time derivative

$$\begin{aligned} \dot{y} = \dot{x}\mathcal{G}'(x) = \dot{x}\frac{1}{\bar{g}(x)} \quad &| \quad \text{insert Eq. (8.21)} \\ = \frac{\bar{f}(x)}{\bar{g}(x)} + \epsilon\delta(t - t_0) \ . \end{aligned}$$

$\bar{g}(x)$, which is multiplied with the delta function has now been cancelled. This is exactly what is needed.

Applying the ansatz Eq. (8.23) to the WS equation (8.20), we obtain

$$\bar{p} = \mathcal{G}(\tilde{z}) = \int_{\tilde{z}} \frac{1}{1 - \bar{r}^2} d\bar{r} = \frac{1}{2} \ln(\frac{1 + \tilde{z}}{1 - \tilde{z}}) \ .$$

And the inverse of $\mathcal{G}$ is

$$\tilde{z} = \mathcal{G}^{-1}(\bar{p}) = \tanh(\bar{p}) \ ,$$

where $\bar{p} = \epsilon = \frac{A}{2}\sqrt{1 - \lambda^2}$.

As mentioned before, $\tilde{z}^- = 0$ is the WS transform parameter for before the kick,

$$\mathcal{G}(\tilde{z}^-) = \ln 1 = 0 \ ,$$

which means

$$\tilde{z}^+ = \tanh(\frac{A}{2}\sqrt{1 - \lambda^2}) \ .$$

General Möbius Map

Transformed phase parameter s is contracted along the circle via a Möbius transform $\mathcal{C}_{\tilde{z}^+}$ parametrized by the delta-kicked WS parameter $\tilde{z}^+$

$$\mathcal{C}_{\tilde{z}^+} \ : \ s^- \to s^+, \quad s^+ = \frac{\tilde{z}^+ + s^-}{1 + \tilde{z}^+ s^-} \tag{8.24}$$

And eventually s is transformed back to z to via $\overline{\mathcal{M}}^{-1} = \mathcal{C}_{-i\Delta}$

$$\overline{\mathcal{M}}^{-1} \ : \ s^+ \to z^+, \quad z^+ = \frac{s^+ - i\Delta}{1 + i\Delta s^+}. \tag{8.25}$$

The composite map without rotation is $\tilde{\mathcal{K}} = \overline{\mathcal{M}}^{-1} \circ \mathcal{C}_{\tilde{z}^+} \circ \overline{\mathcal{M}}$. Plug Eq. (8.24) ($\mathcal{C}_{\tilde{z}^+} : s^- \to s^+$) and Eq. (8.17) ($\overline{\mathcal{M}} : z^- \to s^-$) into Eq. (8.25). After algebraic manipulations, we obtain

$$\tilde{\mathcal{K}} \ : \ z^+ = \frac{(\sigma + i\lambda\tilde{z}^+)z^- + \tilde{z}^+}{\sigma - i\lambda\tilde{z}^+ + z^-\tilde{z}^+} \tag{8.26}$$

where $\sigma = \sqrt{1-\lambda^2}$ and $\tilde{z}^+ = \tanh(\frac{A}{2}\sigma)$. In the main text, $\tilde{z}^+$ is simply denoted Γ.

When rotations are considered as in the Adler equation (4.34), i.e., when the phase shift β is non-zero, map (8.26) can be easily modified. Phase shift β corresponds to the rotation of the frame of reference under which z is transformed by $\tilde{\mathcal{K}}$, which we can obtain by replacing $z^+ \to z^+ e^{-i\beta}$ and $z^- \to z^- e^{-i\beta}$. This concludes the derivation of the kick map $\mathcal{K}_{\lambda,V,\beta}$ (Eq. 8.12). When A is not a delta kick, it can be easily generalized to a cumulative impulse over the kick interval by replacing $A \to V$, where $V = \int_0^\tau A(t)dt$, where τ is the kick duration.

D. Multivariate Taylor Expansion of A Dynamical System

In the following two parts, we expand the coupled ODEs of the Kuramoto-Sakaguchi model $\dot{\varphi}_j = \omega + \mathrm{Im}\left[Ze^{i(\alpha-\varphi_j)}\right]$ in Taylor series, in order to model the errors of the discrete Euler step up to the second and third order in step size h. Without loss of generality, we set identical frequency $\omega = 0$.

To Second Order in Discretization Step Size h

For a smooth dynamics, represented by the ODE $\dot{\varphi}_j = f(\vec{\varphi}, \varphi_j)$, the multivariate Taylor expansion to the first order can be derived as

$$\begin{aligned}
&\varphi_j(t_0+h) - \varphi_j(t_0) = \int_0^h f(\vec{\varphi}, \varphi_j) \\
&= \int_0^h \Bigg\{ f(\vec{\varphi}(t_0), \varphi_j(t_0)) + \sum_k \Big[(\varphi_k(t) - \varphi_k(t_0)) \frac{\partial f(\vec{\varphi}, \varphi_j)}{\partial \varphi_k}\Big|_{t=t_0}\Big] \\
&+ \frac{1}{2!}\sum_{k'}\sum_k \Big[(\varphi_k(t) - \varphi_k(t_0))(\varphi_{k'}(t) - \varphi_{k'}(t_0)) \frac{\partial^2 f(\vec{\varphi}, \varphi_j)}{\partial \varphi_k \partial \varphi_{k'}}\Big|_{t=t_0}\Big] + \dots \Bigg\} dt \\
&\approx h f(\vec{\varphi}(t_0), \varphi_j(t_0)) + \sum_k \Big[\frac{\partial f(\vec{\varphi}, \varphi_j)}{\partial \varphi_k}\Big|_{t=t_0} \int_0^h (\varphi_k(t) - \varphi_k(t_0)) dt\Big]
\end{aligned} \tag{8.27}$$

where h is the step size of integration. In the last line, we truncate to the first-order in h. When the integral is approximated by Euler step $\varphi_k(t) = \varphi_k(t_0) + t f(\vec{\varphi}(t_0), \varphi_k(t_0))$

$$\begin{aligned}
\varphi_j(t_0+h) - \varphi_j(t_0) &\approx h f(\vec{\varphi}(t_0), \varphi_j(t_0)) + \sum_k \Big[\frac{\partial f(\vec{\varphi}, \varphi_j)}{\partial \varphi_k}\Big|_{t=t_0} \int_0^h t f(\vec{\varphi}(t_0), \varphi_k(t_0)) dt\Big] \\
&\approx h f(\vec{\varphi}(t_0), \varphi_j(t_0)) + \frac{h^2}{2} \sum_k \Big[\frac{\partial f(\vec{\varphi}, \varphi_j)}{\partial \varphi_k} f(\vec{\varphi}, \varphi_k)\Big]\Big|_{t=t_0}
\end{aligned} \tag{8.28}$$

Function f and derivative of f for identical Kuramoto-Sakaguchi oscillator dynamics in co-rotating frame are

$$f(\vec{\varphi}, \varphi_j) = \frac{1}{N}\sum_{j'} \sin(\varphi_{j'} - \varphi_j + \alpha) \tag{8.29}$$

$$\frac{\partial f(\vec{\varphi}, \varphi_j)}{\partial \varphi_k} = \begin{cases} \frac{1}{N}\cos(\varphi_k - \varphi_j + \alpha), & k \neq j \\ -\frac{1}{N}\sum\limits_{j' \neq j} \cos(\varphi_{j'} - \varphi_j + \alpha), & k = j \end{cases} \tag{8.30}$$

Plugging into Eq. (8.28)

$$\begin{aligned}
&\varphi_j(t_0+h)-\varphi_j(t_0)\\
&= hf(\vec{\varphi}(t_0),\varphi_j(t_0)) + \frac{h^2}{2}\Big\{\sum_{k\neq j}\Big[\frac{1}{N}\cos(\varphi_k-\varphi_j+\alpha)\frac{1}{N}\sum_{k'}\sin(\varphi_{k'}-\varphi_k+\alpha)\Big]\\
&- \frac{1}{N}\sum_{k\neq j}\cos(\varphi_k-\varphi_j+\alpha)\frac{1}{N}\sum_{k'}\sin(\varphi_{k'}-\varphi_j+\alpha)\Big\}\Big|_{t=t_0}
\end{aligned} \tag{8.31}$$

where the last term contains second-order harmonic coupling of φ_j. In summary,

$$\begin{aligned}
f(\vec{\varphi}(t_0),\varphi_j(t_0)) = \frac{\varphi_j(t_0+h)-\varphi_j(t_0)}{h} &- \frac{h}{2}\Big\{\sum_{k\neq j}\Big[\frac{1}{N}\cos(\varphi_k-\varphi_j+\alpha)\frac{1}{N}\sum_{k'}\sin(\varphi_{k'}-\varphi_k+\alpha)\Big]\\
&- \frac{1}{N}\sum_{k\neq j}\cos(\varphi_k-\varphi_j+\alpha)\frac{1}{N}\sum_{k'}\sin(\varphi_{k'}-\varphi_j+\alpha)\Big\}\Big|_{t=t_0},
\end{aligned} \tag{8.32}$$

so the Euler step actually integrates the following modified ODE to $O(h^2)$

$$\begin{aligned}
\dot{\varphi}_j &= \tilde{f}(\vec{\varphi}(t_0),\varphi_j(t_0))\\
&= \mathrm{Im}(Z_{KS}e^{-i\varphi_j} - \frac{h}{4}(Z_{KS}e^{i\alpha}e^{-i\varphi_j} + Z_{KS}e^{i\alpha}Z^*_{KS,2}e^{i\varphi_j} - Z^2_{KS}e^{-2i\varphi_j}))
\end{aligned} \tag{8.33}$$

where $Z_{KS} = e^{i\alpha}\frac{1}{N}\sum_k e^{i\varphi_k}$ is the Kuramoto-Sakaguchi mean-field.

Using standard definition of Kuramoto mean-field $Z = \frac{1}{N}\sum_k e^{i\varphi_k}$, and second Kuramoto-Daido order parameter $Z_2 = \frac{1}{N}\sum_k e^{i2\varphi_k}$, we obtain from Eq. (8.33)

$$\dot{\varphi}_j = \mathrm{Im}\left[Ze^{i(\alpha-\varphi_j)} - \frac{h}{4}(Ze^{i(2\alpha-\varphi_j)} + ZZ^*_2e^{i\varphi_j} - Z^2e^{i2(\alpha-\varphi_j)})\right]. \tag{8.34}$$

To Third Order in Discretization Step Size h

We can further ask, what is the smooth dynamics that the Euler scheme integrates up to $O(h^3)$? Based on our earlier expansion up to $O(h^2)$, we only need to include one term further in the Taylor expansion Eq. (8.27). When the integral is approximated by Euler step $\varphi_k(t) = \varphi_k(t_0) + tf(\vec{\varphi}(t_0),\varphi_k(t_0))$

$$\begin{aligned}
\varphi_j(t_0+h)-\varphi_j(t_0) \approx hf(\vec{\varphi}(t_0),\varphi_j(t_0)) &+ \frac{h^2}{2}\sum_k\Big[\frac{\partial f(\vec{\varphi},\varphi_j)}{\partial\varphi_k}f(\vec{\varphi},\varphi_k)\Big]\Big|_{t=t_0}\\
&+ \frac{h^3}{6}\sum_{k'}\sum_k\Big[f(\vec{\varphi},\varphi_k)f(\vec{\varphi},\varphi_{k'})\frac{\partial^2 f(\vec{\varphi},\varphi_j)}{\partial\varphi_k\partial\varphi_{k'}}\Big]\Big|_{t=t_0}.
\end{aligned} \tag{8.35}$$

For identical Kuramoto-Sakaguchi oscillator dynamics in co-rotating frame, function f and its first derivative of f are given in Eq. (8.29), Now we just need to

calculate the second derivative of f:

$$\frac{\partial^2 f(\vec{\varphi},\varphi_j)}{\partial\varphi_k\partial\varphi_{k'}} = \begin{cases} 0, & k\neq j, k'\neq j, k\neq k' \\ -\frac{1}{N}\sin(\varphi_k-\varphi_j+\alpha), & k'=k\neq j \\ \frac{1}{N}\sin(\varphi_k-\varphi_j+\alpha), & k'=j\neq k \\ \frac{1}{N}\sin(\varphi_{k'}-\varphi_j+\alpha), & k=j\neq k' \\ -\frac{1}{N}\sum\limits_{j'\neq j}\sin(\varphi_{j'}-\varphi_j+\alpha), & k'=k=j\ . \end{cases} \tag{8.36}$$

Evaluating $\sum\limits_{k'}\sum\limits_{k}\left[f(\vec{\varphi},\varphi_k)f(\vec{\varphi},\varphi_{k'})\frac{\partial^2 f(\vec{\varphi},\varphi_j)}{\partial\varphi_k\partial\varphi_{k'}}\right]$ for these cases we have

$$\sum_{k'}\sum_{k} f(\vec{\varphi},\varphi_k)f(\vec{\varphi},\varphi_{k'})\frac{\partial^2 f(\vec{\varphi},\varphi_j)}{\partial\varphi_k\partial\varphi_{k'}} \tag{8.37}$$

$$\begin{cases} k=j=k', & f^2(\vec{\varphi},\varphi_j)\frac{\partial^2 f(\vec{\varphi},\varphi_j)}{\partial\varphi_j^2} = -\frac{1}{N}f^2(\vec{\varphi},\varphi_j)\sum\limits_{j'\neq j}\sin(\varphi_{j'}-\varphi_j+\alpha) \\ k=j\neq k', & \sum\limits_{k'} f(\vec{\varphi},\varphi_j)f(\vec{\varphi},\varphi_{k'})\frac{\partial^2 f(\vec{\varphi},\varphi_j)}{\partial\varphi_j\partial\varphi_{k'}} = \frac{1}{N}f(\vec{\varphi},\varphi_j)\sum\limits_{k'\neq j} f(\vec{\varphi},\varphi_{k'})\sin(\varphi_{k'}-\varphi_j+\alpha) \\ k\neq j, k'=j, & \sum\limits_{k\neq j} f(\vec{\varphi},\varphi_k)f(\vec{\varphi},\varphi_j)\frac{\partial^2 f(\vec{\varphi},\varphi_j)}{\partial\varphi_k\partial\varphi_j} = \frac{1}{N}f(\vec{\varphi},\varphi_j)\sum\limits_{k\neq j} f(\vec{\varphi},\varphi_k)\sin(\varphi_k-\varphi_j+\alpha) \\ k\neq j, k'=k, & \sum\limits_{k\neq j} f^2(\vec{\varphi},\varphi_k)\frac{\partial^2 f(\vec{\varphi},\varphi_j)}{\partial\varphi_k^2} = -\frac{1}{N}\sum\limits_{k\neq j} f^2(\vec{\varphi},\varphi_k)\sin(\varphi_k-\varphi_j+\alpha)\ . \end{cases} \tag{8.38}$$

Insert the above in Eq. (8.35), we find that the following ODE is being integrated by Euler scheme to third order $O(h^3)$

$$\begin{aligned} \dot{\varphi}_j = {} & \mathrm{Im}(Z_{KS}e^{-i\varphi_j}) - \frac{h}{4}\mathrm{Im}(Z_{KS}e^{i\alpha}e^{-i\varphi_j} + Z_{KS}e^{i\alpha}Z^*_{KS,2}e^{i\varphi_j} - Z^2_{KS}e^{-2i\varphi_j}) \\ & - \frac{h^2}{12}\mathrm{Im}\Big\{|Z_{KS}|^2 Z_{KS,2}e^{i(-2\varphi_j+\alpha)} + Z^2_{KS}Z^*_{KS,2}e^{i\alpha} - Z^2_{KS}e^{i(-2\varphi_j+\alpha)} \\ & - |Z_{KS}|^2 e^{-i\alpha} + \frac{1}{2}Z^3_{KS}e^{-3i\varphi_j} - \frac{3|Z_{KS}|^2}{2}Z_{KS}e^{-i\varphi_j} - \frac{1}{2}|Z_{KS}|^2 Z_{KS}e^{i(-\varphi_j+\alpha)} \\ & + \frac{1}{2}Z^{*2}_{KS}Z_{KS,3}e^{i(\varphi_j-\alpha)}\Big\}\ , \end{aligned} \tag{8.39}$$

where as before $Z_{KS} = e^{i\alpha}\frac{1}{N}\sum\limits_k e^{i\varphi_k}$ is the Kuramoto-Sakaguchi mean-field.

From Eq. (8.39), it is now possible to obtain third and fourth mode couplings by going to the third order of h. We can draw the conclusion that, as h gets larger (or as the integration time gets longer in the case of Ref. [GKM09], where noise combined with repulsive coupling prolongs the integration till the forbidden multiclusters are formed), these terms will play an increasingly significant role in the final dynamics calculated by the numerical scheme.

When there is no phase shift, $\alpha = 0$, we can write Eq. (8.39) as

$$\begin{aligned} \dot{\varphi}_j = {} & \mathrm{Im}(Ze^{-i\varphi_j}) - \frac{h}{4}\mathrm{Im}(Ze^{-i\varphi_j} + ZZ^*_2e^{i\varphi_j} - Z^2e^{-2i\varphi_j}) - \frac{h^2}{12}\mathrm{Im}\Big\{|Z|^2Z_2e^{-2i\varphi_j} \\ & + Z^2Z^*_2 - Z^2e^{-2i\varphi_j} - |Z|^2 + \frac{1}{2}Z^3e^{-3i\varphi_j} - 2|Z|^2Ze^{-i\varphi_j} + \frac{1}{2}Z^{*2}Z_3e^{i\varphi_j}\Big\}\ . \end{aligned} \tag{8.40}$$

E. Integration Schemes for Coupled SDEs

We would like to numerically integrate SDE

$$\dot{x}_j = \bar{f}(\vec{x}, x_j) + \sum_m \bar{g}_m(\vec{x}, t)\Delta W_m(t) \ , \tag{8.41}$$

where m is the noise term index, with Wiener process $\Delta W_m(t) = [W_m(t+h) - W_m(t)] \sim \mathcal{N}(0,1)$. In the order from lower to higher numerical accuracies, we have used the following three integration schemes for the numerical integrations conducted in this thesis.

1. Euler-Maruyama scheme, which has an implicit Itô interpretation:

$$x_{j,n+1} = x_{j,n} + h\bar{f}(\vec{x}, x_j) + \sqrt{h}\sum_m \bar{g}_m(\vec{x}, t)\Delta W_m(t) \ . \tag{8.42}$$

   It has weak order 1, strong order 1/2 [Bur98; BB98; BBT04].

   To obtain the Stratonovich interpretation for the integral of Eq. (8.41), the Stratonovich shift needs to be added to the SDE, i.e, we need to use the following scheme:

$$x_{j,n+1} = x_{j,n} + h\left[\bar{f}(\vec{x}, x_j) - s_j(x,t)\right] + \sqrt{h}\sum_m \bar{g}_m(\vec{x}, t)\Delta W_m(t) \ , \tag{8.43}$$

   where $s_j(x,t) = \frac{1}{2}\sum_{k,m} \bar{g}_m(x_k, t)\partial_{x_k}\bar{g}_m(x_j, t)$ is the Stratonovich shift.

2. Euler-Heun scheme, which has implicit Stratonovich interpretation:

$$\tilde{x}_j = x_{j,n} + \sqrt{h}\sum_m \bar{g}_m(\vec{x}, t)\Delta W_m(t) \tag{8.44}$$

$$x_{j,n+1} = x_{j,n} + h\bar{f}(\vec{x}) + \frac{1}{2}\sqrt{h}\sum_m \left[\bar{g}_m(\vec{\tilde{x}}, t) + \bar{g}_m(\vec{x}, t)\right]\Delta W_m(t) \ , \tag{8.45}$$

   It has strong order 1.

3. Stochastic Runge-Kutta 4th-Order scheme, which has a strong order of 1.5, has been adjusted to have the Stratonovich interpretation as follows:

$$
\begin{aligned}
K_{j1} =& x_{j,n} \\
f_{j1} =& \bar{f}(\vec{x}_n, K_{j1}) - S(K_{j1}, t) \\
K_{j2} =& x_{j,n} + \frac{2}{3} h f_{j1} + \frac{2}{3} \bar{\eta}\bar{g}(K_{j1}) \\
f_{j2} =& \bar{f}(\vec{x}_n, K_{j2}) - S(K_{j2}, t) \\
K_{j3} =& x_{j,n} + \frac{3}{2} h f_{j1} - \frac{1}{3} h f_{j2} + \frac{1}{2} \bar{\eta}\bar{g}(K_{j1}) + \frac{1}{6} \bar{\eta}\bar{g}(K_{j2}) - \frac{2}{3} \bar{\xi}\bar{g}(K_{j1}) \\
K_{j4} =& x_{j,n} + \frac{7}{6} h f_{j1} - \frac{1}{2} \bar{\eta}\bar{g}(K_{j1}) + \frac{1}{2} \bar{\eta}\bar{g}(K_{j3}) + \frac{1}{6} \bar{\xi}\bar{g}(K_{j1}) + \frac{1}{2} \bar{\xi}\bar{g}(K_{j2}) \\
x_{j,n+1} =& x_{j,n} + h\Big\{ \frac{1}{4} f_{j1} + \frac{3}{4} f_{j2} - \frac{3}{4} \left[\bar{f}(\vec{x}_n, K_{j3}) - S(K_{j3}, t) \right] \\
& + \frac{3}{4} \left[\bar{f}(\vec{x}_n, K_{j4}) - S(K_{j4}, t) \right] \Big\} + \bar{\eta} \Big\{ - \frac{1}{2} \bar{g}(K_{j1}) + \frac{3}{2} \bar{g}(K_{j2}) - \frac{3}{4} \bar{g}(K_{j3}) \\
& + \frac{3}{4} \bar{g}(K_{j4}) \Big\} + \bar{\xi} \left[\frac{3}{2} \bar{g}(K_{j1}) - \frac{3}{2} \bar{g}(K_{j2}) \right] ,
\end{aligned}
\tag{8.46}
$$

where $S(x_j, t)$ is the Stratonovich shift, and $\bar{\eta}, \bar{\xi}$ are calculated according to $\bar{\eta} = u\sqrt{h}$ and $\bar{\xi} = \sqrt{h}(\frac{u}{2} + \frac{v}{2\sqrt{3}})$, where u and v are two random Gaussian numbers. Eq. (8.46) is of Itô interpretation if we eliminate all the shift terms.

For the concepts of the Stratonovich and Itô interpretations, please refer to Appendix A.

F. Calculation of the Synchronization Index for Non-identical Oscillators in an Infinite Ensemble Under Common Multiplicative White Noise

We use two methods to calculate the zero-flux solution of the Fokker-Planck equation presented in Eq. (6.29).

Numerical approximation

We first expand P in a

$$
P = \frac{1}{2\pi} \sum_{\tilde{k}=-\infty}^{\infty} p_{\tilde{k}} e^{i\tilde{k}a} \tag{8.47}
$$

Substituting in Eq. (6.29) to obtain

$$
W \sum_{\tilde{k}} p_{\tilde{k}} e^{i\tilde{k}a} - \sum_{\tilde{k}} i\tilde{k} p_{\tilde{k}} e^{i\tilde{k}a} + \frac{\partial}{\partial a} \sum_{\tilde{k}} \frac{e^{ia} + e^{-ia}}{2} p_{\tilde{k}} e^{i\tilde{k}a} = W \ . \tag{8.48}
$$

Rearranging, we obtain

$$
\sum_{\tilde{k}} e^{i\tilde{k}a} [W p_{\tilde{k}} - i\tilde{k} p_{\tilde{k}} + \frac{1}{2} i\tilde{k} (p_{\tilde{k}-1} + p_{\tilde{k}+1})] = W \ . \tag{8.49}
$$

Focusing on the summed term $Wp_{\tilde{k}} - i\tilde{k}p_{\tilde{k}} + \frac{1}{2}i\tilde{k}(p_{\tilde{k}-1} + p_{\tilde{k}+1})$, for $\tilde{k} = 0$

$$Wp_0 - i \cdot 0 \cdot p_0 + \frac{1}{2}i \cdot 0 \cdot (p_{\tilde{k}-1} + p_{\tilde{k}+1}) = Wp_0 \ . \tag{8.50}$$

By letting $p_0 = 1$, the $\tilde{k} > 0$ contribution is all 0, i.e., for general nonzero $\tilde{k}$

$$\frac{im}{2}p_{\tilde{k}-1} + p_{\tilde{k}}(W - i\tilde{k}) + \frac{i\tilde{k}}{2}p_{\tilde{k}+1} = 0 \tag{8.51}$$

Assume $p_{\tilde{k}-1}/p_{\tilde{k}} = r_{\tilde{k}}$, then

$$\begin{aligned} &\frac{i\tilde{k}}{2}r_{\tilde{k}} + W - i\tilde{k} + \frac{i\tilde{k}}{2}\frac{1}{r_{\tilde{k}+1}} = 0 \\ &r_{\tilde{k}} = \frac{2\tilde{k} + 2iW}{\tilde{k}} - \frac{1}{r_{\tilde{k}+1}} \end{aligned} \tag{8.52}$$

The synchronization index (cross-correlation) is

$$\gamma_{12} = |p_1| = |\frac{1}{2 + 2iW - \frac{1}{r_2}}| \ , \tag{8.53}$$

with $r_{\tilde{k}}$ iteratively calculated according to Eq. (8.52).

If we assume the second harmonic coefficient $p_2 \approx 0$, then $r_2 \sim \infty$, i.e., $1/r_2 \approx 0$, then

$$r_1 = \frac{2 + 2iW}{1} \qquad p_1 = \frac{1}{2 + 2iW} \ . \tag{8.54}$$

So the synchronization index (up to first truncation) is

$$\gamma_{12} = |e^{i(\tilde{\psi}_2 - \tilde{\psi}_1)}| = |\langle e^{ia} \rangle| \approx |p_1| = \frac{1}{2\sqrt{1 + W^2}} \tag{8.55}$$

Analytical solution

We use the following transformation to solve Eq. (6.29)

$$x = \cot\frac{a}{2} \qquad \sin^2\frac{a}{2} = \frac{1}{1 + x^2} \qquad \cos a = \frac{x^2 - 1}{x^2 + 1} \qquad \sin a = \frac{2x}{1 + x^2} \tag{8.56}$$

with derivative of the transform

$$dx = -\frac{1 + x^2}{2}da \ . \tag{8.57}$$

The probability density of x should obey $P(a)da = Q(x)dx$. So we derive $Q(x)$ as

$$P(a)da = -P(a)\frac{2}{1 + x^2}dx = Q(x)dx, \tag{8.58}$$

where comparing two sides we obtain

$$Q(x) = -\frac{2P(a)}{1 + x^2} \ . \tag{8.59}$$

We first check for the convergence of the transformed distribution $Q(x)$ at $x \to \pm\infty$, which corresponds to the original variable $a \to 0$. We assume a narrow Gaussian distribution for the original variable a centered around 0

$$P(a) \sim \frac{1}{\epsilon} \exp\left[-\left(\frac{a}{\epsilon}\right)^2\right] , \tag{8.60}$$

which when transformed becomes

$$Q(x) \sim -\frac{2}{1+x^2}\frac{1}{\epsilon} \exp\left[-\left(\frac{2x}{(1+x^2)\epsilon}\right)^2\right] , \tag{8.61}$$

where we used the small-angle approximation $a \approx \sin a$ and the transform above $\sin a = 2x/(1+x^2)$.

For large x, Eq. (8.61) can be simplified to

$$Q(x) \sim -\frac{2}{x^2\epsilon} \exp\left[-\frac{4}{(x\epsilon)^2}\right] , \tag{8.62}$$

and it's easy to see if $x\epsilon \gg 1$, $Q(x) \sim 1/(x^2\epsilon)$, and if $x\epsilon \ll 1$, $Q(x) \sim 0$. So even for an almost delta distribution, in the transformed space, the density at the point which corresponds to the delta peak location goes to 0. Hence after the transformation, the probability density converges to 0 at $|x| \to \infty$.

After transformation, Eq. (6.29) becomes

$$-\frac{\partial Q}{\partial x} - WQ = \frac{W}{(1+x^2)\pi} \tag{8.63}$$

To solve the ODE (8.63), we use the ansatz $Q(x) = C(x)e^{-Wx}$,

$$\begin{aligned} WC(x)e^{-Wx} - C'(x)e^{-Wx} - WC(x)e^{-Wx} &= \frac{W}{(1+x^2)\pi} \\ -C'(x)e^{-Wx} = \frac{W}{(1+x^2)\pi} &\Rightarrow C(x) = -\frac{1}{\pi}\int^x \frac{We^{Wy}}{1+y^2}dy \ . \end{aligned} \tag{8.64}$$

So

$$Q(x) = -e^{-Wx}\frac{1}{\pi}\int^x \frac{We^{Wy}}{1+y^2}dy \ . \tag{8.65}$$

To calculate the synchronization index $\gamma_{12} = \langle e^{ia}\rangle = \langle \cos a\rangle + i\langle \sin a\rangle$, we calculate $\langle \cos a\rangle$ and $\langle \sin a\rangle$ separately. By making substitution $x = v, x - y = u$, ($0 < u < \infty$ and $-\infty < v < \infty$)

$$\begin{aligned} \langle \sin a\rangle = \int_{-\infty}^{\infty} \frac{2x}{1+x^2}Q(x)dx &= -\frac{W}{\pi}\int_{-\infty}^{\infty} \frac{2x}{1+x^2}e^{-Wx}\int^x \frac{e^{Wy}}{1+y^2}dydx \\ &= \frac{W}{\pi}\int_0^{\infty} e^{-Wu}\int_{-\infty}^{\infty} \frac{2v}{1+v^2}\frac{1}{1+(v-u)^2}dvdu \ , \end{aligned} \tag{8.66}$$

which we proceed to solve using complex integration and the residue theorem

$$\int_{-\infty}^{\infty} \frac{2v}{(1+(v-u)^2)(1+v^2)}dv := \int_{-\infty}^{\infty} f(v)dv = (\oint_C - \int_{\text{arc}})f(v)dv \tag{8.67}$$

The arc contribution is negligible, hence we only need to calculate the contour integral

$$\oint_C f(v)dv = 2\pi i \mathrm{Res}(z=i) + 2\pi i \mathrm{Res}(z=i+a) = \frac{2\pi u}{u^2+4} \ . \tag{8.68}$$

Bring it into Eq. (8.66)

$$\langle \sin a \rangle = \frac{W}{\pi} \int_0^\infty e^{-Wu} \frac{2\pi u}{u^2+4} du = 2W \int_0^\infty \frac{e^{-Wu} u}{u^2+4} du \ . \tag{8.69}$$

Using formula 3.354.2 in the integral tables [GR80]

$$\langle \sin a \rangle = 2W[-\mathrm{ci}(2W)\cos(2W) - \mathrm{si}(2W)\sin(2W)] \ , \tag{8.70}$$

where ci and si are sine and cosine integrals

$$\mathrm{ci} = -\int_x^\infty \frac{\cos r}{r} dr \qquad \mathrm{si} = -\int_x^\infty \frac{\sin r}{r} dr \ . \tag{8.71}$$

Similarly, we can solve for $\langle \cos a \rangle$ with formula (3.354.1) in Ref. [GR80]

$$\langle \cos a \rangle = 1 - 2W[\mathrm{ci}(2W)\sin(2W) - \mathrm{si}(2W)\cos(2W)] \ . \tag{8.72}$$

So altogether the synchronization index

$$\begin{aligned} \gamma_{12}^2 &= (\langle \cos a \rangle)^2 + (\langle \sin a \rangle)^2 \\ &= 1 + 4W^2[\mathrm{ci}^2(2W) + \mathrm{si}^2(2W)] - 4W[\mathrm{ci}(2W)\sin(2W) - \mathrm{si}(2W)\cos(2W)] \ . \end{aligned} \tag{8.73}$$

Bibliography

[AS04] D. M. Abrams and H. S. Strogatz. "Chimera States for Coupled Oscillators". In: *Physical Review Letters* 93 (2004), p. 174102.

[Abr+08] D. M. Abrams et al. "Solvable Model for Chimera States of Coupled Oscillators". In: *Physical Review Letters* 101 (8 2008), p. 084103.

[Ace+05] J. A. Acebrón et al. "The Kuramoto model: A simple paradigm for synchronization phenomena". In: *Reviews of Modern Physics* 77.1 (2005), pp. 137–185.

[Adl46] R. Adler. "A study of locking phenomena in oscillators". In: *Proceedings of the IRE* 34.6 (1946), pp. 351–357.

[Arn65] V. I. Arnold. "Small denominators I, Mappings of the Circumference onto Itself'. In: *American Mathematical Society Translations* 46 (1965), pp. 213–284.

[Bai+09] Y. Baibolatov et al. "Periodically forced ensemble of nonlinearly coupled oscillators: From partial to full synchrony". In: *Physical Review E* 80.4 (2009), p. 046211.

[Bar13] G. Barlev. "Synchronization of network coupled chaotic and oscillatory dynamical systems". In: *Ph.D. thesis, University of Maryland, U.S.A* (2013).

[BAO11] G. Barlev, T. M. Antonsen, and E. Ott. "The dynamics of network coupled phase oscillators: An ensemble approach". In: *Chaos* 21.2 (2011), p. 025103.

[BM09] M. Bauer and W. Martienssen. "Coupled circle maps as a tool to model synchronisation in neural networks". In: *Network Computation in Neural Systems* 2 (2009), pp. 345–351.

[BM+16] E. Bianco-Martinez et al. "Successful network inference from time-series data using mutual information rate". In: *Chaos* 26.4 (2016), p. 043102.

[BAR16] C. Bick, P. Ashwin, and A. Rodrigues. "Chaos in generically coupled phase oscillator networks with nonpairwise interactions". In: *Chaos* 26.9 (2016), p. 094814.

[BPR10] G. Bordyugov, A. Pikovsky, and M. Rosenblum. "Self-emerging and turbulent chimeras in oscillator chains". In: *Physical Review E* 82 (3 2010), p. 035205.

[BHD10] M. Breakspear, S. Heitmann, and A. Daffertshofer. "Generative Models of Cortical Oscillations: Neurobiological Implications of the Kuramoto Model". In: *Frontiers in Human Neuroscience* 4 (2010), p. 190.

[BKT10] V. M. Buchstaber, O. V. Karpov, and S. I. Tertychniy. "Rotation number quantization effect". In: *Theoretical and Mathematical Physics* 162.2 (2010), pp. 211–221.

[Buc88] J. Buck. "Synchronous Rhythmic Flashing of Fireflies. II." In: *The Quarterly Review of Biology* 63.3 (1988), pp. 265–289.

[BS09] E. Bullmore and O. Sporns. "Complex brain networks: Graph theoretical analysis of structural and functional systems". In: *Nature reviews. Neuroscience* 10 (2009), pp. 186–198.

[BF04] R. Burden and J. Faires. *Numerical Analysis*. Cengage Learning, 2004.

[BBT04] K. Burrage, P. M. Burrage, and T. Tian. "Numerical methods for strong solutions of stochastic differential equations: an overview". In: *Proceedings of The Royal Society of London. Series A. Mathematical, Physical and Engineering Sciences* 460.2041 (2004), pp. 373–402.

[BB98] K. Burrage and P.M. Burrage. "General order conditions for stochastic Runge-Kutta methods for both commuting and non-commuting stochastic ordinary differential equation systems". In: *Applied Numerical Mathematics* 28.2 (1998), pp. 161 –177.

[Bur98] P. M. Burrage. "Runge–Kutta methods for stochastic differential equations". In: *Ph.D. thesis, University of Queensland, Brisbane, Australia* (1998).

[Buz06] G. Buzsaki. *Rhythms of the Brain*. Oxford University Press, 2006.

[Cab+11] J. Cabral et al. "Role of local network oscillations in resting-state functional connectivity". In: *NeuroImage* 57.1 (2011), pp. 130 –139.

[Cha+14] S. Chakraborty et al. "Neural synchronization based secret key exchange over public channels: A survey". In: *2014 International Conference on Signal Propagation and Computer Technology (ICSPCT 2014)* (2014), pp. 368–375.

[Cha+17] S. Chandra et al. "Modeling the network dynamics of pulse-coupled neurons". In: *Chaos* 27.3 (2017), p. 033102.

[CG96] N. Chatterjee and N. Gupte. "Synchronization in coupled sine circle maps". In: *Physical Review E* 53 (1996), pp. 4457–4466.

[Che17] B. Chen. "Dimensional Reduction for Identical Kuramoto Oscillators". In: *Ph.D. thesis, Boston College* (2017).

[CEM17] B. Chen, J. R. Engelbrecht, and R. Mirollo. "Hyperbolic geometry of Kuramoto oscillator networks". In: *Journal of Physics A* 50.35 (2017), p. 355101.

[Cou+13] B. C. Coutinho et al. "Kuramoto model with frequency-degree correlations on complex networks". In: *Physical Review E* 87.3 (2013), p. 032106.

[Czo+13] K. Czolczynski et al. "Synchronization of the self-excited pendula suspended on the vertically displacing beam". In: *Communications in Nonlinear Science and Numerical Simulation* 18 (2013), pp. 386 –400.

[Dai87] H. Daido. "Scaling behaviour at the onset of mutual entrainment in a population of interacting oscillators". In: *Journal of Physics A* 20.10 (1987), pp. L629–L636.

[Dai92] H. Daido. "Order Function and Macroscopic Mutual Entrainment in Uniformly Coupled Limit-Cycle Oscillators". In: *Progress of Theoretical Physics* 88.6 (1992), pp. 1213–1218.

[Dai93] H. Daido. "Critical Conditions of Macroscopic Mutual Entrainment in Uniformly Coupled Limit-Cycle Oscillators". In: *Progress of Theoretical Physics* 89.4 (1993), pp. 929–934.

[Dai95] H. Daido. "Multi-branch entrainment and multi-peaked order-functions in a phase model of limit-cycle oscillators with uniform all-to-all coupling". In: *Journal of Physics A: Mathematical and General* 28.5 (1995), pp. L151–L157.

[Dau08] T. Dauxois. "Fermi, Pasta, Ulam, and a mysterious lady". In: *Physics Today* 6.1 (2008), pp. 55–57.

[Del19] R. Delabays. "Dynamical equivalence between Kuramoto models with first- and higher-order coupling". In: *Chaos* 29.11 (2019), p. 113129.

[Doe+09] S. M. Doesburg et al. "Rhythms of Consciousness: Binocular Rivalry Reveals Large-Scale Oscillatory Network Dynamics Mediating Visual Perception". In: *PLOS ONE* 4.7 (2009), pp. 1–14.

[DB12] F. Dörfler and F. Bullo. "Synchronization and Transient Stability in Power Networks and Nonuniform Kuramoto Oscillators". In: *SIAM Journal on Control and Optimization* 50.3 (2012), 1616–1642.

[FA11] J. Fell and N. Axmacher. "The role of phase synchronization in memory processes". In: *Nature Reviews Neuroscience* 12 (2011), pp. 105 –118.

[FPU55] E. Fermi, J. Pasta, and S. Ulam. "Studies of Nonlinear Problems". In: *Los Alamos ReportLA-1940* (1955).

[FNP08] G. Filatrella, A. H. Nielsen, and N. F. Pedersen. "Analysis of a power grid using a Kuramoto-like model". In: *The European Physical Journal B* 61.4 (2008), pp. 485–491.

[Fit61] R. Fitzhugh. "Impulses and Physiological States in Theoretical Models of Nerve Membrane". In: *Biophysical Journal* 1.6 (1961), pp. 445–466.

[Fok14] A. D. Fokker. "Die mittlere Energie rotierender elektrischer Dipole im Strahlungsfeld". In: *Annalen der Physik* 348.5 (1914), pp. 810–820.

[Fok17] A. D. Fokker. "Ueber einen Satz der statistichen Dynamik und eine Erweiterung in der Quantumtheorie". In: *Sitzungsberichte der Preussischen Akademie der Wissenschaften* (1917), pp. 324–341.

[Fri15] P. Fries. "Rhythms for Cognition: Communication through Coherence". In: *Neuron* 88.1 (2015), pp. 220 –235.

[FK79] T. Fujimura and A. Komamine. "Synchronization of Somatic Embryogenesis in a Carrot Cell Suspension Culture". In: *Plant Physiology* 64.1 (1979), pp. 162–164.

[Fur63] K. Furutsu. "On the statistical theory of electromagnetic waves in a fluctuating medium (I)". In: *Journal of Research of the National Bureau of Standards, Section D, Radio Propagation* 67 (1963), p. 303.

[Gar+74] C. S. Gardner et al. "Korteweg-devries equation and generalizations. VI. methods for exact solution". In: *Communications on Pure and Applied Mathematics* 27.1 (1974), pp. 97–133.

[GKM09] S. Gil, Y. Kuramoto, and A. S. Mikhailov. "Common noise induces clustering in populations of globally coupled oscillators". In: *EPL* 88.6 (2009), p. 60005.

[GL50] V. L. Ginzburg and L. D. Landau. "On the Theory of Superconductivity". In: *The Journal of Experimental and Theoretical Physics* 20 (1950), pp. 1064–1082.

[GGB16] C. Giusti, R. Ghrist, and D. S. Bassett. "Two's company, three (or more) is a simplex". In: *Journal of Computational Neuroscience* 41.1 (2016), pp. 1–14.

[Goe95] C. J. Goebel. "Comment on "Constants of motion for superconductor arrays"". In: *Physica D* 80.1 (1995), pp. 18 –20.

[GD19] D. S. Goldobin and A. V. Dolmatova. "Ott-Antonsen ansatz truncation of a circular cumulant series". In: *Physical Review Research* 1 (3 2019), p. 033139.

[GP06] D. S. Goldobin and A. Pikovsky. "Antireliability of noise-driven neurons". In: *Physical Review E* 73.6 (2006), p. 061906.

[GP04] D. S. Goldobin and A. S. Pikovsky. "Synchronization of periodic self-oscillations by common noise". In: *Radiophysics and Quantum Electronics* 47.10 (2004), pp. 910–915.

[GP05] D. S. Goldobin and A. S. Pikovsky. "Synchronization and desinchronization of self-sustained oscillators by common noise". In: *Physical Review E* 71 (2005), 045201(R).

[Gol+11] E. Goldobin et al. "Josephson Junction with a Magnetic-Field Tunable Ground State". In: *Physical Review Letters* 107.22 (2011), p. 227001.

[Gol+13] E. Goldobin et al. "Phase Retrapping in a Pointlike φ Josephson Junction: The Butterfly Effect". In: *Physical Review Letters* 111.5 (2013), p. 057004.

[Gol+92] D. Golomb et al. "Clustering in globally coupled phase oscillators". In: *Physical Review A* 45.6 (1992), pp. 3516–3530.

[GP19] C. C. Gong and Arkady Pikovsky. "Low-dimensional dynamics for higher-order harmonic, globally coupled phase-oscillator ensembles". In: *Physical Review E* 100 (6 2019), p. 062210.

[GTP20] C. C. Gong, R. Toenjes, and A. Pikovsky. "Coupled Moebius Maps as a Tool to Model Kuramoto Phase Synchronization". In: *arXiv e-prints* (2020). arXiv: `arXiv:2001.07593`.

[Gon+19] C. C. Gong et al. "Repulsively coupled Kuramoto-Sakaguchi phase oscillators ensemble subject to common noise". In: *Chaos* 29.3 (2019), p. 033127.

[GR80] I.S. Gradsteyn and I.M. Ryzhik. *Tables of Integrals, Series and Products*. Academic Press, 1980.

[GR93] M. D. Greenfield and I. Roizen. "Katydid synchronous chorusing is an evolutionarily stable outcome of female choice". In: *Nature* 364.6438 (1993), pp. 618–620.

[GH94] M. Griniasty and V. Hakim. "Correlations and dynamics in ensembles of maps: Simple models". In: *Physical Review E* 49 (4 1994), pp. 2661–2667.

[HT82] P. Hänggi and H. Thomas. "Stochastic processes: Time evolution, symmetries and linear response". In: *Physics Reports* 88.4 (1982), pp. 207 –319.

[HFB18] K. M. Hannay, D. B. Forger, and V. Booth. "Macroscopic models for networks of coupled biological oscillators". In: *Science Advances* 4.8 (2018), e1701047.

[HMM93] D. Hansel, G. Mato, and C. Meunier. "Clustering and slow switching in globally coupled phase oscillators". In: *Physical Review E* 48.5 (1993), pp. 3470–3477.

[Har+05] M. Hartbauer et al. "Mechanisms for synchrony and alternation in song interactions of the bushcricket Mecopoda elongata (Tettigoniidae: Orthoptera)". In: *Journal of Comparative Physiology A* 191.2 (2005), pp. 175–188.

[Hon+07] H. Hong et al. "Entrainment Transition in Populations of Random Frequency Oscillators". In: *Physical Review Letters* 99.18 (2007), p. 184101.

[Hon+15] H. Hong et al. "Finite-size scaling, dynamic fluctuations, and hyperscaling relation in the Kuramoto model". In: *Physical Review E* 92.2 (2015), p. 022122.

[HI00] F. C. Hoppensteadt and E. M. Izhikevich. "Pattern recognition via synchronization in phase-locked loop neural networks". In: *IEEE Transactions on Neural Networks* 11.3 (2000), pp. 734–738.

[IRF11] Yu. S. Ilyashenko, D. A. Ryzhov, and D. A. Filimonov. "Phase-lock effect for equations modeling resistively shunted Josephson junctions and for their perturbations". In: *Functional Analysis and Its Applications* 45.3 (2011), p. 192.

[JPP08] J. Javaloyes, M. Perrin, and A. Politi. "Collective Atomic Recoil Laser as a synchronization transition". In: *Physical Review E* 78 (2008), p. 011108.

[Joh+13] F. Johansson et al. *mpmath: a Python library for arbitrary-precision floating-point arithmetic (version 0.18)*. `http://mpmath.org`. 2013.

[Jus95] W. Just. "Globally coupled maps: phase transitions and synchronization". In: *Physica D* 81.4 (1995), pp. 317–340.

[Kal+17] P. Kalle et al. "Chimera states and the interplay between initial conditions and non-local coupling". In: *Chaos* 27.3 (2017), p. 033110.

[Kan89] K. Kaneko. "Chaotic but regular posi-nega switch among coded attractors by claster–size variations". In: *Physical Review Letters* 63.3 (1989), pp. 219–223.

[Kan90] K. Kaneko. "Globally coupled chaos violates the law of large numbers but not the central-limit theorem". In: *Physical Review Letters* 65 (12 1990), pp. 1391–1394.

[Kan91] K. Kaneko. "Globally coupled circle maps". In: *Physica D* 54.1 (1991), pp. 5 –19.

[KZH05] I. Z. Kiss, Y. Zhai, and J. L. Hudson. "Predicting Mutual Entrainment of Oscillators with Experiment-Based Phase Models". In: *Physical Review Letters* 94.24 (2005), p. 248301.

[KZH06] I. Z. Kiss, Y. Zhai, and J. L. Hudson. "Characteristics of Cluster Formation in a Population of Globally Coupled Electrochemical Oscillators: An Experiment-Based Phase Model Approach". In: *Progress of Theoretical Physics Supplement* 161 (2006), pp. 99–106.

[KP15] M. Komarov and A. Pikovsky. "Finite-size-induced transitions to synchrony in oscillator ensembles with nonlinear global coupling". In: *Physical Review E* 92.2 (2015), 020901(R).

[KP13] M. Komarov and A. S. Pikovsky. "Multiplicity of Singular Synchronous States in the Kuramoto Model of Coupled Oscillators". In: *Physical Review Letters* 111 (2013), p. 204101.

[Kor] Hiroshi Kori. *Kuramoto talks about the Kuramoto model [Video File].* Retrieved from https://youtu.be/lac4TxWyBOg, Feb 2. 2015.

[Kur75] Y. Kuramoto. "Self-entrainment of a population of coupled nonlinear oscillators". In: *International Symposium on Mathematical Problems in Theoretical Physics, Lecture Notes in Physics, Vol. 39,* ed. by H. Araki. New York, NY, USA: Springer, 1975, pp. 420–422.

[Kur78] Y. Kuramoto. "Diffusion-Induced Chaos in Reaction Systems". In: *Progress of Theoretical Physics Supplement* 64 (1978), pp. 346–367.

[Kur84] Y. Kuramoto. *Chemical Oscillations, Waves, and Turbulence.* Mineola, NY: Dover Publications, 1984.

[KB02] Y. Kuramoto and D. Battogtokh. "Coexistence of coherence and incoherence in nonlocally coupled phase oscillators". In: *Nonlinear Phenomena in Complex Systems* 5.4 (2002), pp. 380–385.

[LAP13] Y. M. Lai and M. A Porter. "Noise-induced synchronization, desynchronization, and clustering in globally coupled nonidentical oscillators". In: *Physical Review E* 88 (2013), p. 012905.

[Lop+16] M. A. Lopes et al. "Synchronization in the random-field Kuramoto model on complex networks". In: *Physical Review E* 94.1 (2016), p. 012308.

[Lor63] E. N. Lorenz. "Deterministic Nonperiodic Flow". In: *Journal of the Atmospheric Sciences* 20.2 (1963), pp. 130–141.

[Lor07] J. Lorenz. "Continuous opinion dynamics under bounded confidence: A survey". In: *International Journal of Modern Physics C* 18.12 (2007), pp. 1819–1838.

[Lyn+10] M. Lynall et al. "Functional Connectivity and Brain Networks in Schizophrenia". In: *Journal of Neuroscience* 30.28 (2010), pp. 9477–9487.

[MPR14] Y. Maistrenko, B. Penkovsky, and M. Rosenblum. "Solitary state at the edge of synchrony in ensembles with attractive and repulsive interactions". In: *Physical Review E* 89.6 (2014), 060901(R).

[Mai+14] Y. L. Maistrenko et al. "Cascades of Multiheaded Chimera States for Coupled Phase Oscillators". In: *International Journal of Bifurcation and Chaos* 24.08 (2014), p. 1440014.

[Mal+15] D. Malagarriga et al. "Synchronization-based computation through networks of coupled oscillators". In: *Frontiers in Computational Neuroscience* 9 (2015), p. 97.

[MPMA16] E. Martens, M. Panaggio, and D. M. Abrams. "Basins of Attraction for Chimera States". In: *New Journal of Physics, Fast Track Communication* 18 (2016), p. 022002.

[Mar+13] E. A. Martens et al. "Chimera states in mechanical oscillator networks". In: *Proceedings of the National Academy of Sciences* 110.26 (2013), pp. 10563–10567.

[MMS09] S. A. Marvel, R. E. Mirollo, and S. H. Strogatz. "Identical phase oscillators with global sinusoidal coupling evolve by Möbius group action". In: *Chaos* 19.4 (2009), p. 043104.

[Mat+19] M. H. Matheny et al. "Exotic states in a simple network of nanoelectromechanical oscillators". In: *Science* 363.6431 (2019).

[Miu76] R. M. Miura. "The Korteweg-de Vries Equation: A Survey of Results". In: *SIAM Review* 18.3 (1976), pp. 412–459.

[MP18] E. Montbrió and D. Pazó. "Kuramoto Model for Excitation-Inhibition-Based Oscillations". In: *Physical Review Letters* 120.24 (2018), p. 244101.

[MA19] C. A. Moreira and M. A.M. de Aguiar. "Modular structure in C. elegans neural network and its response to external localized stimuli". In: *Physica A* 533 (2019), p. 122051.

[NK10] K. H. Nagai and H. Kori. "Noise-induced synchronization of a large population of globally coupled nonidentical oscillators". In: *Physical Review E* 81.6 (2010), p. 065202.

[NYK12] K. Nakada, S. Yakata, and T. Kimura. "Noise-induced synchronization in spin torque nano oscillators". In: *Journal of Applied Physics* 111.7 (2012), p. 07C920.

[NM15] T. Nishikawa and A. E. Motter. "Comparative analysis of existing models for power-grid synchronization". In: *New Journal of Physics* 17.1 (2015), p. 015012.

[Nov64] E. A. Novikov. "Functional and random-force method in turbulence theory". In: *The Journal of Experimental and Theoretical Physics* 47.5 (1964), p. 1919.

[Noz92] H. Nozawa. "A neural network model as a globally coupled map and applications based on chaos". In: *Chaos* 2.3 (1992), pp. 377–386.

[OK19] O. E. Omel'chenko and E. Knobloch. "Chimerapedia: coherence–incoherence patterns in one, two and three dimensions". In: *New Journal of Physics* 21.9 (2019), p. 093034.

[OK02] G. Osipov and J. Kurths. "Regular and chaotic phase synchronization of coupled circle maps". In: *Physical Review E* 65 (2002), p. 016216.

[OPK02] G. V. Osipov, A. S. Pikovsky, and J. Kurths. "Phase Synchronization of Chaotic Rotators". In: *Physical Review Letters* 88.5 (2002), p. 054102.

[OA08] E. Ott and T. M. Antonsen. "Low dimensional behavior of large systems of globally coupled oscillators". In: *Chaos* 18.3 (2008), p. 037113.

[OA09] E. Ott and T. M. Antonsen. "Long time evolution of phase oscillator systems". In: *Chaos* 19.2 (2009), p. 023117.

[PA15] M. J. Panaggio and D. M. Abrams. "Chimera states: coexistence of coherence and incoherence in networks of coupled oscillators". In: *Nonlinearity* 28.3 (2015), R67.

[PC90] L. M. Pecora and T. L. Carroll. "Synchronization in chaotic systems". In: *Physical Review Letters* 64.8 (1990), pp. 821–824.

[Pec+14] L. M. Pecora et al. "Cluster synchronization and isolated desynchronization in complex networks with symmetries". In: *Nature Communications* 5 (2014), p. 4079.

[Per+00] J. Perelló et al. “Black–Scholes option pricing within Itô and Stratonovich conventions”. In: *Physica A* 278.1 (2000), pp. 260–274.

[PGP19] F. Peter, C. C. Gong, and A. Pikovsky. “Microscopic correlations in the finite-size Kuramoto model of coupled oscillators”. In: *Physical Review E* 100.3 (2019), p. 032210.

[PP18] F. Peter and A. S. Pikovsky. “Transition to collective oscillations in finite Kuramoto ensembles”. In: *Physical Review E* 97.3 (2018), p. 032310.

[PPJ18] S. Petkoski, J. M. Palva, and V. K. Jirsa. “Phase-lags in large scale brain synchronization: Methodological considerations and in-silico analysis”. In: *PLOS Computational Biology* 14.7 (2018), pp. 1–30.

[Pet+14] G. Petri et al. “Homological scaffolds of brain functional networks”. In: *Journal of The Royal Society Interface* 11.101 (2014), p. 20140873.

[PD19] B. Pietras and A. Daffertshofer. “Network dynamics of coupled oscillators and phase reduction techniques”. In: *Physics Reports* 819 (2019), pp. 1 –105.

[PR09] A. Pikovsky and M. Rosenblum. “Self-organized partially synchronous dynamics in populations of nonlinearly coupled oscillators”. In: *Physica D* 238.1 (2009), pp. 27 –37.

[Pik84] A. S. Pikovsky. “Synchronization and stochastization of the ensamble of autogenerators by external noise”. In: *Radiophysics and Quantum Electronics* 27.5 (1984), pp. 390–395.

[PDG19] A. S. Pikovsky, A. V. Dolmatova, and D. S. Goldobin. “Correlations of the States of Non-Entrained Oscillators in the Kuramoto Ensemble with Noise in the Mean Field”. In: *Radiophysics and Quantum Electronics* 61.8 (2019), pp. 672–680.

[PK94] A. S. Pikovsky and J. Kurths. “Collective behavior in ensembles of globally coupled maps”. In: *Physica D* 76 (1994), pp. 411–419.

[PP16] A. S. Pikovsky and A. Politi. *Lyapunov Exponents: A Tool to Explore Complex Dynamics*. Cambridge University Press, 2016.

[PPM01] A. S. Pikovsky, O. Popovych, and Y. Maistrenko. “Resolving Clusters in Chaotic Ensembles of Globally Coupled Identical Oscillators”. In: *Physical Review Letters* 87.4 (2001), p. 044102.

[PR08] A. S. Pikovsky and M. Rosenblum. “Partially Integrable Dynamics of Hierarchical Populations of Coupled Oscillators”. In: *Physical Review Letters* 101 (26 2008), p. 264103.

[PR11] A. S. Pikovsky and M. Rosenblum. “Dynamics of heterogeneous oscillator ensembles in terms of collective variables”. In: *Physica D* 240.9 (2011), pp. 872 –881.

[PR15a] A. S. Pikovsky and M. Rosenblum. “Dynamics of globally coupled oscillators: Progress and perspectives”. In: *Chaos* 25.097616 (2015).

[PRK01] A. S. Pikovsky, M. Rosenblum, and J. Kurths. *Synchronization: A Universal Concept in Nonlinear Sciences*. Cambridge Nonlinear Science Series. Cambridge University Press, 2001.

[Pim+16] A. V. Pimenova et al. “Interplay of coupling and common noise at the transition to synchrony in oscillator populations”. In: *Scientific Reports* 6 (2016), p. 38518.

[PLR05] A. Pluchino, V. Latora, and A. Rapisarda. "Changing Opinions in a Changing World: a New Perspective in Sociophysics". In: *International Journal of Modern Physics C* 16.04 (2005), pp. 515–531.

[PR15b] A. Politi and M. Rosenblum. "Equivalence of phase-oscillator and integrate-and-fire models". In: *Physical Review E* 91.4 (2015), p. 042916.

[Ris96] H. Risken. *The Fokker-Planck equation. Methods of solution and applications. 2nd ed.* Vol. 18. 1996.

[RP07] M. Rosenblum and A. Pikovsky. "Self-Organized Quasiperiodicity in Oscillator Ensembles with Global Nonlinear Coupling". In: *Physical Review Letters* 98.6 (2007), p. 064101.

[RPK96] M. G. Rosenblum, A. S. Pikovsky, and J. Kurths. "Phase Synchronization of Chaotic Oscillators". In: *Physical Review Letters* 76.11 (1996), pp. 1804–1807.

[Sak88] H. Sakaguchi. "Cooperative Phenomena in Coupled Oscillator Systems under External Fields". In: *Progress of Theoretical Physics* 79.1 (1988), pp. 39–46.

[SK86] H. Sakaguchi and Y. Kuramoto. "A soluble active rotater model showing phase transitions via mutual entertainment". In: *Progress of Theoretical Physics* 76 (1986), pp. 576–581.

[Sch+14] L. Schmidt et al. "Coexistence of synchrony and incoherence in oscillatory media under nonlinear global coupling". In: *Chaos* 24.1 (2014), p. 013102.

[Sch16] E. Schöll. "Synchronization patterns and chimera states in complex networks: Interplay of topology and dynamics". In: *The European Physical Journal Special Topics* 225.6 (2016), pp. 891–919.

[SH01] A. Silvescu and V. Honavar. "Temporal Boolean Network Models of Genetic Networks and Their Inference from Gene Expression Time Series". In: *Complex Systems* 13 (2001), 61–78.

[Sin93] W. Singer. "Synchronization of Cortical Activity and its Putative Role in Information Processing and Learning". In: *Annual Review of Physiology* 55.1 (1993), pp. 349–374.

[Siv80] G. I. Sivashinsky. "On Flame Propagation Under Conditions of Stoichiometry". In: *SIAM Journal on Applied Mathematics* 39.1 (1980), pp. 67–82.

[Siv77] G.I. Sivashinsky. "Nonlinear analysis of hydrodynamic instability in laminar flames—I. Derivation of basic equations". In: *Acta Astronautica* 4.11 (1977), pp. 1177 –1206.

[Siz+18] A. E. Sizemore et al. "Cliques and cavities in the human connectome". In: *Journal of Computational Neuroscience* 44.1 (2018), pp. 115–145.

[SOGR11] P. Skardal, E. Ott, and J. G Restrepo. "Cluster Synchrony in Systems of Coupled Phase Oscillators with Higher-Order Coupling". In: *Physical Review E* 84 (2011), p. 036208.

[SA19] P. S. Skardal and A. Arenas. "Abrupt Desynchronization and Extensive Multistability in Globally Coupled Oscillator Simplexes". In: *Physical Review Letters* 122.24 (2019), p. 248301.

[SMC18] K. Soman, V. Muralidharan, and V. S. Chakravarthy. "An Oscillatory Neural Autoencoder Based on Frequency Modulation and Multiplexing". In: *Frontiers in Computational Neuroscience* 12 (2018), p. 52.

[Ste+00] P. N. Steinmetz et al. "Attention modulates synchronized neuronal firing in primate somatosensory cortex". In: *Nature* 404.6774 (2000), pp. 187 –190.

[Str00a] S. H. Strogatz. "From Kuramoto to Crawford: exploring the onset of synchronization in populations of coupled oscillators". In: *Physica D* 143.1 (2000), pp. 1 –20.

[Str00b] S. H. Strogatz. *Nonlinear Dynamics and Chaos: With Applications to Physics, Biology, Chemistry and Engineering*. Westview Press, 2000.

[Str12] S. H. Strogatz. *Sync: How Order Emerges From Chaos In the Universe, Nature, and Daily Life*. Hachette Books, 2012.

[SM91] S. H. Strogatz and R. E. Mirollo. "Stability of incoherence in a population of coupled oscillators". In: *Journal of Statistical Physics* 63.3 (1991), pp. 613–635.

[Str+05] S.H. Strogatz et al. "Theoretical mechanics: crowd synchrony on the Millennium Bridge". In: *Nature* 438.7064 (2005), pp. 43–44.

[SW13] H. Su and X. Wang. *Pinning Control of Complex Networked Systems: Synchronization, Consensus and Flocking of Networked Systems via Pinning*. Springer Berlin Heidelberg, 2013.

[TSP10] N. Tabareau, J.-J. Slotine, and Q.-C. Pham. "How Synchronization Protects from Noise". In: *PLOS Computational Biology* 6.1 (2010), pp. 1–9.

[TA11] T. Tanaka and T. Aoyagi. "Multistable Attractors in a Network of Phase Oscillators with Three-Body Interactions". In: *Physical Review Letters* 106.22 (2011), p. 224101.

[Tem+12] A. A. Temirbayev et al. "Experiments on oscillator ensembles with global nonlinear coupling". In: *Physical Review E* 85.1 (2012), p. 015204.

[TT04] J. Teramae and D. Tanaka. "Robustness of the Noise-Induced Phase Synchronization in a General Class of Limit Cycle Oscillators". In: *Physical Review Letters* 93.20 (2004), p. 204103.

[TFS08] P. Tiesinga, J.-M. Fellous, and T. J. Sejnowski. "Regulation of spike timing in visual cortical circuits". In: *Nature Reviews Neuroscience* 9.2 (2008), pp. 97–107.

[TNS12] M. R. Tinsley, S. Nkomo, and K. Showalter. "Chimera and phase-cluster states in populations of coupled chemical oscillators". In: *Nature Physics* 8.9 (2012), pp. 662–665.

[TKP01] D. Topaj, W.-H. Kye, and A. Pikovsky. "Transition to coherence in populations of coupled chaotic oscillators: A linear response approach". In: *Physical Review Letters* 87.7 (2001), p. 074101.

[Tot+18] J. Totz et al. "Spiral wave chimera states in large populations of coupled chemical oscillators". In: *Nature Physics* 14 (2018), pp. 282–285.

[Tyu+18] I. V. Tyulkina et al. "Dynamics of Noisy Oscillator Populations beyond the Ott-Antonsen Ansatz". In: *Physical Review Letters* 120.26 (2018), p. 264101.

[Ves11] A. Vespignani. "Modelling dynamical processes in complex socio-technical systems". In: *Nature Physics* 8.32 (2011), pp. 32–39.

[VRP16] V. Vlasov, M. Rosenblum, and A. Pikovsky. "Dynamics of weakly inhomogeneous oscillator populations: perturbation theory on top of Watanabe–Strogatz integrability". In: *Journal of Physics A* 49.31 (2016), 31LT02.

[VZP14] V. Vlasov, Y. Zou, and T. Pereira. "Explosive Synchronization is Discontinuous". In: *Physical Review E* 92 (2014), p. 012904.

[Vod+16] D. Vodenicarevic et al. "Synchronization detection in networks of coupled oscillators for pattern recognition". In: *2016 International Joint Conference on Neural Networks (IJCNN)*. 2016, pp. 2015–2022.

[Wal69] T. J. Walker. "Acoustic Synchrony: Two Mechanisms in the Snowy Tree Cricket". In: *Science* 166.3907 (1969), pp. 891–894.

[WHY17] H. Wang, W. Han, and J. Yang. "Synchronous dynamics in the Kuramoto model with biharmonic interaction and bimodal frequency distribution". In: *Physical Review E* 96.2 (2017), p. 022202.

[WS94] S. Watanabe and S. H. Strogatz. "Constants of motion for superconducting Josephson arrays". In: *Physica D* 74 (1994), pp. 197–253.

[WS95] K. Wiesenfeld and J. W. Swift. "Averaged equations for Josephson junction series arrays". In: *Physical Review E* 51.2 (1995), pp. 1020–1025.

[Win67] A. T. Winfree. "Biological rhythms and the behavior of populations of coupled oscillators". In: *Journal of Theoretical Biology* 16.1 (1967), pp. 15 –42.

[Wol19] N. Wolchover. "Scientists Discover Exotic New Patterns of Synchronization". In: *Quanta Magazine* (2019).

[Xu+16] C. Xu et al. "Collective dynamics of identical phase oscillators with high-order coupling". In: *Scientific Reports* 6 (2016), p. 31133.

[Yan+14] Y. Yaniv et al. "Synchronization of sinoatrial node pacemaker cell clocks and its autonomic modulation impart complexity to heart beating intervals". In: *Heart Rhythm* 11.7 (2014), pp. 1210 –1219.

[Yoo+15] S. Yoon et al. "Critical behavior of the relaxation rate, the susceptibility, and a pair correlation function in the Kuramoto model on scale-free networks". In: *Physical Review E* 91.3 (2015), p. 032814.

[Yua+16] D. Yuan et al. "Dynamics in the Kuramoto model with a bi-harmonic coupling function". In: *Communications in Nonlinear Science and Numerical Simulation* 38 (2016), pp. 23 –29.

[Zha+19] T. Zhang et al. "An Oscillatory Neural Network Based Local Processing Unit for Pattern Recognition Applications". In: *Electronics* 8.1 (2019), p. 64.

[ZSD06] W. Zhao, E. Serpedin, and E. R. Dougherty. "Inferring gene regulatory networks from time series data using the minimum description length principle". In: *Bioinformatics* 22.17 (2006), pp. 2129–2135.

[ZSD08] W. Zhao, E. Serpedin, and E. R. Dougherty. "Inferring Connectivity of Genetic Regulatory Networks Using Information-Theoretic Criteria". In: *IEEE/ACM Transactions on Computational Biology and Bioinformatics* 5.2 (2008), pp. 262–274.